A chemical biological approach identifies OTULIN as a regulator of the SNX27-retromer

Dissertation

der Fakultät für Biologie

der Ludwig-Maximilians-Universität München

Aurelia Weber

München, den 9. Januar 2019

Diese Dissertation wurde angefertigt
unter der Leitung von **Prof. Dr. Daniel Krappmann**
am **Helmholtz Zentrum München**
Deutsches Forschungszentrum für Gesundheit und Umwelt
Institut für Molekulare Toxikologie und Pharmakologie
Abteilung Zelluläre Signalintegration

Erstgutachter:	Prof. Dr. Daniel Krappmann
Zweitgutachterin:	Prof. Dr. Barbara Conradt
Tag der Abgabe:	09.01.2019
Tag der mündlichen Prüfung:	23.05.2019

TABLE OF CONTENTS

LIST OF FIGURES

1. Summary

The ubiquitination of proteins is a crucial and reversible post-translational modification in eukaryotes, which influences all cellular processes. Various types of ubiquitin polymers exist that differ in the linkage of the individual ubiquitin molecules. The seven lysine (Lys) residues within the ubiquitin molecule as well as its N-terminal methionine (Met1) can be linked to the C-terminus of another ubiquitin molecule by specific enzymes. Attached to protein substrates, different linkage-specific polyubiquitin chains exert distinct functions. For instance, Lys48- and Lys63-linked ubiquitin chains regulate protein stability and activity, respectively. Met1-linked ubiquitin chains, also referred to as linear chains, have attracted attention in the last decade since they play an important role in the activation of inflammatory signaling pathways. Met1-linked ubiquitin chains are synthesized by the linear ubiquitin chain assembly complex (LUBAC), with HOIP/RNF31 as the catalytic subunit.
Recently, OTULIN was identified as the deubiquitinating enzyme (DUB) that specifically cleaves Met1-linked ubiquitin chains. OTULIN interacts with LUBAC via the E3 ligase HOIP, and thus counteracts LUBAC-mediated generation of linear chains. Moreover, OTULIN acts as a general homeostatic control factor that balances cellular amounts of Met1-linked ubiquitin.

To better understand the cellular activity of OTULIN, we took a chemical biological approach. An activity-based probe (ABP) was designed that covalently couples to the active site of OTULIN and thus captures OTULIN in its active conformation. The chemically synthesized OTULIN ABP is based on a complete Met1-linked diubiquitin substrate, in which the C-terminal glycine (Gly76) of the distal ubiquitin moiety has been substituted with the electrophilic non-canonical amino acid dehydroalanine (bio-Ub^{G76Dha}-Ub).
The OTULIN ABP displays strong reactivity toward recombinant and cellular OTULIN. Some cross-reactivity was only detected with the DUB USP5 and the ubiquitin-activating (E1) enzymes UBA1 and UBA6, confirming the high selectivity for OTULIN. In fact, labeling of USP5 and E1 enzymes by the OTULIN ABP was abolished by the removal of the C-terminal glycine in the proximal ubiquitin molecule and the resulting OTULIN ABP ΔG76 specifically labels OTULIN. The OTULIN ABP facilitates the detection of active endogenous OTULIN and its enrichment from cell extracts, along with OTULIN-associated protein complexes, such as LUBAC.

Using mass spectrometric analysis after OTULIN ABP pull-down, we identified Sorting Nexin 27 (SNX27) as a new OTULIN interactor. SNX27 is a PDZ (post-synaptic density 95/discs large/zonula occludens) domain-containing adaptor protein of the endosomal retromer complex, which mediates the fast transport of internalized transmembrane proteins, the so called cargos, from early endosomes back to the plasma membrane. Co-immunoprecipitations revealed that the OTULIN-SNX27 interaction takes place in various cell lines as well as in primary cells. Further, analytical gel filtration indicated that the majority of OTULIN and SNX27 form a stable cytosolic complex.

Structural, biophysical and cellular analyses demonstrated that OTULIN-SNX27 binding relies on a C-terminal PDZ-binding motif (PDZbm) in OTULIN, which interacts with the canonical cargo-binding site in the SNX27 PDZ domain. Moreover, a second interface was identified that contributes to the high affinity and selectivity of the OTULIN-SNX27 interaction. Cellular binding studies provided evidence that OTULIN counteracts binding of the retromer complex to SNX27. Thus, OTULIN cannot be a cargo for SNX27-dependent sorting processes. Functionally, SNX27 has no impact on the hydrolase activity of OTULIN, the OTULIN-LUBAC association, or LUBAC-mediated signaling. However, through binding to SNX27, OTULIN restricts access for cargos and the retromer complex, and additionally prevents endosomal localization of SNX27. Accordingly, OTULIN counteracts fast recycling of internalized plasma membrane proteins by the SNX27-retromer complex. While activity of OTULIN is critical for controlling the abundance of linear ubiquitin chains, regulation of the SNX27-retromer by OTULIN occurs independently from its catalytic hydrolase activity.

Thus, a chemical biological approach facilitated the characterization of cellular OTULIN activity and allowed the identification of a new non-catalytic function of OTULIN in controlling endosomal sorting processes.

1. Zusammenfassung

Die Ubiquitinierung von Proteinen ist eine essentielle und reversible post-translationale Modifikation in Eukaryoten, die alle zellulären Vorgänge beeinflusst. Es existieren verschiedene Arten von Ubiquitin-Polymeren, die sich in der Verknüpfung der einzelnen Ubiquitin-Moleküle unterscheiden. Sowohl die sieben Lysin-Reste (Lys) innerhalb des Ubiquitin-Moleküls als auch dessen N-terminales Methionin (Met1) können durch spezifische Enzyme mit dem C-Terminus eines anderen Ubiquitin-Moleküls verknüpft werden. Gebunden an Proteinsubstrate, üben unterschiedliche verbindungsspezifische polyUbiquitin-Ketten verschiedene Funktionen aus. So regulieren zum Beispiel Lys48- und Lys63-verknüpfte Ubiquitin-Ketten die Protein-Stabilität beziehungsweise die Protein-Aktivität. Met1-verknüpfte Ubiquitin-Ketten, welche auch lineare Ketten genannt werden, haben im letzten Jahrzehnt große Aufmerksamkeit auf sich gezogen, da sie eine wichtige Rolle bei der Aktivierung inflammatorischer Signalwege spielen. Lineare Ubiquitin-Ketten werden durch den ‚Linear ubiquitin chain assembly complex' (LUBAC) mit HOIP/RNF31 als katalytischer Untereinheit synthetisiert.
Kürzlich wurde OTULIN als deubiquitinierendes Enzym (DUB) identifiziert, das spezifisch Met1-verknüpfte Ubiquitin-Ketten spaltet. OTULIN interagiert über die E3 Ligase HOIP mit LUBAC, und wirkt der LUBAC-vermittelten Bildung linearer Ketten entgegen. Außerdem fungiert OTULIN als wesentlicher homöostatischer Kontrollfaktor, der die zelluläre Konzentration von Met1-verknüpftem Ubiquitin im Gleichgewicht hält.

Um die zelluläre Aktivität von OTULIN besser zu verstehen, wählten wir einen chemisch-biologischen Ansatz. Eine aktivitätsbasierte Sonde (‚activity-based probe', ABP) wurde generiert, die kovalent an das aktive Zentrum von OTULIN bindet und OTULIN so in der aktiven Konformation arretiert. Die chemisch synthetisierte OTULIN ABP basiert auf einem vollständigen Met1-verknüpften diUbiquitin-Substrat, in dem das C-terminale Glycin (Gly76) des distalen Ubiquitins durch die elektrophile nicht-kanonische Aminosäure Dehydroalanin ersetzt wurde (bio-Ub^{G76Dha}-Ub). Die OTULIN ABP zeigt eine starke Reaktivität gegenüber rekombinantem und zellulärem OTULIN. Eine gewisse Kreuzreaktivität konnte nur mit dem DUB USP5 und den Ubiquitin aktivierenden E1 Enzymen UBA1 und UBA6 festgestellt werden, sodass die OTULIN ABP eine hohe Selektivität für OTULIN aufweist. Die geringe Kreuzreaktivität der OTULIN ABP gegenüber USP5 und E1 Enzymen wurde durch Entfernung des C-terminalen Glycins im proximalen Ubiquitin-Molekül aufgehoben und die

hierdurch entstandene OTULIN ABP ΔG76 markiert spezifisch das aktive OTULIN. Die OTULIN ABP ermöglicht somit die Detektion von aktivem endogenen OTULIN und dessen Anreicherung aus Zellextrakten, zusammen mit OTULIN-assoziierten Proteinkomplexen, wie dem LUBAC.

Mittels massenspektrometrischer Analyse nach OTULIN ABP Pull-down identifizierten wir Sorting Nexin 27 (SNX27) als einen neuen OTULIN-Interaktor. SNX27 ist ein PDZ (post-synaptic density 95/discs large/zonula occludens)-Domäne enthaltendes Adapterprotein des endosomalen Retromerkomplexes, welches den schnellen Transport internalisierter Transmembranproteine (so genannter Cargos) von frühen Endosomen zurück zur Plasmamembran vermittelt. Co-Immunopräzipitationen zeigten, dass die OTULIN-SNX27 Interaktion sowohl in verschiedenen Zelllinien als auch in primären Zellen erfolgt. Überdies deutete analytische Gelfiltration darauf hin, dass ein Großteil zellulären OTULINs und SNX27‘ einen stabilen zytosolischen Komplex bilden.
Strukturelle, biophysikalische und zelluläre Analysen zeigten, dass die OTULIN-SNX27 Bindung auf einem C-terminalen PDZ-Bindemotiv (PDZbm) in OTULIN beruht, welches mit der kanonischen Cargo-Bindestelle in der SNX27 PDZ-Domäne interagiert. Außerdem wurde eine zweite Interaktionsoberfläche identifiziert, die zur hohen Affinität und Selektivität der OTULIN-SNX27 Interaktion beiträgt.
Zelluläre Bindungsstudien erbrachten den Nachweis, dass OTULIN der Bindung des Retromerkomplexes an SNX27 entgegenwirkt. Demnach kann OTULIN kein Cargo für SNX27-abhängige Sortiervorgänge sein. Funktional hat SNX27 weder Auswirkungen auf die Hydrolase-Aktivität OTULINs, noch auf die OTULIN-LUBAC Interaktion oder die LUBAC-vermittelte Signalübermittlung. OTULIN hingegen beschränkt durch die Bindung an SNX27 den Zugang für Cargos und den Retromer-Komplex und verhindert zusätzlich die endosomale Lokalisation von SNX27. Dementsprechend wirkt OTULIN dem schnellen Rücktransport internalisierter Plasmamembran-Proteine durch den SNX27-Retromer-Komplex entgegen. Während die Aktivität von OTULIN entscheidend für die Kontrolle der Abundanz linearer Ubiquitin-Ketten ist, geschieht die Regulation des SNX27-Retromer-Komplexes durch OTULIN unabhängig von dessen Hydrolase-Aktivität. So erlaubte der chemisch-biologische Ansatz die Charakterisierung der zellulären Aktivität von OTULIN und die Identifikation einer neuen nicht-katalytischen Funktion von OTULIN bei der Kontrolle endosomaler Sortierungsprozesse.

2. Introduction

2.1 Ubiquitination – a versatile post-translational protein modification

The post-translational modifier ubiquitin (Ub) is an important regulator of almost every cellular process in eukaryotic organisms (Komander and Rape, 2012). This small (8.5 kDa) protein consists of 76 amino acids (aa) whose sequence is highly conserved from yeast to humans. Its globular structure exhibits an exposed C-terminal tail, which can be covalently linked to lysine (Lys) residues in cellular proteins in a post-translational process called ubiquitination. Target proteins can become monoubiquitinated at one (monoubiquitination), or multiple sites (multi-monoubiquitination), or they can become polyubiquitinated by the formation of a polymeric Ub chain on their surface (polyubiquitination) (Figure 2-1A). Different Ub modifications affect the fate of a target protein in a variety of ways and function as signals for succeeding cellular events (Komander and Rape, 2012). Proteins may, for instance, become activated or inhibited, stabilized or destabilized by ubiquitination or provide a platform for protein interactions. Thus, cellular processes such as protein degradation or endocytosis and signaling pathways leading to the activation of transcription factors can be regulated and tightly controlled (Komander and Rape, 2012).

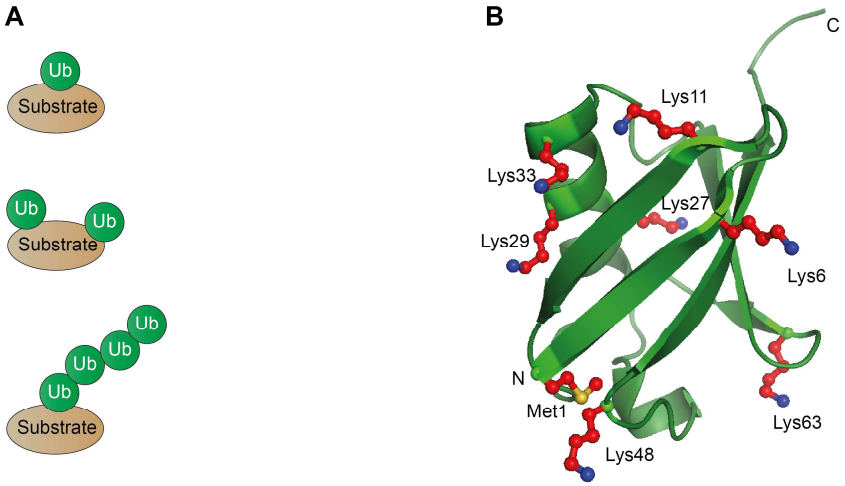

Figure 2-1: Ubiquitin – a versatile post-translational modifier.
A) Kinds of ubiquitination as post-translational modification: monoubiquitination, multi-monoubiquitination and polyubiquitination.
B) Ribbon representation of Ub depicted in green (PDB ID: 1ubq) (Vijay-Kumar et al., 1987). The seven Lys residues and the N-terminal Met are highlighted as these can serve as conjunction sites for another Ub molecule during polyubiquitination.

As well as cellular substrates, Ub itself can become ubiquitinated. All ε-amino groups of the seven Lys residues (Lys6, Lys11, Lys27, Lys29, Lys33, Lys48, Lys63) within the Ub molecule or the α-amino group of the N-terminal methionine (Met1) can serve as conjunction sites for the C-terminal carboxyl group of another Ub (Figure 2-1B). Thus, eight different

linkages can be formed between two Ub molecules creating a large variety of possible chain architectures. In homotypic or linkage-specific Ub chains, the molecules are connected by the same linkage type. The most extensively studied linkage-specific chains are Lys48- and Lys63-Ub. Lys48-Ub usually denotes target proteins for proteasomal degradation (Chau et al., 1989; Hershko and Ciechanover, 1998), whereas Lys63-Ub mostly has non-degradative roles and acts as a scaffold in signaling cascades triggering, for example, kinase activation, the DNA damage response or intracellular trafficking (Chen and Sun, 2009). Besides these typical chains, Met1-linked linear Ub chains have attracted increasing attention in the last decade due to their role in NF-κB (nuclear factor kappa B) signaling (Iwai and Tokunaga, 2009).

Depending on the linkage type, Ub chains differ in their three-dimensional conformations. Lys6-, Lys11- and Lys48-Ub, for instance, exhibit compact structures that are generated by non-covalent interactions between the hydrophobic patches of adjacent Ub molecules (Bremm et al., 2010; Eddins et al., 2007; Virdee et al., 2010). K63- and Met1-Ub, on the other hand, form open chain structures, in which the covalent linkages are the only interaction surfaces (Komander et al., 2009b; Varadan et al., 2004).

Besides the homotypic Ub chains, heterotypic, or branched Ub chains also exist, in which the Ub moieties are connected by different linkages, and which considerably increase the complexity of Ub modifications (Komander and Rape, 2012).

2.1.1 Ubiquitin conjugation

Ub is covalently attached to substrates in a three-step enzymatic process by enzymes referred to as E1, E2 and E3s (Figure 2-2). In humans, two E1s named UBA1 and UBA6, about 40 E2, and more than 600 E3 enzymes exist. This large number of E2 and E3 enzymes emphasizes the diversity and complexity of the Ub-mediated signaling network and the basic importance of linkage and substrate specificity (Zinngrebe et al., 2014).

In the first ATP-dependent step of the ubiquitination cascade, the E1 or Ub-activating enzyme recognizes the C-terminal di-glycine (di-Gly) motif in the Ub molecule and binds the C-terminal carboxyl group of Ub via a high-energy thioester bond. In a second step, the Ub is transferred to the active Cys of an E2 or Ub-conjugating enzyme. And finally, an E3 Ub ligase catalyzes the Ub transfer onto the target protein, interacting with both E2 and substrate (Hershko and Ciechanover, 1998).

The precise transfer mechanism is dependent on the domain structure of the respective E3 enzyme (Figure 2-2). HECT (Homologous to the E6AP Carboxyl Terminus) E3s have a C-terminal HECT domain with an active Cys residue that takes over the Ub from the E2~Ub

intermediate before attaching it to the substrate. RING (Really Interesting New Gene) E3 ligases catalyze the direct Ub transfer from the E2 onto the substrate by bringing both into very close proximity. The third subfamily of RING-between-RING (RBR) E3 enzymes carries a RING domain (RING1) followed by an in-between-RING (IBR) and a second RING domain (RING2). The RING1 domain initially binds the E2~Ub complex as is the case with classical RING E3s. Then, however, the Ub is transferred to a catalytic Cys in the RING2 domain before becoming attached to the substrate. This mechanism is called the RING-HECT hybrid mechanism and is characteristic of the E3 ligases Parkin, HHARI and HOIP (Rotin and Kumar, 2009; Smit et al., 2012; Zinngrebe et al., 2014).

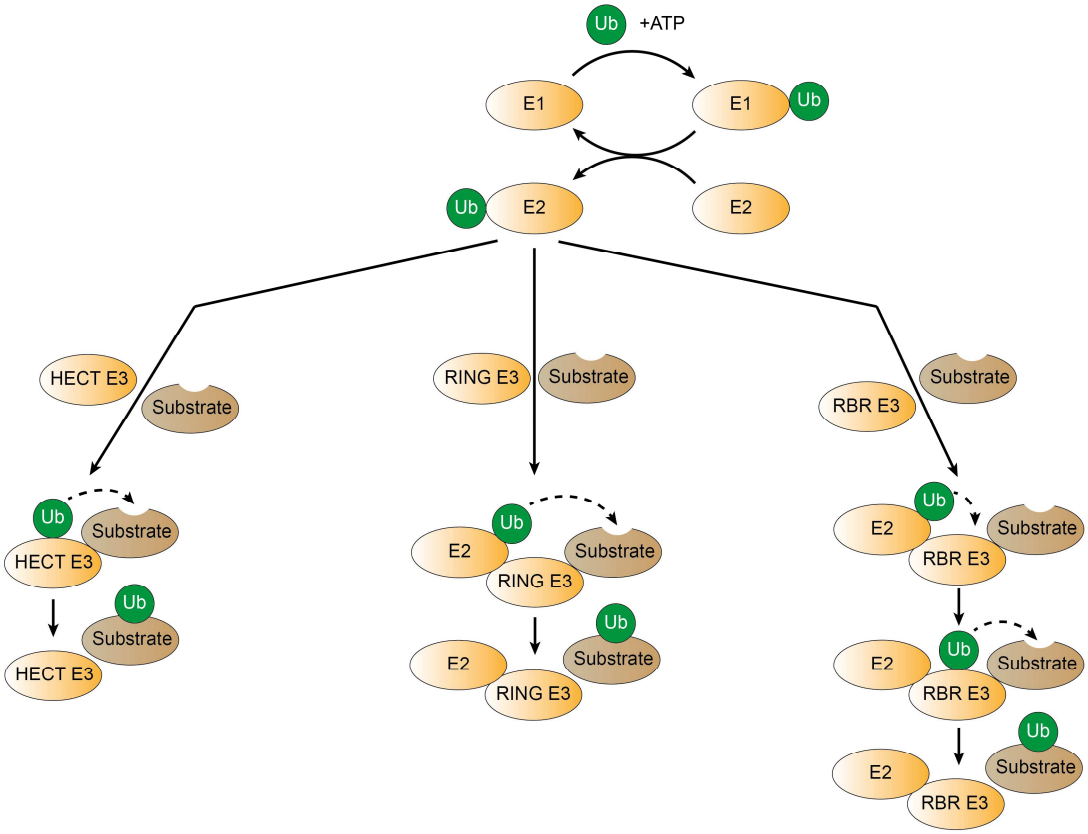

Figure 2-2: Ubiquitin conjugation.
Ubiquitination is a three-step enzymatic process. First, Ub is activated in an ATP-dependent reaction by an E1 enzyme by forming an E1~Ub intermediate. Then, the activated Ub is transferred to an E2 enzyme. Finally, E3 enzymes mediate the Ub transfer onto the target protein either by bridging the E2-substrate interaction or by serving as E3~Ub intermediate.

In the ubiquitination process, E3 enzymes mediate substrate specificity and sometimes linkage specificity of polyUb chains, whereas E2 enzymes mostly determine linkage specificity and the length of generated Ub chains (Ye and Rape, 2009; Zinngrebe et al., 2014). E3 ligases often ubiquitinate themselves and thus affect their own stability and activity (Keusekotten et al., 2013; Lorenz, 2018; Zheng and Shabek, 2017).

2.1.2 Ubiquitin recognition by ubiquitin-binding proteins

Ubiquitin attachment primarily mediates its effects by offering interaction platforms for other proteins. Ub can interact non-covalently with other proteins via several surfaces (Figure 2-3A). The main interaction surface is a hydrophobic area formed by Ile44, Leu8, Val70, and His68 (Dikic et al., 2009; Komander and Rape, 2012). This Ile44 patch is flexible around Leu8 and mediates the interaction with most Ub-binding proteins. Further important interaction surfaces are the hydrophobic Ile36 patch (Ile36, Leu71 and Leu73), the Phe4 patch (Phe4, Gln2 and Thr12) and the TEK-box (Thr12, Thr14, Glu34, Lys6, and Lys11) (Husnjak and Dikic, 2012; Komander and Rape, 2012).
MonoUb and polyUb are recognized by a plethora of Ub-binding proteins (UBPs). These UBPs contain at least one Ub-binding domain (UBD). UBPs are, for example, enzymes that are required for conjugation and deconjugation of Ub chains. These enzymes must have the ability to interact with Ub to ensure the signaling function of the post-translational modifier.

UBDs can be subdivided into approximately 20 families and their structures differ widely in some cases (Dikic et al., 2009; Husnjak and Dikic, 2012). Nevertheless, all UBDs are able to interact with the highly conserved Ub surfaces (see Figure 2-3A). Most UBDs recognize the Ub Ile44 patch (Beal et al., 1998; Dikic et al., 2009). The Ile36 patch is, among others, recognized by some proteins of the Ub chain assembly and disassembly machinery (Hu et al., 2002; Kamadurai et al., 2009; Komander and Rape, 2012; Reyes-Turcu et al., 2006). The Phe4 patch and the TEK-box provide further interaction surfaces for UBDs (Husnjak and Dikic, 2012; Komander and Rape, 2012).

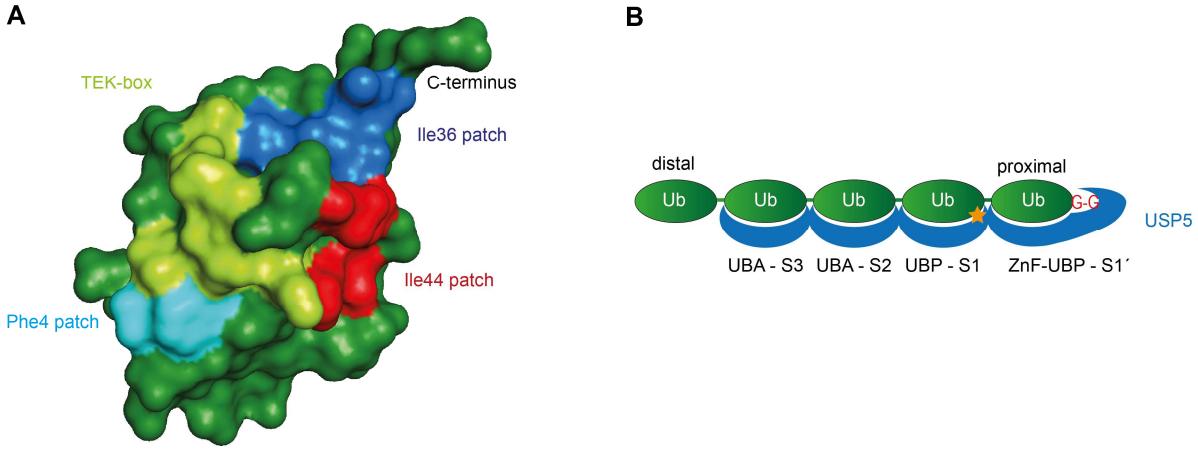

Figure 2-3: Ubiquitin sensing by Ub-binding proteins.
A) Molecular surface representation of Ub (green) with important recognition patches highlighted in color (PDB ID: 1ubq) (Vijay-Kumar et al., 1987).
B) The four UBDs of USP5. The C-terminal di-Gly motif in unanchored Ub chains is recognized and bound by the ZnF-UBP domain (S1´ site). This binding is required for the cleavage of Ub chains from the proximal end. The UBP domain (S1 site) comprises the active site, whereas two UBA domains bind the distal Ub molecules.

Many UBPs possess several UBDs. The deubiquitinating enzyme Ub-specific protease 5 (USP5), also referred to as isopeptidase T (IsoT), is an interesting example, because it has four UBDs (Figure 2-3B): A zinc-finger Ub-binding protein (ZnF-UBP) domain with a deep binding pocket (S1´site) recognizes the highly conserved C-terminal di-Gly motif (Gly75-Gly76) of Ub in unanchored chains and thus enables fast hydrolysis of free polymers in the cell (Reyes-Turcu et al., 2006). The Ub-binding protein (UBP) domain contains the catalytic center (S1 site), and two Ub-associated (UBA) domains (S2 and S3 site) bind the distally linked Ub molecules (Reyes-Turcu et al., 2008).

Many proteins are equipped with specific UBDs, which enable them to distinguish between distinct Ub modifications by sensing the specific linkage between two Ub molecules or the overall conformation of Ub chains (Dikic et al., 2009; Husnjak and Dikic, 2012). This is, among others, an important feature of proteins that act in cellular signaling cascades and link specific Ub signals with a downstream effect. The protein NEMO (NF-κB essential modulator, IKKγ), for instance, binds to Met1-Ub through its UBAN (Ub binding in ABIN and NEMO) domain (Ivins et al., 2009; Komander et al., 2009b; Rahighi et al., 2009). More precisely, this domain interacts with both the distal Ile44 patch and the proximal Phe4 patch of Met1-diUb, providing specificity for the linear linkage (Rahighi et al., 2009). The NEMO UBAN-Met1-Ub interaction is important for proper NF-κB activation. Patients carrying a mutation in the Met1-Ub binding site of NEMO suffer from ectodermal dysplasia with immune deficiency (Hubeau et al., 2011; Rahighi et al., 2009). Interestingly, NEMO is not only recruited to Met1-Ub, but is also a substrate for linear ubiquitination (Tokunaga et al., 2009).

Further examples of UBPs with specific UBDs are the TAK1-binding proteins 2 and 3 (TAB2/3) that are found in a complex with the transforming growth factor β-activated kinase 1 (TAK1). TAB2 and TAB3 contain nuclear protein localization 4 zinc finger (NZF) domains that specifically interact with Lys63-linked Ub chains (Kulathu et al., 2009; Sato et al., 2009). This interaction recruits TAK1 to Lys63-Ub and induces kinase activation, which is also required for NF-κB activation and mitogen-activated protein kinase (MAPK) signaling.

2.1.3 Ubiquitin deconjugation

In common with other post-translational modifications (e.g. phosphorylation or acetylation), ubiquitination is a reversible and highly dynamic process in cells. The action of E3 ligases is counteracted by deubiquitinating enzymes (DUBs) that disassemble Ub chains. This degradation prevents continuous activation of cellular signaling pathways and ensures that the cellular equilibrium can be restored. Moreover, DUBs process Ub precursor proteins to maintain the cellular pool of free Ub. These Ub precursors are encoded by the *UBC, UBB,*

UBA52 and UBA80 genes and are translated either as fusions of three to nine Ub molecules or as fusions of one Ub and a ribosomal protein (Komander et al., 2009a).

In humans, approximately 100 DUBs exist that can be classified into six different families: The Ub-specific proteases (USPs), the ovarian tumor domain-containing proteases (OTUs), the Ub C-terminal hydrolases (UCHs), the Josephin domain-containing proteases and the motif interacting with Ub (MIU)- containing novel DUB family (MINDY) are all Cys proteases with a catalytic diad (Cys-His) or triad (Cys-His-Asn/Asp), whereas the zinc-dependent JAB1/MPN/MOV34 (JAMM) DUBs are metalloproteases (Mevissen and Komander, 2017).

Structures of the catalytic DUB domains in unbound (apo) and substrate-bound states, have given an insight into DUB reactivities. Some DUBs, like USP7, are inactive in the apo state due to a disordered catalytic site. Upon substrate binding, the catalytic residues are reorganized and adopt an active configuration (Hu et al., 2002). Other DUBs, like the proteasome-associated USP14, already exhibit a functional active site in the apo state, but the access to the catalytic pocket is blocked by a structural element, such as a surface loop (Hu et al., 2005).

All DUBs have the ability to interact with the highly conserved hydrophobic surfaces in the Ub molecule (see Figure 2-3A), through a primary Ub-binding site, the S1 site in the catalytic domain (Mevissen and Komander, 2017). This interaction orients the C-terminus of the distal Ub and its linkage towards the catalytic center. Additional substrate or Ub-binding sites provide DUBs with specificity and the ability to distinguish between distinct Ub linkages. A second Ub-binding site inside or outside of the catalytic domain enables DUBs to bind two consecutive Ub molecules in Ub chains. This S1´ site can accommodate the proximal Ub only in a particular orientation and thus determines what linkage is within reach of the active site (Mevissen and Komander, 2017).

The extent of linkage specificity varies among the DUB families. All MINDY family members, for example, are Lys48-specific (Abdul Rehman et al., 2016) and most OTU DUBs, give preference to one particular linkage type or to a small selection of linkages (Mevissen et al., 2013): Cezanne exclusively disassembles Lys11-Ub (Mevissen et al., 2016), OTUB1 specifically cleaves Lys48-Ub (Edelmann et al., 2009) and OTULIN is the only known DUB that is specific for the cleavage of Met1-Ub (Keusekotten et al., 2013). Usually linkage-specific enzymes cannot cleave off the remaining substrate-bound monoUb since their minimal substrate is a diUb. In contrast, most USPs unspecifically cleave a broad range of Ub linkages (Komander et al., 2009b) and are also capable of removing substrate-bound monoUb (Mevissen and Komander, 2017). Even though they are very promiscuous in terms of Ub linkages, they often specifically recruit target proteins that they deubiquitinate by means of substrate-specific binding sites. It is important to mention that the USP CYLD

(Cylindromatosis) is an exception, since it preferentially cleaves Lys63- and Met1-Ub chains (Komander et al., 2008; Komander et al., 2009b; Sato et al., 2015).

In addition, a polyUb chain can be cleaved by DUBs at different sites. In the case of internal cleavage by DUBs with so-called endo-activity, modified substrates can quickly become deubiquitinated, and the released unanchored polyUb chains have to be processed afterwards. Endo-activity is a common feature of DUBs that modulate Ub-mediated signaling, as for example CYLD (Komander et al., 2008). If the Ub chain is attacked from the distal end by a DUB with exo-activity, monoUb is released at each cleavage step and the complete deubiquitination of substrates requires more cleavage steps than complete deubiquitination by endopeptidases. Exo-activity is a characteristic of the proteasome-associated DUB USP14 (Hu et al., 2005) and the MINDY family (Abdul Rehman et al., 2016). Whether a DUB deconjugates polyUb with endo- or exo-activity, mainly depends on the accessibility of the catalytic site for the respective chain type. Interestingly, USP21 hydrolyzes Lys6-Ub with exo- (Hospenthal et al., 2013), Lys63-Ub with endo-activity (Ye et al., 2012) based on the structural conditions of its USP domain.

Specialized 'recycling' DUBs exist for the cleavage of free unattached Ub chains. USP5 (IsoT), for instance, recognizes and binds the C-terminal di-Gly motif in unanchored Ub chains via its ZnF-UBP domain, and efficiently disassembles them from the proximal end, regardless of the linkage type (see also section 2.1.2) (Reyes-Turcu et al., 2006).

DUB abundance, localization and post-translational modifications can additionally influence and fine-tune DUB activity and function (Mevissen and Komander, 2017). Some DUBs, such as the proteasome-bound USP14, associate with large protein complexes to fulfill their function (Borodovsky et al., 2001; Hu et al., 2005). DUBs can also form complexes with E3 ligases (Elliott et al., 2014; Schaeffer et al., 2014; Sowa et al., 2009), indicating that the synthesis and degradation of Ub chains are often closely linked and regulated.

2.1.4 Ubiquitination in the NF-κB signaling pathway

Transcription factors of the NF-κB family are crucial for proper functioning of our immune system since they regulate the expression of target genes, which induce pro-inflammatory immune responses, cell survival, cell proliferation and cell differentiation (Hayden and Ghosh, 2012).

Under unstimulated conditions, NF-κB dimers are bound and retained in the cytoplasm by the inhibitor of NF-κB alpha (IκBα). Stimulation of immune receptors, such as cytokine receptors, pattern recognition receptors (PRRs) or antigen receptors, by their respective ligands triggers activation of the canonical NF-κB signaling pathway. Owing to this activation,

IκBα is phosphorylated and subsequently modified with Lys48-linked Ub chains. This ubiquitination with Lys48-linked polyUb results in the proteasomal degradation of IκBα and in the release of the transcription factors. Free NF-κB dimers can finally translocate into the nucleus and induce gene transcription (Hayden and Ghosh, 2012; Liu and Chen, 2011).
Besides ubiquitination of IκBα, adaptor proteins and E3 ligases are recruited to the receptors and form receptor-associated initial complexes upon stimulation of immune receptors. In the case of tumor necrosis factor receptor 1 (TNFR1), for example, TRADD (TNFR1-associated death domain protein) and the kinase RIPK1 (receptor-interacting serine/threonine protein kinase 1), as well as the E3 enzymes cIAP1/2 (cellular inhibitor of apoptosis 1 and 2) and TRAF2 (TNF receptor-associated factor 2) represent the receptor-proximal signaling complex (Fiil and Gyrd-Hansen, 2014; Hayden and Ghosh, 2012; Lork et al., 2017). This cluster of adaptor proteins and enzymes enables ubiquitination of complex components, predominantly with Lys63-linked Ub chains, creating a binding platform for additional protein complexes (Figure 2-4).

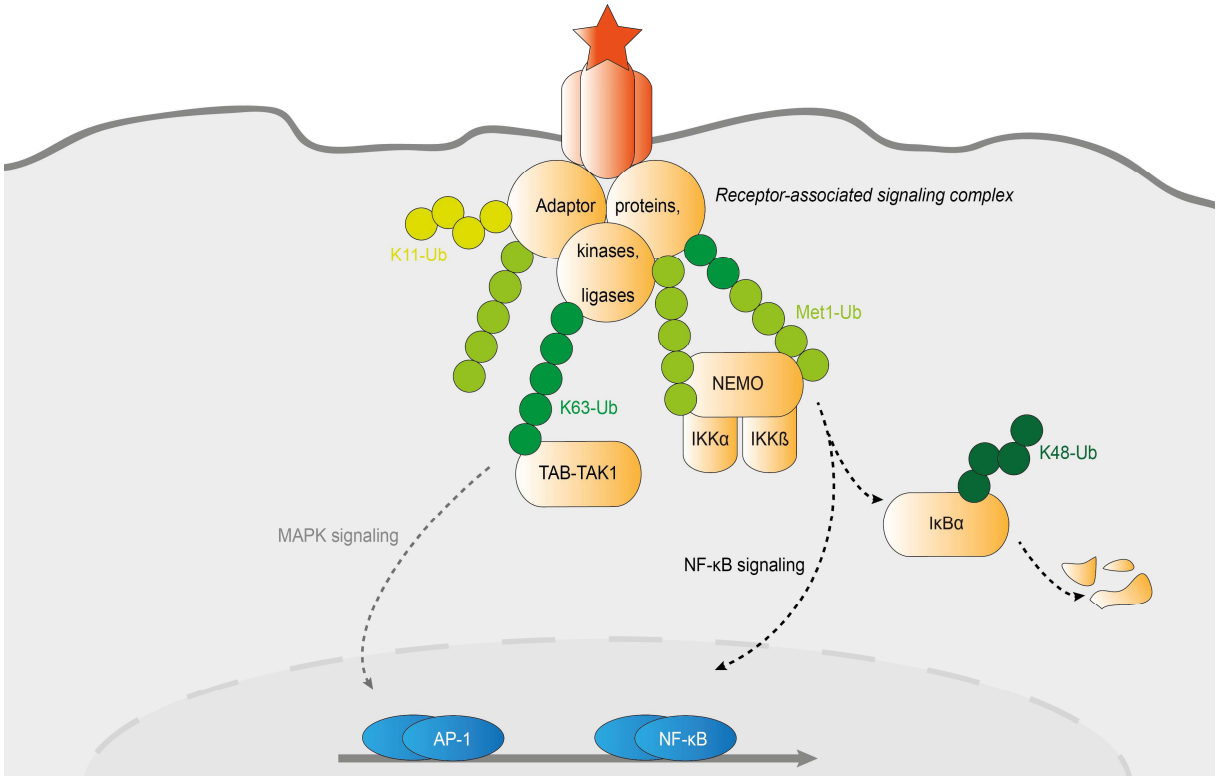

Figure 2-4: Ubiquitin-mediated NF-κB activation.
Engagement of immune receptors by ligands leads to the assembly of receptor-associated signaling complexes composed of adaptor proteins, E3 ligases and kinases. These complexes are modified with Lys63-Ub, Met1-Ub and other Ub chain types, which are recognized and bound by two key kinase complexes. The TAB-TAK1 complex induces MAPK signaling and activates the IKK complex. The activated IKK complex phosphorylates IκBα leading to its proteasomal degradation. Released NF-κB dimers translocate into the nucleus, which together with AP-1 up-regulates target gene expression.

Among others, the linear Ub chain assembly complex (LUBAC) is also recruited to receptor-associated signaling complexes, as it has been shown for TNFR1 and NOD2

(nucleotide-binding oligomerization domain-containing protein 2) (Damgaard et al., 2012; Haas et al., 2009). Recruitment of LUBAC results in the additional conjugation of Met1-Ub on signaling components, which, along with Lys63-Ub, promotes the attraction and activation of two important kinase complexes (Figure 2-4): The IκB kinase (IKK) complex, composed of IKKα, IKKβ and NEMO (IKKγ) is recruited to Met1-Ub via the regulatory subunit NEMO (Rahighi et al., 2009), whereas the TAK1-binding proteins TAB2 and TAB3 lead the TAB-TAK1 complex to Lys63-Ub chains (see section 2.1.2). TAK1 induces downstream MAPK signaling and phosphorylates the adjacent IKKβ subunit of the IKK complex leading to its activation (Zhang et al., 2014). Activated IKKβ, in turn, phosphorylates IκBα, which leads to the ubiquitination and proteasomal degradation of IκBα, as mentioned above (Hayden and Ghosh, 2012).

2.2 Linear ubiquitin (Met1-Ub)

Linear Ub, also referred to as Met1-Ub, contrasts strongly with all other Ub chain types, since peptide bonds (Figure 2-5A) and not isopeptide bonds (Figure 2-5B) link the Ub molecules to one another. This creates a unique chemical and structural surrounding at the linkage sites (Figure 2-5). Compared to isopeptide bonds, the peptide bond has limited rotational freedom and the Met1 side chain occupies much space next to the carboxyl group (Komander et al., 2009b).

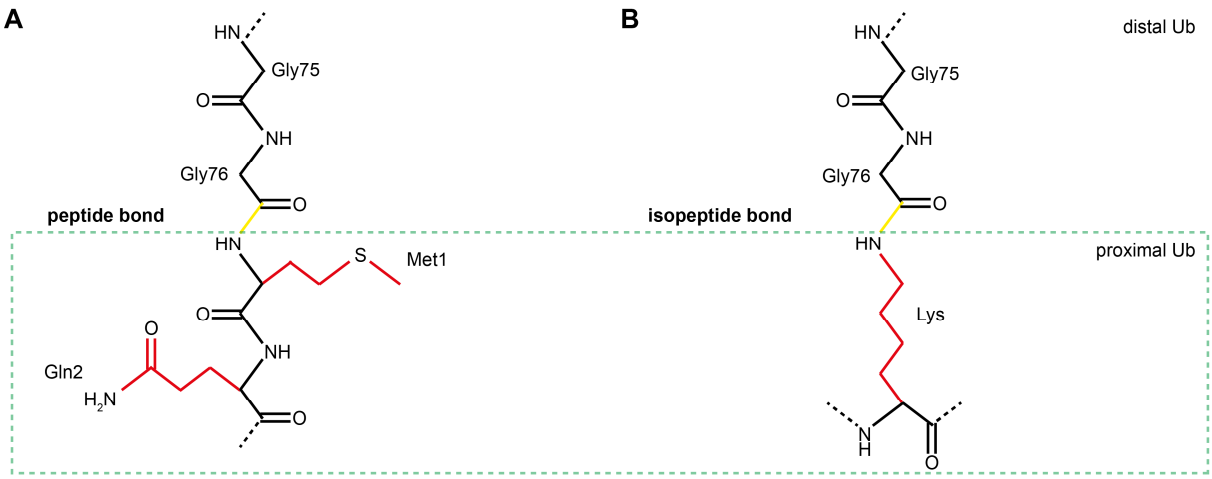

Figure 2-5: Chemical environment of peptide and isopeptide bonds in Ub chains.
A) In Met1-Ub, the C-terminal Gly76 of the distal Ub is linked to the α-amino group of Met1 in the proximal Ub via a peptide bond. Met1 and Gln2 side chains are in close vicinity to the peptide bond and limit the rotational freedom of the Ub linkage.
B) In Lys-linked Ub chains, distal Gly76 is connected to the ε-amino group of a proximal Lys side chain.
The peptide and isopeptide bonds, respectively, are colored in yellow, amino acid side chains in red.

The structural conformation of Met1-Ub is similar to that of Lys63-Ub (Komander et al., 2009b; Varadan et al., 2004) and just as Lys63-Ub, it is also essential for the regulation of various signaling pathways (Shimizu et al., 2015).

In human cells, two sources exist for Met1-Ub. On the one hand, the *UBB* and *UBC* genes encode Met1-linked Ub precursors that are composed of three to nine Ub molecules (Ozkaynak et al., 1984) and are post-translationally processed by DUBs like USP5 to maintain the cellular availability of free Ub (Amerik et al., 1997). On the other hand, Met1-Ub is generated by a specific E3 ligase complex, the linear Ub chain assembly complex (LUBAC) (Kirisako et al., 2006). Met1-Ub is disassembled by the recently identified Met1-specific OTU domain-containing DUB OTULIN (Keusekotten et al., 2013) and by the USP CYLD, which is selective for Met1- and Lys63-Ub (Hrdinka et al., 2016; Komander et al., 2008; Sato et al., 2015). Some other promiscuous USPs can also hydrolyze Met1-Ub, but only with very low efficiency compared to other chain types (Faesen et al., 2011; Komander et al., 2009b). DUBs of other families are unreactive towards Met1-Ub (Komander et al., 2009b; Mevissen et al., 2013).

Linear Ub is an important regulator of inflammatory and cell death signaling and has been linked with Wnt signaling during embryonic development (Rittinger and Ikeda, 2017; Rivkin, 2013; Sasaki and Iwai, 2015; Shimizu et al., 2015). Deficiencies in the Met1-Ub machinery impair the function of the immune system and cause disease (Hrdinka and Gyrd-Hansen, 2017; Rittinger and Ikeda, 2017).

2.2.1 LUBAC

To this day, LUBAC is the only known E3 ligase complex that specifically generates Met1-Ub. It is composed of the proteins HOIL-1L (Heme-oxidized IRP2 Ub ligase-1, also termed RBCK1 or RNF54), HOIP (HOIL-1-interacting protein, also termed RNF31 or ZIBRA), and SHARPIN (Shank-associated RH domain-interacting protein, also termed hSIPL1) (Gerlach et al., 2011; Ikeda et al., 2011; Kirisako et al., 2006; Tokunaga et al., 2011). Although both HOIP and HOIL-1 are E3 ligases with functional RBR domains, the ability of the complex to generate Met1-Ub originates from the catalytic activity of HOIP (Emmerich et al., 2013; Stieglitz et al., 2012). Being an RBR E3 ligase, HOIP catalyzes the assembly of Met1-Ub by means of a RING/HECT hybrid mechanism (Figure 2-6). After an initial interaction between the RING1 domain and the incoming E2-Ub complex, the Ub is taken over by Cys885 in the RING2 domain and subsequently connected to the amino-terminus of the target Ub (Smit et al., 2012; Stieglitz et al., 2012; Stieglitz et al., 2013).

It was shown that LUBAC can at least *in vitro* form linear chains with various E2 enzymes (Kirisako et al., 2006). However, Met1-linkage specificity is not determined by these E2s, but is an intrinsic feature of HOIP. It is based on a C-terminal linear Ub chain-determining domain (LDD) that forms a structural unit with the RING2 domain. The LDD binds the acceptor Ub and brings its N-terminus in close proximity to the donor Ub in the RING2 domain, thus enabling formation of the peptide bond (Smit et al., 2012; Stieglitz et al., 2013). So far, it is unclear whether LUBAC may only generate linear Ub on existing Ub chains or whether it is capable of recognizing the target substrate and attaching the first Ub (Emmerich et al., 2016; Emmerich et al., 2013; Fujita et al., 2014; Hrdinka et al., 2016; Smit et al., 2012; Tokunaga et al., 2009). *In vitro* isolated HOIP is present in an auto-inhibited state (Stieglitz et al., 2012). The binding of HOIL-1 or SHARPIN releases this state and promotes HOIP activity (Figure 2-6) (Gerlach et al., 2011; Kirisako et al., 2006; Stieglitz et al., 2012). It is known that the binding of only one component is sufficient to promote HOIP activity, the exact stoichiometric composition of cellular LUBAC, however, is still unclear. It cannot be ruled out that distinct LUBAC complexes with different properties are present in cells. Gel filtration analyses of cell extracts revealed that all components associate into a complex with an apparent molecular weight of approximately 600 kDa (Kirisako et al., 2006; Tokunaga et al., 2011).

LUBAC stability strongly depends on the prescence of all three sububnits. Loss of a single component results in LUBAC destabilization and functional impairment (Boisson et al., 2015; Boisson et al., 2012; Ikeda et al., 2011; Tokunaga et al., 2011).

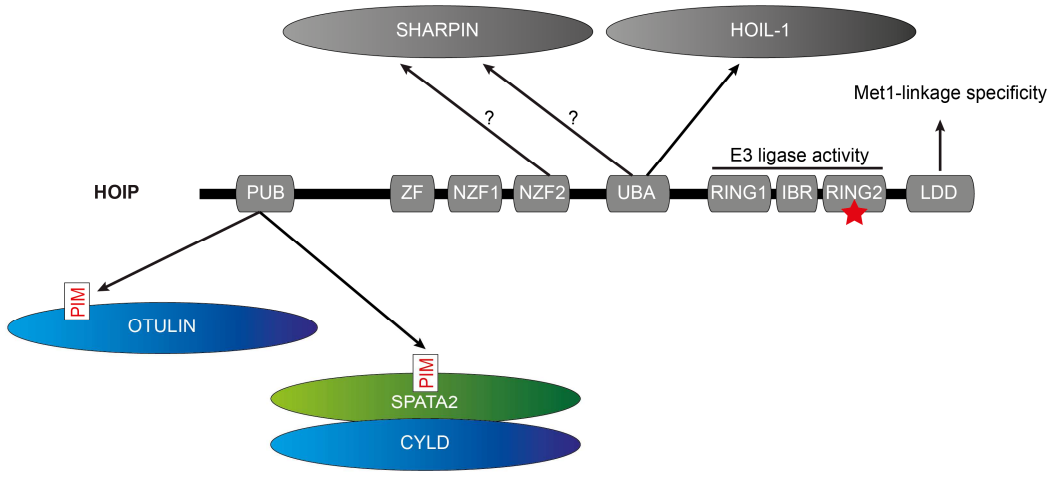

Figure 2-6: HOIP interacts with LUBAC subunits and DUBs.
HOIP, the catalytic subunit of LUBAC, generates Met1-Ub by a RING-HECT hybrid mechanism. Met1-Ub specificity is mediated by the linear Ub chain-determining domain (LDD). HOIP activity requires interaction with the other LUBAC components (HOIL-1 or SHARPIN). Moreover, HOIP interacts with the Met1-Ub cleaving DUBs OTULIN and CYLD via its PUB domain. Whereas OTULIN directly associates with HOIP via a PUB-interacting motif, the HOIP-CYLD interaction is mediated by the bridging factor SPATA2.

HOIP additionally interacts with the DUBs OTULIN and CYLD (Figure 2-6). OTULIN exclusively disassembles linear Ub (Keusekotten et al., 2013), whereas CYLD cleaves both Met1-Ub and K63-Ub (Hrdinka et al., 2016; Komander et al., 2009b; Sato et al., 2015). OTULIN directly binds to the PUB (peptide:N-glycanase/UBA- or UBX-containing proteins) domain of HOIP by means of a PUB-interacting motif (PIM) (Elliott et al., 2014; Schaeffer et al., 2014), CYLD, however, is linked to HOIP via the bridging factor SPATA2 (Spermatogenesis-associated protein 2) (Elliott et al., 2016; Kupka et al., 2016a; Schlicher et al., 2016; Wagner et al., 2016). SPATA2 also carries a PIM and engages the same PIM-binding pocket in HOIP as OTULIN (Elliott et al., 2016). Therefore, OTULIN and SPATA2-CYLD cannot simultaneously form a complex with HOIP, but it remains to be defined whether the two distinct LUBAC-DUB complexes are stably associated or whether they are subjected to a dynamic exchange (Draber et al., 2015; Elliott et al., 2016).

The generation of Met1-Ub by LUBAC facilitates the activation of the transcription factor NF-κB in response to the stimulation of various immune receptors, like TNFR, IL-1R or TLRs (see section 2.1.4) (Ikeda, 2015; Shimizu et al., 2015). Upon stimulation, LUBAC is recruited to pre-assembled receptor-associated signaling complexes (Damgaard et al., 2012; Gerlach et al., 2011; Haas et al., 2009). Accordingly, all LUBAC subunits comprise NZF domains that allow interaction with Met1-Ub and Lys63-Ub (Emmerich et al., 2013; Gerlach et al., 2011; Haas et al., 2009; Ikeda et al., 2011; Sato et al., 2011; Shimizu et al., 2016). The NZF domain of SHARPIN, for example, is required for LUBAC recruitment to the activated TNFR1 complex (Shimizu et al., 2016). Integrated in the receptor-associated signaling complexes, LUBAC decorates signaling mediators, like RIPKs, NEMO, TNFR1, MYD88 and IRAK1/4, with Met1-Ub (Draber et al., 2015; Emmerich et al., 2013; Fiil et al., 2013; Gerlach et al., 2011; Hrdinka et al., 2016; Tokunaga et al., 2009).

The HOIP-associated DUBs OTULIN and CYLD counteract LUBAC-mediated NF-κB activation (Draber et al., 2015; Elliott et al., 2014; Keusekotten et al., 2013; Schaeffer et al., 2014; Takiuchi et al., 2014). When HOIP null MEFs are reconstituted with a HOIP PUB mutant that cannot interact with OTULIN and CYLD, TNF-induced NF-κB activation is enhanced (Takiuchi et al., 2014). Interestingly, LUBAC-associated SPATA2-CYLD is recruited to receptor-associated signaling complexes after stimulation of TNFR1 and NOD2, whereas minimal or no OTULIN is detected in activated signaling complexes (Draber et al., 2015; Elliott et al., 2016; Schlicher et al., 2016; Wagner et al., 2016). Nevertheless, OTULIN was shown to limit ubiquitination of receptor-associated proteins (Fiil et al., 2013; Hrdinka et al., 2016; Keusekotten et al., 2013). Further studies are necessary to elucidate more precisely the role of OTULIN in the activated NF-κB signaling pathway.

LUBAC not only assembles Met1-Ub on substrates but also on itself (Fiil et al., 2013; Hrdinka et al., 2016; Keusekotten et al., 2013). This auto-ubiquitination is controlled by LUBAC-bound OTULIN but not by CYLD (Elliott et al., 2014; Hrdinka et al., 2016). The purpose of LUBAC auto-ubiquitination is not completely clarified, but it was suggested to affect LUBAC activity (Damgaard et al., 2016; Draber et al., 2015; Fiil et al., 2013; Hrdinka et al., 2016). In addition to the role of LUBAC in NF-κB-mediated immune signaling, it is also implicated in cell death regulation (Sasaki and Iwai, 2015; Shimizu et al., 2015).

2.2.2 OTULIN – the only known Met1-specific DUB

In 2013, two groups identified independently the first DUB that exclusively disassembles Met1-Ub: On the one hand by studying mutations in mice that lead to embryonic lethality due to angiogenic abnormalities (Rivkin, 2013), on the other hand by a bioinformatical screen in search of unannotated OTU DUBs (Keusekotten et al., 2013).

Keusekotten et al. found an OTU domain with complete catalytic triad (Cys129, His339, Asn341) in the previously unannotated protein FAM105B and named the protein OTULIN (OTU DUB with linear linkage specificity). OTULIN is composed of 352 aa and the highly conserved OTU domain that was shown to be sufficient for OTULIN´s Met1-linkage specificity spans a large part of the protein (aa 80-352, Figure 2-7A) (Keusekotten et al., 2013). Structural analyses of this domain revealed that substrate-unbound OTULIN exists in an auto-inhibited state, in which the catalytic residues His339 and Cys129 are maintained in an inactive conformation by Asp336 (Keusekotten et al., 2013). MonoUb is unable to induce a conformational change in the inactive catalytic pocket, which makes OTULIN unreactive towards monoUb-based suicide inhibitors such as Ub-AMC (Keusekotten et al., 2013; Rivkin, 2013). The minimal substrate cleaved by OTULIN is Met1-linked diUb. Its binding to OTULIN causes release of the auto-inhibited state and elicits enzymatic activity.

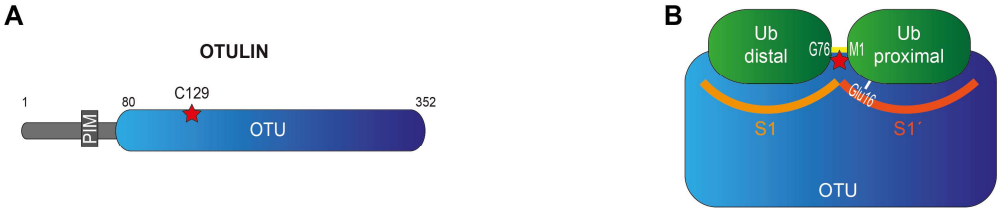

Figure 2-7: OTULIN specifically disassembles Met1-Ub.
A) Schematic representation of OTULIN. OTULIN consists of a flexible N-terminus and a catalytic OTU domain, which is sufficient for both Met1-linkage specificity and cleavage activity. The PUB-interacting motif (PIM) in the N-terminus mediates the interaction with HOIP.
B) Met1-linked proximal Ub is specifically bound by the S1´ binding site in OTULIN. Upon binding, Glu16 of the proximal Ub is inserted into the catalytic pocket, where it co-ordinates the catalytic triad for the cleavage reaction (substrate-assisted catalysis). Asterisk: catalytic center.

OTULIN´s unique specificity for Met1-linked Ub chains can be attributed to two molecular circumstances (Keusekotten et al., 2013): On the one hand, OTULIN has a very selective Met1-Ub binding site. Besides the common interaction between the S1 site and the distal Ub, the S1´ site of OTULIN orients the proximal Ub in such a way that the peptide bond points towards the catalytic center (Figure 2-7B). Even structurally similar Lys63-Ub would not fit properly into the S1´ binding site, which explains the 100-fold lower affinity of OTULIN towards Lys63-Ub. Moreover, OTULIN is not able to hydrolyze Lys63-Ub since the isopeptide bond is shielded from the catalytic center by a dedicated binding pocket. On the other hand, Met1-specificity of OTULIN can be attributed to a cleavage mechanism referred to as substrate-assisted catalysis (Keusekotten et al., 2013). The specific attachment of Met1-Ub leads to the insertion of the proximal Ub residue Glu16 into the catalytic pocket, where it rearranges the catalytic residues and hence enables the own cleavage (Figure 2-7B).

Gumby mice carrying a homozygous mutation (*Gum*^{W96R} or *Gum*^{D336E}) die during embryonic development between E12.5 and E14 due to defects in angiogenesis. The W96R mutation is located in the S1´ site of Otulin/gumby and drastically reduces affinity of Otulin towards Met1-Ub. Thus, the enzymatic activity is functionally impaired, leading to increased Met1-Ub steady-state levels in gumby mice (Rivkin, 2013). Also samples from patients carrying a homozygous mutation in *OTULIN* that compromises OTULIN stability and activity showed strong accumulation of linear Ub chains (Damgaard et al., 2016; Zhou et al., 2016), emphasizing that OTULIN is crucial for the homeostatic control of cellular Met1-Ub levels. Interestingly, depletion of CYLD which also cleaves linear Ub chains does not have an impact on basal Met1-Ub levels (Draber et al., 2015).

Moreover, OTULIN counteracts LUBAC-mediated linear ubiquitination of immune receptor-associated proteins and auto-ubiquitination of LUBAC (Fiil et al., 2013; Hrdinka et al., 2016; Keusekotten et al., 2013). OTULIN was shown to directly interact with the E3 ligase HOIP (Elliott et al., 2014; Schaeffer et al., 2014). A highly conserved peptide sequence of five amino acids (Asp54-Met55-Tyr56-Arg57-Ala58) in the OTULIN N-terminus mediates the interaction with the HOIP PUB domain, with Met55 and Tyr56 being the key residues (Figure 2-7A) (Elliott et al., 2014). Other PUB domains, as they are found in PNGase or UBXD1, are not bound by this PIM of OTULIN. Phosphorylation of Tyr56 prevents the OTULIN-HOIP association and thus might represent a regulatory mechanism for the interaction in cells (Elliott et al., 2014; Schaeffer et al., 2014).

OTULIN depletion in immune cells has cell type-specific consequences: In T and B cells, LUBAC is degraded leading to massive impairment of Met1-Ub signaling. In contrast,

Met1-Ub accumulates in myeloid cells resulting in constitutive NF-κB activation and overproduction of inflammatory cytokines (Damgaard et al., 2016), resembling the autoimmune disease termed ORAS (OTULIN-related autoinflammatory syndrome) from patients with hypomorphic mutations in the *OTULIN* gene (Damgaard et al., 2016; Zhou et al., 2016). Consistent with a critical requirement for OTULIN catalytic activity, adult OTULIN C129A mutant mice exhibit auto-inflammation, which relies on aberrant induction of cell death (Heger et al., 2018).

Since the aberrant angiogenesis in gumby mice results from defective Wnt signaling, OTULIN has also been associated with canonical Wnt signaling during embryonic development (Rivkin, 2013), besides its regulatory function in signaling pathways of the immune system. In line with this, Wnt reporter assays revealed that the generation of Met1-Ub by LUBAC suppresses Wnt signaling, and OTULIN counteracts this suppression (Rivkin, 2013; Takiuchi et al., 2014). Moreover, an interaction between the OTULIN N-terminus and the protein DVL2, which is involved in Wnt signaling, was identified (Rivkin, 2013). Importantly, so far all functions of OTULIN have been attributed to its role in Ub homeostasis by catalyzing deconjugation of Met1-linked Ub chains and LUBAC binding.

2.3 Activity-based probes

Activity-based probes (ABPs) are powerful tools to study enzyme activities and functions. They are composed of a reactive group, also referred to as a warhead, which is fused to a detection marker (Cravatt et al., 2008). In most cases the reactive group is an electrophile. In a nucleophilic attack by an active enzyme, the electrophilic warhead becomes covalently linked to the active site (Figure 2-8). In consequence of covalently modifying the active site, enzymes get irreversibly inhibited (Cravatt et al., 2008). The detection marker, for example a fluorophore or an affinity tag, is needed to detect the enzyme-coupled probe in subsequent experimental steps. ABPs often target large groups of enzymes that display similar catalytic features, like serine hydrolases, cysteine proteases or kinases.

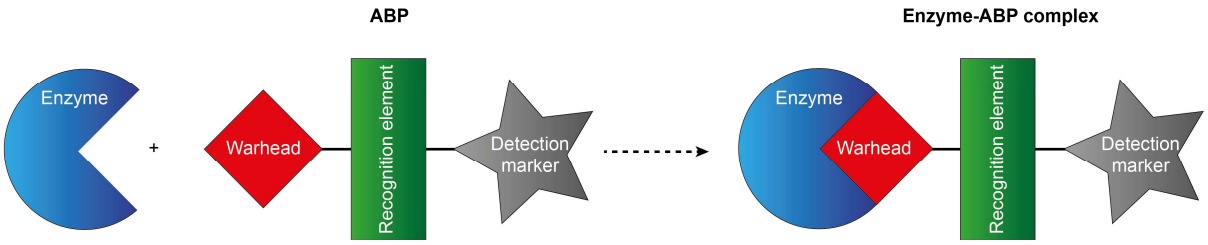

Figure 2-8: Schematic representation of an ABP.
By a nucleophilic enzymatic attack, the electrophilic warhead becomes covalently coupled to the active site of the enzyme. Recognition elements increase target specificity of the probes. Detection markers such as affinity tags or fluorophors enable the detection of enzyme-ABP complexes in subsequent assays.

This enables acquisition of the functional state of the proteome in physiological and pathophysiological settings, a process that is called activity-based protein profiling (Cravatt et al., 2008). In order to reduce promiscuity and enhance target specificity, ABPs often additionally carry a recognition element that is based on the respective enzyme substrate (Figure 2-8) (Ovaa, 2007).

2.3.1 ABPs for deubiquitinating enzymes

The first ABPs for detecting DUB activities consisted of a Ub molecule as recognition element, which is C-terminally fused to an electrophilic group such as vinyl methyl ester (VME) or propargylamide (PA) (Figure 2-9A) (Borodovsky et al., 2002; de Jong et al., 2012). These commonly called suicide probes are attacked by the nucleophilic active site Cys that exists in most DUBs, generating a covalent bond between the probe and the enzyme. MonoUb-based ABPs like Ub-PA or Ub-VME promiscuously label DUBs from different DUB families (Borodovsky et al., 2002; Ekkebus et al., 2013). On the basis of this characteristic, such probes have been successfully used to analyze DUB activities in cell extracts (activity profiling) and to determine efficiency and specificity of DUB inhibitors (Altun et al., 2011). Moreover, the use of ABPs led to the identification of new DUBs (Borodovsky et al., 2002). For many DUBs it is still not known, in which cellular processes they are implicated. In this case, ABPs will help to identify new functions of deubiquitinating enzymes.

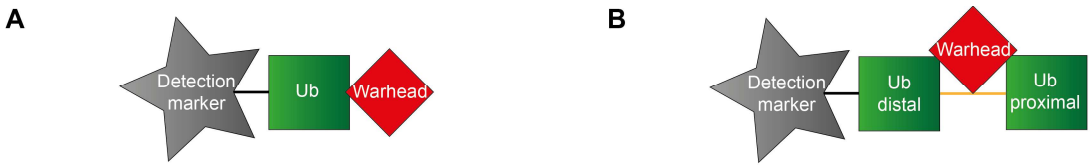

Figure 2-9: Schematic respresentation of monoUb-based and linkage-specific diUb-based ABPs for DUBs.
A) In monoUb-based suicide probes, the recognition element Ub is C-terminally fused to an electrophilic warhead.
B) DiUb-based ABPs are used to profile linkage specificity of DUBs. The electrophilic warhead is positioned next to the scissile bond (yellow) between distal and proximal Ub.

To profile Ub chain linkage specificity of DUBs, ABPs have been generated that are based on linkage-specific diUbs. In these probes, the electrophilic warhead is mostly positioned between the two Ub moieties, where the DUB attack takes place (Figure 2-9B) (Li et al., 2014; McGouran et al., 2013; Mulder et al., 2014). The challenge in designing a diUb-based ABP is that the introduced warhead has to mimic the linkage of the Ub molecules as accurately as possible. Only in this way, the ABP structurally resembles native diUb. Mulder et al. took advantage of the non-enzymatic native chemical ligation technique to generate diUb ABPs that are based on all seven Lys-linked diUbs (Mulder et al., 2014) and structurally closely resemble the native isopeptide-linked diUbs. However, this strategy was not applicable to the generation of Met1-linked diUb-based probes since the peptide bond

between two linearly connected Ub molecules contrasts strongly with an isopeptide bond regarding structure and chemical nature (see Figure 2-5). The insertion of an appropriate electrophile mimicking the Gly-Met environment of a linear diUb linkage has caused difficulties to date. McGouran et al. generated a probe based on Met1-diUb (McGouran et al., 2013), which labeled many USPs that usually cleave linear Ub chains only with low efficiency (Faesen et al., 2011; Komander et al., 2009b). More importantly, the Met1-specific DUB OTULIN was not labeled with this probe (McGouran et al., 2013). In this context, one should mention again that OTULIN does not react with common monoUb-based suicide inhibitors, since the substrate-assisted Ub chain hydrolysis relies on a native Met1-linked diUb as substrate (Keusekotten et al., 2013; Mevissen et al., 2013). The low specificity of the probe was attributed to the greater flexibility of the introduced electrophile and the loss of the Met1 side chain (McGouran et al., 2013).

In another attempt to generate an ABP based on linear diUb, Met1 in the proximal Ub moiety was replaced by the electrophilic non-canonical amino acid dehydroalanine (Dha) (Haj-Yahya et al., 2014). Dha is a small warhead that is easily generated by conversion of Cys through oxidative elimination (Bernardes et al., 2008). However, instead of becoming covalently attached to the active site of OTULIN, the probe was cleaved by OTULIN and by USP2 as well (Haj-Yahya et al., 2014). To date, no DUB ABP has been generated that closely resembles native Met1-linked diUb and labels Met1-specific active OTULIN. In addition, all DUB ABPs generated so far target a broad range of DUBs and do not exhibit specificity towards one particular enzyme.

2.4 Endosomal sorting by the retromer complex

The endosomal network is an essential traffic system for proteins. As a result of endocytosis, the cellular plasma membrane is constantly engulfed and forms intracellular membrane-coated early endosomes. Along with the plasma membrane, transmembrane proteins such as nutrient transporters, ion channels or surface receptors are also internalized. These proteins, referred to as cargos, are sorted and can take different routes through the cell: Either they are directly transported back to the plasma membrane for reuse (‘recycling’) (Hsu et al., 2012) or they migrate to the trans-Golgi network (TGN) by retrograde transport (Figure 2-10) (Johannes and Wunder, 2011). Remaining in the endosome, cargos undergo the process of endosomal maturation and are finally degraded in the lysosome. Proper functioning of endosomal sorting is crucial for the maintenance of cellular homeostasis. It must be ensured that essential membrane proteins are excluded from lysosomal degradation (Burd and Cullen, 2014).

In eukaryotes, an important mediator of this sorting process is the retromer complex, which is assembled on endosomes. The mammalian retromer is a heterotrimeric protein complex composed of the vacuolar protein sorting-associated proteins (VPS)26, VPS29 and VPS35 (Gallon and Cullen, 2015). Composed of 796 amino acids, VPS35 is the largest retromer subunit that interacts via its C-terminus with VPS29 and via its N-terminus with VPS26 (Norwood et al., 2011). Three paralogous genes for VPS26 exist in mammals: *VPS26A*, *VPS26B* and Down´s syndrome critical region 3 (*DSCR3*) (Kerr et al., 2005; Koumandou et al., 2011). VPS26A and VPS26B display 69% amino acid sequence identity and 82% similarity and adopt very similar arrestin-fold structures (Kerr et al., 2005). They form two distinct retromer complexes with VPS35 and VPS29 as both utilize the same binding site in VPS35 and cannot bind simultaneously (Collins et al., 2008; Gallon and Cullen, 2015). To date, it is unclear whether DSCR3 contributes to retromer function.

The retromer regulates export of cargos from the endosomes to the TGN or to the plasma membrane (Gallon and Cullen, 2015). It forms functionally distinct complexes with different family members of the sorting nexins (SNXs). The specific complex composition determines which cargo is transported and where it is transported to (Figure 2-10).

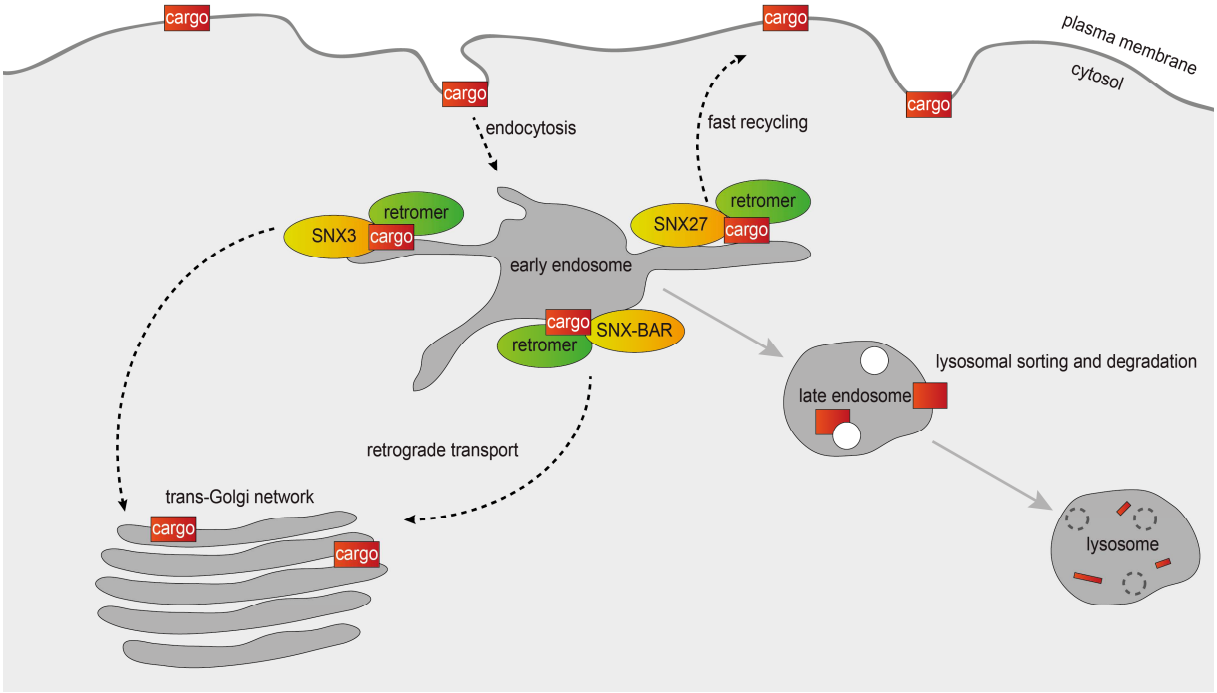

Figure 2-10: Retromer-mediated endosomal sorting of cargos.
Endocytosis leads to the internalization of plasma membrane proteins (cargos) into early endosomes. Distinct SNX-retromer complexes then mediate cargo export from the endosomes to the plasma membrane or to the TGN to prevent lysosomal degradation.

In mammals, 33 SNX proteins (Cullen, 2008) have been identified to date, six of which (SNX1, SNX2, SNX3, SNX5, SNX6 and SNX27) interact with the retromer complex (Gallon and Cullen, 2015; Lucas and Hierro, 2017). All SNX proteins have a characteristic Phox

homology (PX) domain that preferentially binds phosphatidylinositol 3-phosphate (PI(3)P) membrane lipids. Therefore, most SNXs are recruited to PI(3)P-rich early endosomes (Teasdale and Collins, 2012).

As the retromer itself is not able to directly bind membranes, association with SNX proteins facilitates its recruitment to endosomes (Gallon and Cullen, 2015). For instance, SNX3 can recruit the retromer by interacting with VPS26. This SNX3-retromer complex formation enables recognition and binding of the divalent cation transporter DMT1-II at the SNX3-VPS26 interface and its transport to the TGN (Figure 2-10) (Lucas et al., 2016). SNX1, SNX2, SNX5 and SNX6 carry a Bin/Amphiphysin/Rvs (BAR) domain in addition to the PX domain (van Weering et al., 2010). BAR domains form hetero- or homo-dimers that adopt concave structures enabling sensing and binding of curved membranes (Gallon and Cullen, 2015). It has been proposed that higher-order helical arrays of SNX-BAR proteins might also trigger and stabilize membrane tubules to generate carrier structures for cargos (Frost et al., 2008; Gallon and Cullen, 2015; Lucas and Hierro, 2017; van Weering et al., 2012). The SNX-BAR-retromer complex also mediates the retrograde transport of cargos to the TGN (Gallon and Cullen, 2015).

The SNX27-retromer, however, transports cargos such as the β2-adrenergic receptor (β2-AR) or the glucose transporter GLUT1 from the early endosomes to the plasma membrane (Figure 2-10) (Lauffer et al., 2010; Steinberg et al., 2013). Recognition of cargos is achieved by sorting signals. In the case of transmembrane proteins sequence motifs are present in the cytoplasmic tail and are bound by adaptor proteins. Both the retromer and retromer-associated SNXs can function as adaptors (Gallon and Cullen, 2015).

Proper sorting of cargos not only relies on appropriate functioning of SNX-retromer complexes, but also on the dynamic formation of actin polymers on the endosomal membrane. Actin patches control endosomal biogenesis and maturation, regulate endosomal morphology and motility and stabilize endosomal subdomains, providing a scaffold for cargo sorting at the endosomes (Simonetti and Cullen, 2018). Inhibition of actin polymerization by drugs leads to defects in cargo segregation and in endosomal maturation (Ohashi et al., 2011). The Wiskott-Aldrich syndrome protein and SCAR homologue (WASH) complex is composed of the five proteins WASH1, strumpellin, SWIP, FAM21 and coiled-coil domain containing protein 53 (CCDC53) and promotes the nucleation of filamentous actin by the actin-related protein 2/3 (Arp2/3) complex at the endosomes (Derivery et al., 2009; Seaman et al., 2013). The interaction of FAM21 with the retromer complex and with SNX27, respectively, links the actin nucleation-promoting activity of the WASH complex to the targeted sorting process of cargos (Jia et al., 2012; Lee et al., 2016).

2.4.1 SNX27-dependent endosome-to-plasma trafficking

Like all other SNX proteins, SNX27 also has a PX domain, which recruits SNX27 to early endosomes (Figure 2-11A) (Cai et al., 2011; Lauffer et al., 2010; Rincon et al., 2007). Additionally, SNX27 has a less well-characterized C-terminal FERM (4.1, ezrin, radixin, moesin)-like domain, which interacts with the SNX-BAR protein SNX1 and with the WASH complex, and comprises another lipid-binding site that preferentially binds bi- and tri-phosphorylated phosphatidylinositol lipids (Ghai et al., 2015; Lee et al., 2016; Steinberg et al., 2013). Among the SNX proteins, SNX27 is the only member that also bears a unique post-synaptic density 95/discs large/zonula occludens (PDZ) domain (Figure 2-11A) (Gallon et al., 2014). PDZ domains commonly mediate protein-protein interactions by binding to C-terminal peptide sequences, the so-called PDZ-binding motifs (PDZbms) in the binding partner (Doyle et al., 1996). In line with this, the SNX27 PDZ domain binds C-terminal PDZbms with the class I consensus sequence X-[Thr/Ser]-X-Φ, where X is any and Φ a bulky amino acid (Gallon and Cullen, 2015; Hung and Sheng, 2002; Lunn et al., 2007). Such PDZbms are found in transmembrane proteins such as GLUT1 (Steinberg et al., 2013) or β2-AR (Lauffer et al., 2010) that are recycled by the SNX27-retromer complex. These sorting signals are recognized and bound by SNX27 and transported from the endosomes to the plasma membrane in association with the retromer complex (Cullen and Korswagen, 2011; Gallon and Cullen, 2015; Temkin et al., 2011).

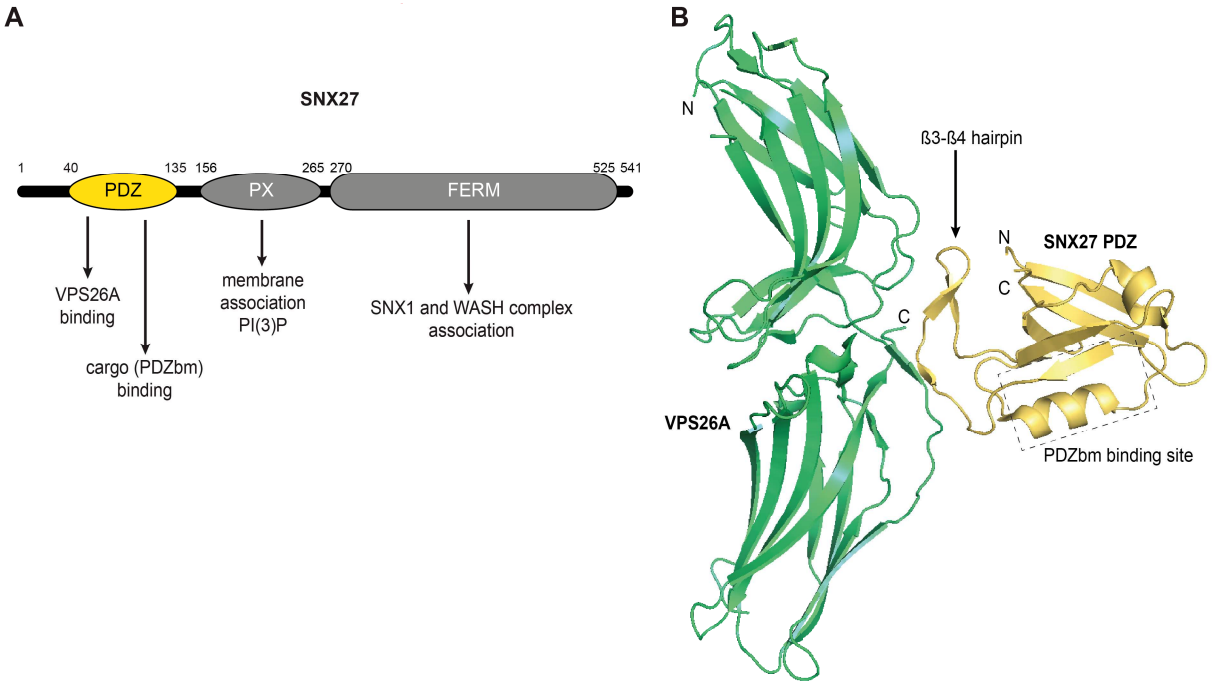

Figure 2-11: The PDZ domain of SNX27 interacts with VPS26A and PDZbm-containing cargos.
A) Schematic representation of SNX27. The PDZ domain that interacts with both VPS26A and PDZbm-containing cargos is highlighted in yellow.
B) Crystal structure of the rat SNX27 PDZ domain (yellow) bound to mouse VPS26A (green) depicted as ribbon (PDB ID: 4P2A) (Gallon et al., 2014). The putative PDZbm binding pocket and the β3-β4 loop that interacts with VPS26A are highlighted.

Besides transmembrane proteins, cytoplasmic proteins with PDZbms like diacylglycerol kinase ζ (DGKζ) (Rincon et al., 2007) or β-PIX (Valdes et al., 2011) can also bind to the SNX27 PDZ domain.

Structural analysis of the SNX27 PDZ domain revealed that it corresponds to the core structure of other PDZ domains with the exception that it contains an additional β-hairpin loop (β3-β4 loop) that protrudes from this core structure (Balana et al., 2011; Gallon et al., 2014). This β3-β4 loop directly binds to both paralogs of the retromer component VPS26 and allows simultaneous binding of cargos in the spatially divided PDZbm binding pocket (Figure 2-11B) (Gallon et al., 2014). Taken together, the SNX27 PDZ domain mediates the binding of cargos as well as the retromer association, enabling rapid endosome-to-plasma membrane transport. Proteomic analyses revealed that the surface expression of more than 100 cargos depends on both SNX27 and retromer (Steinberg et al., 2013). Through the additional interaction of the FERM domain with the WASH complex and SNX1, SNX27 brings components of the endosomal trafficking machinery closely together and thus regulates fast cargo recycling to the plasma membrane (Lee et al., 2016; Steinberg et al., 2013).
The particular importance of SNX27 and retromer in neurons is recognizable by numerous neuropathologies like Parkinson´s disease, Alzheimer´s disease, Down syndrome and infantile epilepsy caused by mutations or altered expression patterns (Li et al., 2016). SNX27 knockout (KO) mice die either in utero or within three weeks after birth. Born mice are small, fail to thrive and display neuronal deficits in the brain (Cai et al., 2011; Wang et al., 2013). Moreover, SNX27 deficiency in mice leads to synaptic dysfunction, memory and learning deficits and to a reduction in surface levels of NMDA (N-methyl-D-aspartate) and AMPA (α-amino-3-hydroxy-5-methyl-4-isoxazolepropionic acid) receptors (Loo et al., 2014; Wang et al., 2013). Finally, it was shown that endosomal SNX27 is recruited to the immunological synapse in activated T cells and tumor-engaged natural killer cells but its role at the immunological synapse has not been well defined (Ghai et al., 2015; MacNeil and Pohajdak, 2007; Rincon et al., 2011). So far, it is unclear, whether all SNX27 functions are connected to cargo sorting.

3. Aims of the study

OTULIN is the only known DUB that exclusively cleaves Met1-linked Ub chains. Due to its hydrolase activity, it is of central importance for the homeostatic control of Met1-Ub levels. Besides its role as homeostatic factor, OTULIN has been associated with signaling pathways, which are regulated by linear Ub chains, such as NF-κB or cell death signaling.
While the molecular basis for the specific cleavage of Met1-Ub by OTULIN has been clarified, it remains unclear, how much of the endogenous OTULIN is active, and whether catalytic activity of OTULIN is affected by various stimuli. Additionally, only the interaction with HOIP and LUBAC has been described in detail to date, and it is not known if OTULIN binds to other proteins and controls other cellular pathways.

Therefore, the main aim of this study was to better characterize the DUB OTULIN with regard to its cellular activity and its cellular functions. To this end, a diUb-based active site-directed probe was chemically synthesized, which covalently labels OTULIN (OTULIN ABP). Initially, reactivity of OTULIN towards the new probe was validated using recombinant OTULIN in direct DUB assays and structural analyses as well as with endogenous OTULIN in cellular extracts. To enrich OTULIN and other ABP-binding proteins from cell extracts, the ABP was equipped with an affinity tag. By OTULIN ABP pull-downs from cell extracts and their subsequent mass spectrometric analysis, the selectivity of the OTULIN-directed ABP was analyzed. The very few cross-reactions were abolished by a small change in the probe design, yielding a specific OTULIN ABP.

In the second part, the newly developed and well-characterized tool was used to search for OTULIN interactors. By mass spectrometric analysis of OTULIN ABP pull-downs, we identified SNX27 as a new interaction partner of OTULIN. Cellular interaction was verified by co-immunoprecipitations, confocal microscopy and analytical gel filtration analysis. Moreover, structural, biophysical and cellular analyses were performed in order to specify the mechanism of this interaction. The final aim of this study was to investigate the function of the OTULIN-SNX27 interaction and thus to describe a potential novel role of OTULIN in the cell.

4. Results

4.1 A linear diubiquitin-based ABP for efficient and selective detection of OTULIN

To develop an experimental tool to function as OTULIN ABP, the following criteria needed to be met: (i) the ABP should be based on Met1-linked diUb since this corresponds to the minimal native OTULIN substrate (Keusekotten et al., 2013) and, (ii) the amino acid dehydroalanine (Dha) should be positioned near the scissile bond between the two Ub molecules as a small electrophilic warhead. The probe was designed and chemically synthesized by our collaboration partner Farid El Oualid (UbiQ, The Netherlands). He generated an N-terminally biotin-labeled Met1-diUb, in which the Gly76 of the distal Ub was substituted with Dha (bio-Ub^{G76Dha}-Ub**,** Figure 4-1). Introducing the small electrophile at this site prevents alterations (in terms of structure and flexibility) in the peptide bond environment between the two linearly linked Ub molecules. In order to facilitate efficient access to the biotin tag, an aminohexanoic (Ahx) linker was inserted between the tag and the N-terminus of Ub, generating some extra space (de Jong et al., 2012).

Figure 4-1: Bio-Ub^{G76Dha}-Ub closely resembles native Met1-diUb.
Schematic of Met1-diUb in comparison with the active site-directed probe, bio-Ub^{G76Dha}-Ub (OTULIN ABP). The peptide bond linking the two Ub molecules is depicted in yellow, while the electrophilic Dha residue is displayed in red.

The detailed protocol for the total chemical synthesis of bio-Ub^{G76Dha}-Ub is published in (Weber et al., 2017). Here, the synthesis is described only briefly: First, the two basic modules, bio-Ahx-labeled Ub1-75 and Cys-Ub, were produced by means of Fmoc (fluorenylmethoxycarbonyl)-based solid-phase peptide synthesis. Following fusion of the distal and proximal Ub moieties by native chemical ligation, the Cys residue was finally converted into Dha by oxidative elimination (Bernardes et al., 2008).

4.1.1 Recombinant OTULIN is labeled by bio-Ub^{G76Dha}-Ub (OTULIN ABP)

To test the reactivity of OTULIN toward the newly developed probe, the recombinantly produced catalytic OTU domain of OTULIN (OTULIN$_{cat}$, aa 80-352) was incubated with bio-Ub^{G76Dha}-Ub. The probe formed a covalent adduct with OTULIN$_{cat}$, which can be observed

from a molecular weight (MW) shift in OTULIN by SDS-PAGE and Coomassie staining (Figure 4-2A, asterisk). The increase in MW corresponds to the MW of a diUb (~17 kDa). The catalytically inactive OTULIN mutant (C129A) did not react with the probe. Since catalytic activity is required for covalent probe attachment, bio-Ub^{G76Dha}-Ub represents the first described OTULIN ABP. A point mutation in the S1´ binding site of OTULIN$_{cat}$ (W96A), previously shown to drastically diminish Met1-diUb affinity (Keusekotten et al., 2013), also prevented covalent adduct formation (Figure 4-2A).

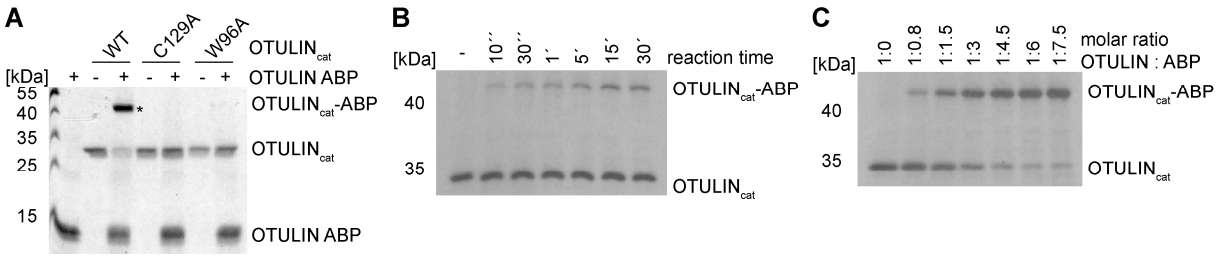

Figure 4-2: Recombinant OTULIN$_{cat}$ is labeled by the OTULIN ABP.
A) Recombinant OTULIN$_{cat}$ (1 µg) was incubated with 4 µg bio-Ub^{G76Dha}-Ub (2 hrs, 37°C). OTULIN-ABP complex formation was assessed by SDS-PAGE and Coomassie staining. Asterisk: OTULIN-ABP complex.
B) 250 ng OTULIN$_{cat}$ was incubated at 30°C in a 1:1 molar ratio with OTULIN ABP. OTULIN-ABP complex formation was monitored by Silver Staining after SDS-PAGE.
C) 250 ng OTULIN$_{cat}$ was incubated with increasing OTULIN ABP concentrations for 15 min at 30°C. OTULIN-ABP complex formation was monitored by Silver Staining after SDS-PAGE.

To monitor kinetics of the OTULIN-ABP complex formation, OTULIN$_{cat}$ was incubated with OTULIN ABP at 30°C and equimolar concentrations. Adduct formation was detected after 10 seconds, but within 30 minutes the educts were not completely converted (Figure 4-2B). Approximately 5-fold molar excess of ABP was required for almost complete labeling of OTULIN$_{cat}$ within 15 minutes (Figure 4-2C).

As expected for an ABP that covalently and irreversibly labels the active site of an enzyme, the probe inhibited Met1-tetraUb cleavage by OTULIN$_{cat}$ in a dose-dependent manner (Figure 4-3A).

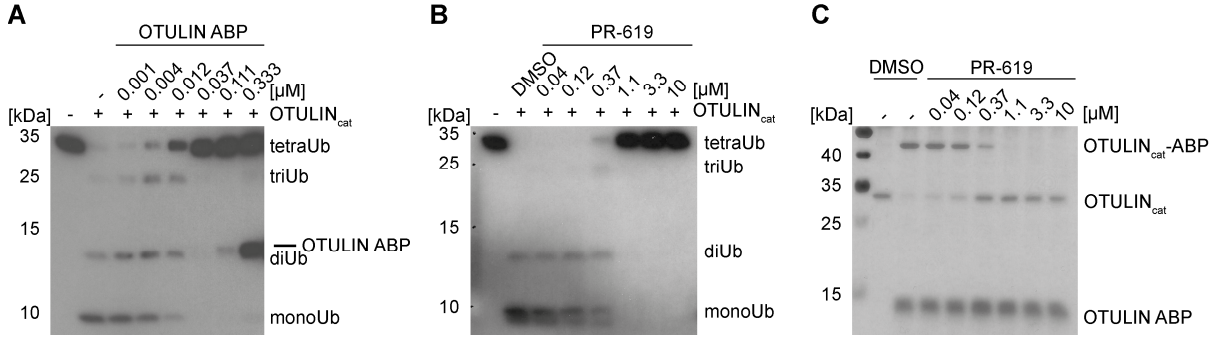

Figure 4-3: OTULIN is inhibited by covalent attachment of the ABP.
A) A TetraUb cleavage assay was performed after pre-treatment of OTULIN with increasing ABP concentrations. TetraUb chain cleavage was analyzed by Western Blot (WB) using anti-Ub antibody.
B) A TetraUb cleavage assay was performed after pre-treatment of OTULIN with increasing PR-619 concentrations. TetraUb chain cleavage was assessed by WB using anti-Ub antibody.
C) Following pre-treatment with increasing PR-619 concentrations, OTULIN$_{cat}$ (500 ng) was incubated with 2 µg OTULIN ABP (5 min, 30°C). OTULIN-ABP complex formation was monitored by Silver staining.

Under these *in vitro* conditions, the ABP blocked OTULIN activity and tetraUb cleavage in a concentration range from 12 to 37 nM. To confirm that our probe only labels active OTULIN, we made use of the small-molecule inhibitor PR-619, which inhibits a broad range of DUBs (Altun et al., 2011). PR-619 dose-dependently inhibited Met1-tetraUb cleavage by OTULIN (Figure 4-3B) and prevented OTULIN-ABP complex formation (Figure 4-3C). PR-619 concentrations between 370 nM and 1.1 µM rendered OTULIN inactive towards both tetraUb chains and OTULIN ABP. Altogether these data demonstrate that the OTULIN ABP efficiently labels the active site of recombinant $OTULIN_{cat}$.

4.1.2 Structural analysis of the OTULIN-ABP complex

To better characterize the OTULIN-ABP interaction, the complex was crystallized and analyzed by X-ray crystallography by our collaboration partner Paul Elliott (MRC, Cambridge; University of Oxford). The detailed analysis is published in (Weber et al., 2017). The OTULIN-ABP complex structure (PDB ID: 5OE7) was determined at 3 Å resolution (Figure 4-4A) and is nearly indistinguishable from the published OTULIN C129A-Met1-diUb complex structure (PDB: 3ZNZ) (Keusekotten et al., 2013). The distal and proximal Ub moieties are arranged identically on the $OTULIN_{cat}$ surface (Figure 4-4B). Further, the OTULIN active site adopts a similar conformation (Figure 4-4C). The structural analysis confirmed that the active site-directed probe reacts with OTULIN as expected. The electron density in the well-ordered active site enabled complete building of the thioether bond formed by the reaction between the Dha and catalytic Cys129 of OTULIN (Figure 4-4C, left). The inserted proximal Glu16 of the probe reveals that the ABP enables OTULIN to react with the ABP through substrate-assisted catalysis.

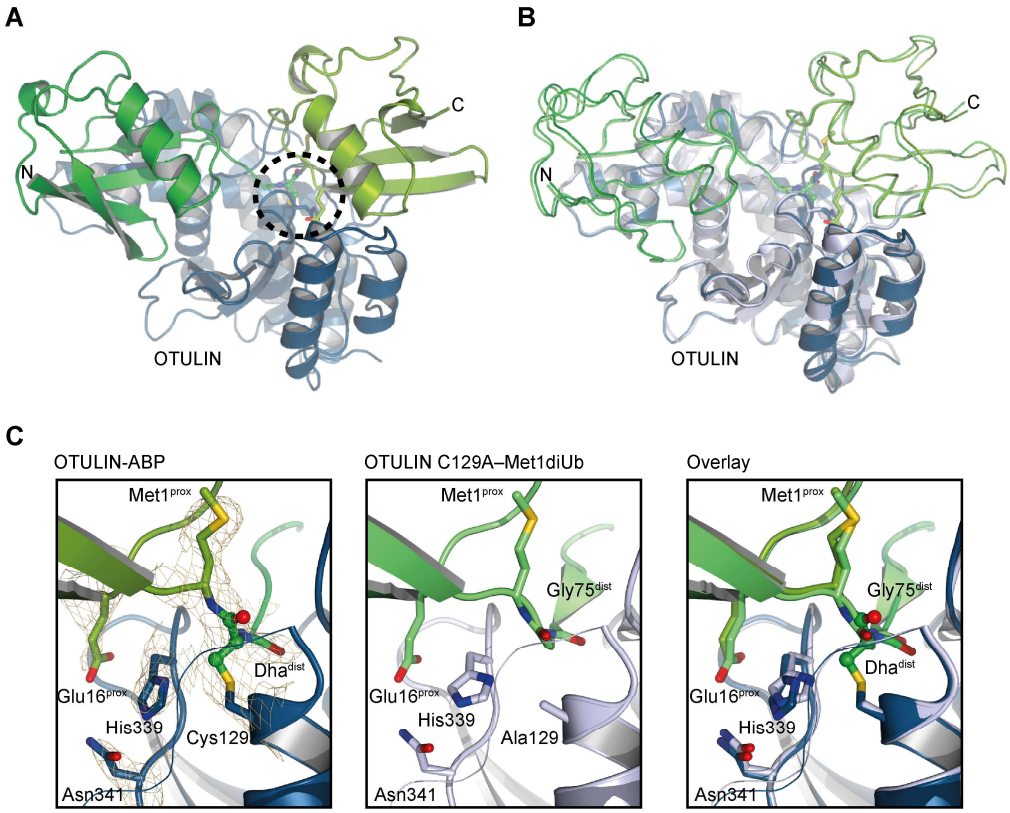

Figure 4-4: Structural analysis of the OTULIN-ABP complex.
A) Structure of the OTULIN-ABP complex is depicted as ribbon. $OTULIN_{cat}$ (aa 80–352) is shown in blue with the distal and proximal Ub moieties of the OTULIN ABP colored in dark and light green, respectively. Circle: catalytic triad of OTULIN. (PDB ID: 5OE7) (Weber et al., 2017)
B) Superimposition of the OTULIN-ABP complex structure (dark blue) and the OTULIN C129A-Met1-diUb complex structure (OTULIN C129A – grey; PDB ID: 3ZNZ) (Keusekotten et al., 2013).
C) Close-up views of the OTULIN active site bound to OTULIN ABP (left) or bound to Met1-diUb (C129A, middle) and overlay of both structures highlighting the identical arrangement of the catalytic triad. Relevant residues are shown in stick format.
A-C) Illustrations provided by P. Elliott (MRC, Cambridge; University of Oxford) (Weber et al., 2017).

4.1.3 Selectivity analysis of the OTULIN ABP towards recombinant DUBs

To acquire a first impression of the OTULIN ABP selectivity, the probe was incubated with recombinant DUBs from different families (Figure 4-5A). Although the OTU domains of OTULIN and OTUB1 structurally closely resemble each other (Keusekotten et al., 2013), Lys48-specific OTUB1 did not react with the probe, to a similar extent as A20, another OTU DUB, and UCHL1 and UCHL3 from the UCH DUB family. The Ub-specific proteases USP2, USP7 and USP8 also did not form a covalent adduct with the ABP, although many USPs cleave a broad range of Ub chains (Komander et al., 2009a; Ritorto et al., 2014). In contrast, a small proportion of USP5 (IsoT) was covalently labeled by the OTULIN ABP, evident from a MW shift in SDS-PAGE (Figure 4-5A, asterisks).

In parallel, the DUBs were either incubated with the suicide inhibitor Ub-PA or with Lys48-linked diUb to ensure that all DUBs are active and that an inability to react with the ABP cannot be attributed to a lack of DUB activity.

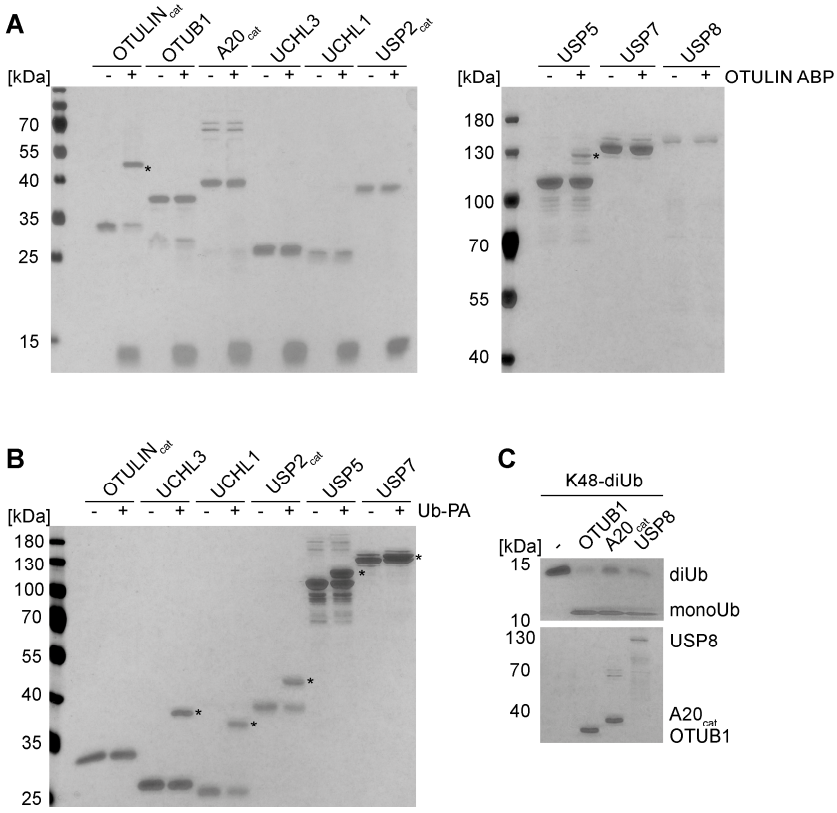

Figure 4-5: OTULIN ABP selectively labels recombinant OTULIN and USP5.
A) Recombinant DUBs (0.5 - 1 µM) were incubated with 3 µM OTULIN ABP (1 h, 30°C). Covalent adduct formation was assessed by Silver staining. Asterisks: DUB-ABP adducts.
B) Recombinant DUBs (0.5 µM) were incubated with 5 µM Ub-PA (1 h, 30°C). Covalent adduct formation was determined by Silver staining. Asterisks: DUB-Ub adducts.
C) OTUB1, $A20_{cat}$ and USP8 (0.5 µM) were incubated with 500 ng Lys48-linked diUb (1 h, 30°C). DiUb cleavage was examined by Silver staining.

Beside OTULIN that fails to react with Ub-PA, because it requires an entire diUb substrate (Keusekotten et al., 2013; Mevissen et al., 2013), all tested DUBs formed Ub adducts with the suicide inhibitor and consequently were active (Figure 4-5B). Lys48-diUb was hydrolyzed by OTUB1, A20 and USP8, proving their catalytic activity (Figure 4-5C).

Since OTULIN and USP5 can hydrolyze Met1-Ub, two additional Met1-Ub cleaving USP DUBs, USP21 and CYLD (Komander et al., 2009b; Sato et al., 2015; Ye et al., 2011), were assessed for their reactivity toward the OTULIN ABP (Figure 4-6A). Neither $USP21_{cat}$ nor CYLD reacted with the probe, even though they were proven to be active by means of Ub-PA (Figure 4-6B). Especially for CYLD, which preferentially cleaves Met1- and Lys63-Ub, this finding was unexpected. For both OTULIN and CYLD, it has been shown that they fail to hydrolyze Ub chains with G76S mutations (Keusekotten et al., 2013; Komander et al., 2008). Still, OTULIN reacts with the ABP, approving the G76Dha substitution, whereas CYLD does not do so. Referring to our ABP design, we wanted to determine whether the G76A mutation in the distal Ub (His-Ub^{G76A}-Ub) would be tolerated.

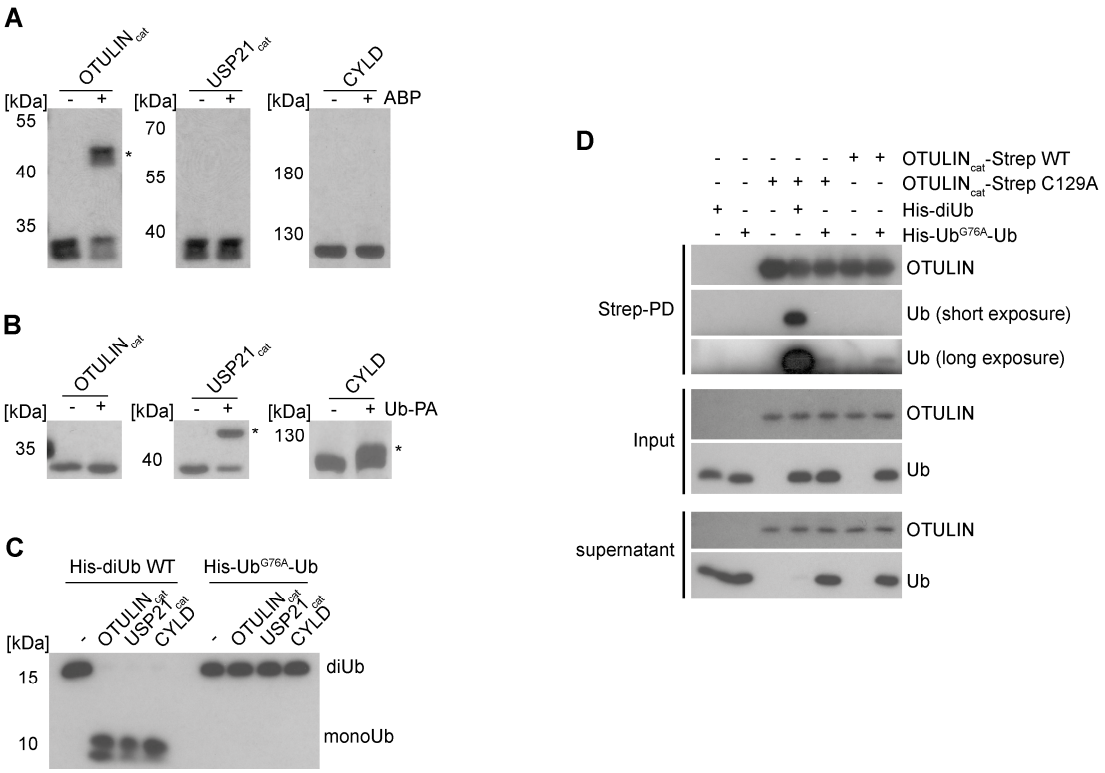

Figure 4-6: The Met1-Ub cleaving DUBs USP21 and CYLD do not react with OTULIN ABP.
A) Recombinant DUBs (0.5 - 1 µM) were incubated with 3 µM OTULIN ABP (1 h, 30°C). Covalent adduct formation was assessed by Silver staining. Asterisk: DUB-ABP adduct.
B) Recombinant DUBs (0.5 µM) were incubated with 5 µM Ub-PA (1 h, 30°C). Covalent adduct formation was determined by Silver staining. Asterisks: DUB-Ub adducts.
C) Recombinant $OTULIN_{cat}$, $USP21_{cat}$ or CYLD (1 µg) were incubated with either Met1-linked diUb WT or Ub^{G76A}-Ub (1 h, 37°C). DiUb cleavage was analyzed by WB.
D) Strep-PD of $OTULIN_{cat}$-Strep in the presence of Met1-linked His-diUb WT or His-Ub^{G76A}-Ub. Interaction between the proteins was analyzed by WB.

$OTULIN_{cat}$, $USP21_{cat}$ and CYLD hydrolyzed wild-type (WT) Met1-diUb, but were unable to cleave the G76A mutant (Figure 4-6C). To determine whether the mutation impairs binding of His-Ub^{G76A}-Ub to OTULIN, pull-down (PD) experiments of StrepII-tagged OTULIN ($OTULIN_{cat}$-Strep) with either Met1-diUb or Ub^{G76A}-Ub were performed (Figure 4-6D). WT Met1-diUb was strongly bound and pulled down by the catalytically inactive $OTULIN_{cat}$ C129A mutant. The binding affinity of OTULIN WT or C129A for Ub^{G76A}-Ub, by contrast, was strongly reduced. This suggests that the binding affinity of OTULIN towards Met1-diUb strongly depends on the distal Gly76 and that the replacement of Gly76 by Dha in the ABP diminishes affinity. Nevertheless, the weak interaction is apparently sufficient to facilitate the reaction of OTULIN with the electrophilic Dha in our probe, which does not apply to CYLD.

In addition to the desired ABP reactivity towards OTULIN, the first ABP selectivity analysis revealed that the probe slightly cross-reacts with recombinant USP5, which disassembles unanchored polyUb chains in cells (Amerik et al., 1997; Reyes-Turcu et al., 2006).

4.1.4 OTULIN ABP reacts with OTULIN in cell extracts

To determine whether the OTULIN ABP reacts with full-length OTULIN in cell extracts, HEK293 lysates from Flag-tagged OTULIN overexpressing cells were incubated with the ABP. The extracts were separated via SDS-PAGE and transferred to membranes by Western Blotting. Complex formation was analyzed by probing the membranes with anti-Flag antibody.

Indeed, overexpressed OTULIN WT was entirely labeled by the probe and formed a covalent complex with the ABP (Figure 4-7A). The catalytically inactive OTULIN mutant, however, did not react with the probe as seen with recombinant OTULIN C129A (see Figure 4-2A).

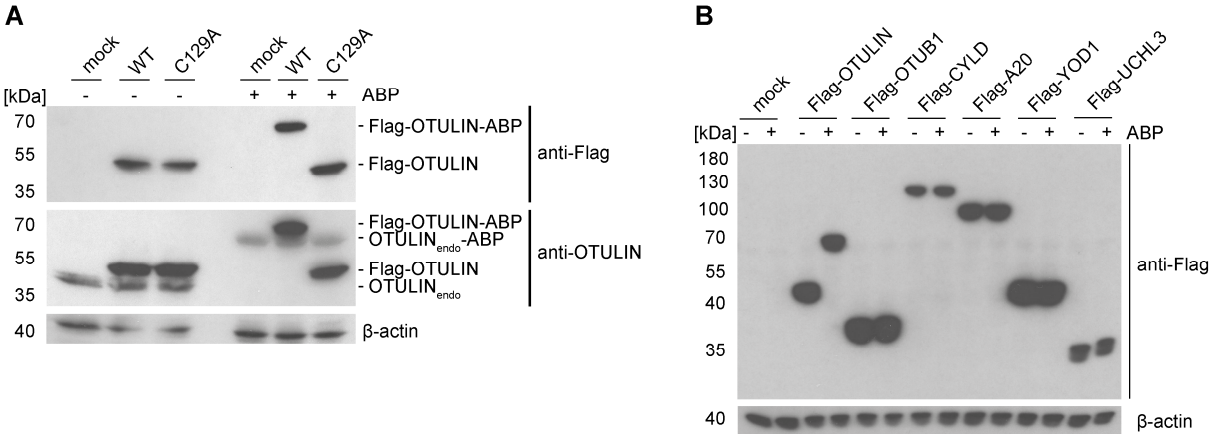

Figure 4-7: OTULIN ABP labels active OTULIN in cell extracts.
A) Extracts from HEK293 cells overexpressing Flag-OTULIN WT or C129A were incubated with 1 µg OTULIN ABP (~2.5x10^5 cells/reaction, 30 min, 30°C). Labeling of exo- and endogenous OTULIN was analyzed by WB.
B) Experiment was performed as in A) with extracts from HEK293 cells overexpressing Flag-tagged DUBs (incubation time: 1 h).

Probing the Western Blot (WB) membranes with anti-OTULIN antibody revealed that endogenous OTULIN was also labeled by OTULIN ABP (Figure 4-7A). Interestingly, all OTULIN present in HEK293 cells seems to be active or is activated through the ABP interaction as no uncoupled endogenous OTULIN could be detected following OTULIN ABP incubation. Reactivity of other overexpressed DUBs towards the OTULIN ABP was assessed in a similar manner (Figure 4-7B), even though the limited number of plasmids restricted the extent of the analysis. None of the tested full-length DUBs formed a covalent complex with the ABP.

To test whether the observed cross-reactivity of the OTULIN ABP towards recombinant USP5 also persists towards cellular USP5, lysates of untransfected HEK293 cells were incubated with ABP. In accordance with the previous results, a small proportion of endogenous USP5 formed a covalent complex with the ABP (Figure 4-8A). However, it is important to mention that the majority of cellular USP5, contrary to OTULIN, did not become covalently attached to the ABP. Probing the WB membranes with other available

DUB-specific antibodies confirmed that endogenous UCHL3, OTUB1 and CYLD did not react with the electrophilic Dha in the OTULIN ABP.

To monitor the kinetics of the coupling reaction between cellular OTULIN and the ABP, extracts from 2x10^7 Jurkat T cells were incubated at room temperature (RT) with increasing amounts of ABP for 15 min (Figure 4-8B). As observed for HEK293 cells, the entire cellular OTULIN amount reacted with the active site-directed probe in T cells, and thus seems to be active.

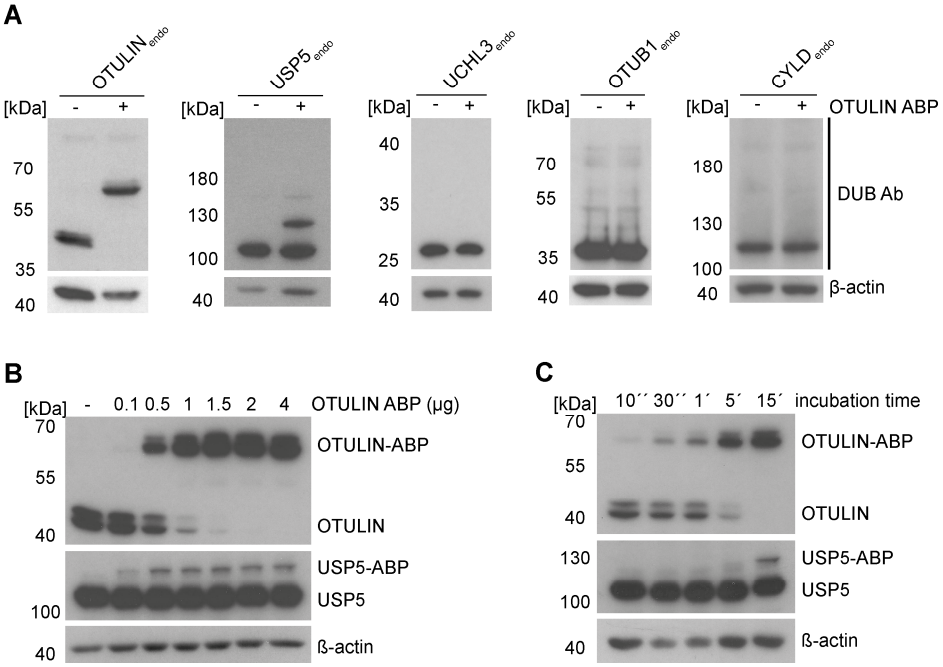

Figure 4-8: Endogenous OTULIN and USP5 react with OTULIN ABP in cell extracts.
A) Incubation of HEK293 cell extracts was performed as in Figure 4-7A. Cross-reactivity of OTULIN ABP was assessed by WB using the indicated anti-DUB antibodies.
B and C) Extracts of Jurkat T cells (2x10^7 cells/sample) were incubated at RT with increasing OTULIN ABP amounts for 15 min (B) or with 1 µg OTULIN ABP for different times (C).

The reaction proceeded dose-dependently and 1 µg ABP was sufficient to achieve almost complete binding of OTULIN to the ABP. The USP5-ABP adduct was already detectable after incubation with 0.5 µg ABP, the amount of USP5-ABP complex did not accumulate with increasing ABP concentrations though. Upon incubation of the lysates with 1 µg ABP, OTULIN-ABP complex formation was already observed after 10 to 30 seconds, whereas the USP5-ABP complex formed with delay after 15 min (Figure 4-8C). However, to achieve almost complete coupling a 15-minute incubation time was required at RT.

Thus, incubation of cellular extracts with ABP showed that active cellular OTULIN can also be detected with the probe and confirmed the cross-reactivity of the probe towards USP5.

4.1.5 Incubation of cell extracts with ABP induces polyUb chain formation

To further examine the selectivity of our OTULIN ABP, HEK293 cell extracts were treated with OTULIN ABP as in previous experiments and analyzed for ABP adducts by probing the WB membranes with an antibody that specifically binds Met1-linked Ub. Since our ABP is based on Met1-diUb, the anti-Met1-Ub antibody should recognize both the free ABP and ABP-labeled proteins. Indeed, uncoupled ABP and the OTULIN-ABP complex were detectable with this antibody (Figure 4-9A).

30-minute incubation at 30°C led to the appearance of a ladder-like pattern with smear in the high-MW range that closely resembles Met1-linked polyUb chains (Figure 4-9A). Reducing the incubation time (ice control, 2 min, 30°C) and a subsequent incubation on ice, gave rise to considerably less Met1-Ub smearing, suggesting that the generation of this Met1-Ub pattern is enzymatically driven.

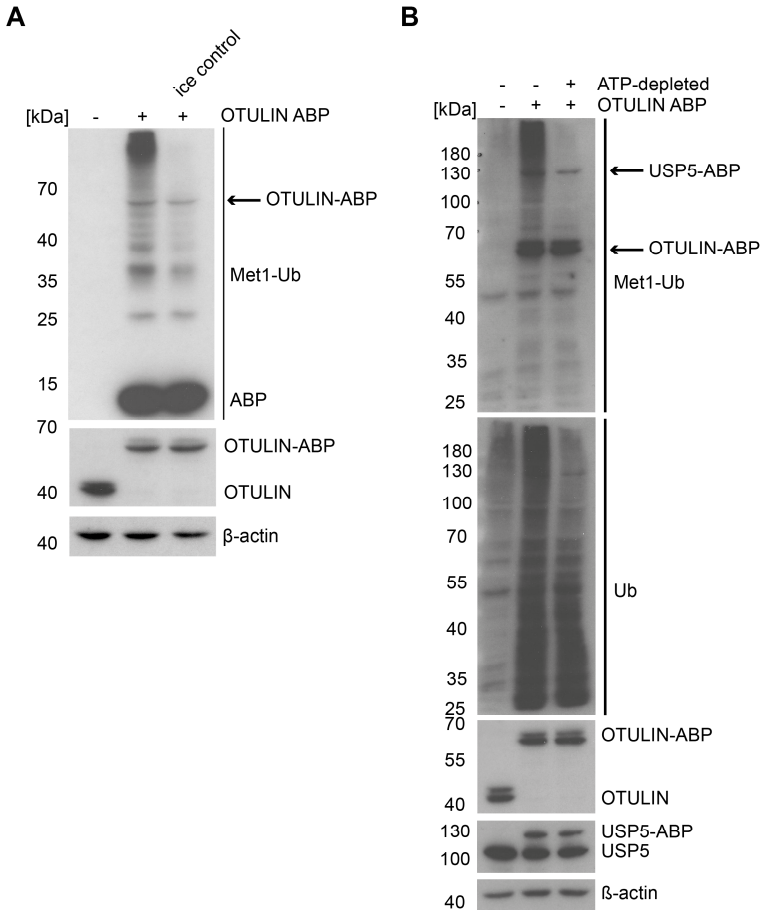

Figure 4-9: ABP treatment of cell extracts causes polyUb chain formation.
A) HEK293 cell extracts (~2.5x10^5 cells/reaction) were incubated with 1 µg OTULIN ABP for 30 min at 30°C. As control, the enzymatic reaction was put on ice following an initial 2-minute incubation at 30°C. Formation of ABP adducts was analyzed by WB.
B) For ATP depletion, extracts from 6x10^5 HEK293 cells were incubated with apyrase prior to the incubation with 1 µg OTULIN ABP for 30 min. Ubiquitin chain formation and ABP adducts were determined by WB.

Removal of ATP from the extracts by recombinant apyrase before ABP incubation prevented the *in vitro* formation of polyUb chains that could be detected not only with anti-Met1-Ub, but also with a general anti-Ub antibody (Figure 4-9B). Two distinct bands at ~60 kDa and ~130 kDa were detected with the anti-Met1-Ub antibody after ATP depletion (Figure 4-9B). The MW of these proteins corresponds to the MW and the electrophoretic migration pattern of the OTULIN-ABP and USP5-ABP adducts that were detected by OTULIN- and USP5-specific antibodies. Importantly, besides these two protein bands only very weak background signals were detected following ATP depletion with the anti-Met1-Ub antibody. This suggests that OTULIN and USP5 are selectively labeled by the OTULIN ABP.
Furthermore, the data indicate that incubation of the lysates with OTULIN ABP and inhibition of the two Met1-Ub cleaving DUBs, OTULIN and USP5, results in the assembly of polyUb chains via the ATP-dependent enzymatic ubiquitination cascade.

4.1.6 Global selectivity analysis of the OTULIN ABP by LC-MS/MS

To accurately define the OTULIN ABP specificity, the ABP was subjected to a global mass spectrometric analysis. Following incubation of cell extracts with the ABP, the N-terminal biotin tag enabled us to enrich the ABP and ABP binders in a biotin-PD using streptavidin beads. Under non-stringent conditions, the OTULIN-ABP complex could be precipitated in the ABP-PD, as well as the known OTULIN interactor HOIP (Figure 4-10A). In order to identify covalently bound ABP interactors, PD stringency was optimized. Up to 1% SDS in the washing buffer did not have a negative impact on PD efficiency of the OTULIN-ABP complex, whereas detection of non-covalently bound HOIP was already greatly reduced after washing with 0.1% SDS-containing buffer (Figure 4-10A). Accordingly, for the mass spectrometry (MS) analysis of covalent ABP adducts, all PD samples were washed with 1% SDS-containing buffer to deplete most non-covalent interactors. In the LC-MS/MS (liquid chromatography-tandem MS) analysis we compared a sample that had been incubated with the OTULIN ABP (sample 2) with a control sample, to which no ABP had been added (sample 1). Additionally, in sample 3, ATP was depleted by apyrase to abolish interactions that result from the polyUb chains that are generated upon ABP incubation (see 4.1.5). As additional control, the general DUB inhibitor PR-619 was added to sample 4, to prevent DUB-ABP complex formation. For statistical significance, four biological replicates were prepared. OTULIN-ABP complex formation and pull-down were detected by WB independently from apyrase treatment, whereas PR-619 prevented OTULIN labeling and its pull-down (Figure 4-10B). After performing PD experiments, PD eluates were sent to Adan

Pinto-Fernandez and Sarah Bonham (Benedikt M. Kessler group, University of Oxford) for the MS analysis including protein digest, LC-MS/MS and data analysis.

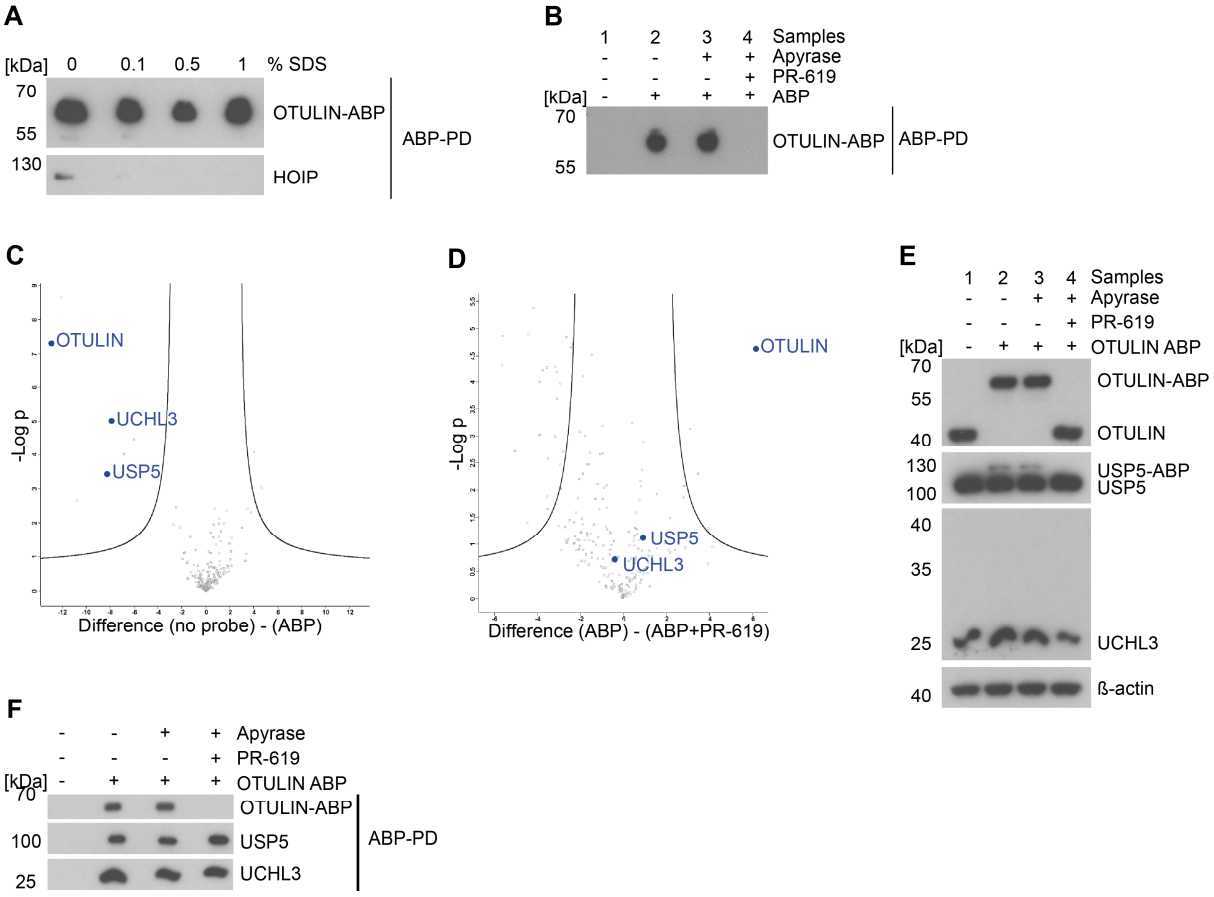

Figure 4-10: LC-MS/MS analysis confirms high selectivity of OTULIN ABP.
A) Biotin-PD of OTULIN ABP under highly stringent conditions to enrich covalent ABP interactors. Jurkat T cell extracts ($18x10^6$ cells/sample) were incubated with 4 µg OTULIN ABP (15 min, RT). Following PD, beads were washed twice with buffer containing different SDS concentrations. PD of the OTULIN-ABP complex and the non-covalent HOIP association were assessed by WB.
B) Control of OTULIN-ABP PD in samples before LC-MS/MS analysis. Jurkat T cell extracts ($5x10^7$ cells/sample) were treated with apyrase and PR-619 as indicated prior to the incubation with ABP. Following PD, beads were washed with 1% SDS-containing buffer. 5% of the PD eluates were analyzed by WB, the rest was sent to LC-MS/MS analysis.
C) Volcano plot illustrating enrichment of identified DUBs (blue) after ABP-PD (sample 1 vs. 2). Curves depict significant enrichment or depletion, respectively. Illustration provided by A. Fernandez (Benedikt M. Kessler group, University of Oxford).
D) Volcano plot illustrating loss of DUB binding (blue) to ABP upon DUB inhibition by PR-619 (sample 3 vs. sample 4). Curves depict significant enrichment or depletion, respectively. Illustration provided by A. Fernandez (Benedikt M. Kessler group, University of Oxford).
E) Jurkat T cell extracts were treated like LC-MS/MS samples. Labeling of proteins in extracts was analyzed by WB.
F) ABP-PDs were performed under the same conditions as for LC-MS/MS analysis (extracts from $2x10^7$ Jurkat T cells) and analyzed by WB to verify the MS results.

The comparison of the samples with and without OTULIN ABP (1 vs. 2) revealed that only three DUBs, namely OTULIN, USP5 and UCHL3, were significantly enriched in the ABP-PD (Figure 4-10C). The enrichment of OTULIN and USP5 confirmed the labeling by the ABP in previous experiments. However, the enrichment of UCHL3 was unexpected, because using recombinant, transfected or endogenous UCHL3 no UCHL3-ABP complex formation was detected (see Figure 4-5, Figure 4-7B and Figure 4-8A). DUB inhibitor PR-619 treatment led to the significant depletion of OTULIN from the PD samples, validating that the catalytic

activity of OTULIN is required for covalent binding (3 vs. 4, Figure 4-10D). In contrast, neither USP5 nor UCHL3 were depleted from the ABP-PD by PR-619, suggesting that these DUBs bind to the ABP even under highly stringent conditions (1% SDS) in a non-covalent manner (3 vs. 4, Figure 4-10D).

To exclude that PR-619 does not affect USP5 activity, Jurkat T cell extracts were treated in the same manner as the LC-MS/MS samples and directly analyzed for USP5-ABP complex formation by WB. Loss of the USP5-ABP adduct following inhibitor treatment proved that PR-619 inhibits USP5, as well as OTULIN (Figure 4-10E). The experiment also confirmed again that UCHL3 did not become covalently attached to the ABP. This suggests that the binding affinities between USP5 or UCHL3 and the OTULIN ABP are very high and that the interactions seem to be mostly non-covalent. The validation of the MS results by WB analysis confirmed that USP5 and UCHL3 bind the OTULIN ABP and are pulled down, regardless of whether the extracts were treated with apyrase or PR-619 (Figure 4-10F). It is important to note that both DUBs were detected at MWs that correspond to the MWs of the unbound proteins and not of the ABP adducts. This proves that the DUBs USP5 and UCHL3 are strong Ub binders and mostly non-covalently interact with the OTULIN ABP. Altogether, the LC-MS/MS analysis revealed that the OTULIN ABP is very selective for OTULIN and that its cross-reactivity towards USP5 is negligible.

4.1.7 LC-MS/MS analysis reveals coupling of E1 enzymes to ABP

Next, global reactivity of the OTULIN ABP was examined by comparing the entire interactome enriched by ABP-PD in sample 1 versus sample 2 (Figure 4-11A). Besides the three DUBs (blue), only four other proteins (red) were identified, namely UBC, NEDD8, UBA1 and UBA6. The Ub precursor protein UBC corresponds to the probe itself, which consists of two Ub moieties. Interestingly, binding of the mammalian E1 enzymes UBA1 and UBA6 to the ABP was prevented by ATP depletion (Figure 4-11B). This ATP-dependent ABP binding of E1 enzymes could be confirmed by WB (Figure 4-11C) and closely resembles the first Ub-activating step of the ubiquitination cascade, in which a Ub C-terminus reacts under ATP consumption with the catalytic Cys in the E1 enzyme and a high-energy thioester bond is formed. The covalent ABP-E1 enzyme complex could not be visualized under reducing conditions by SDS-PAGE (Figure 4-11D), supporting that binding is most likely achieved through a thioester bond. In accordance with the fact that incubation of cell extracts with ABP leads to the ATP-dependent formation of polyUb chains (4.1.5), the diUb-based ABP seems to be activated by E1 enzymes, in common with monoUb. Moreover, MS results indicate that

the ATP-dependent assembly of polyUb chains by the probe may not be based on inhibition of OTULIN or other DUBs but on the insertion of the probe itself into Ub chains.

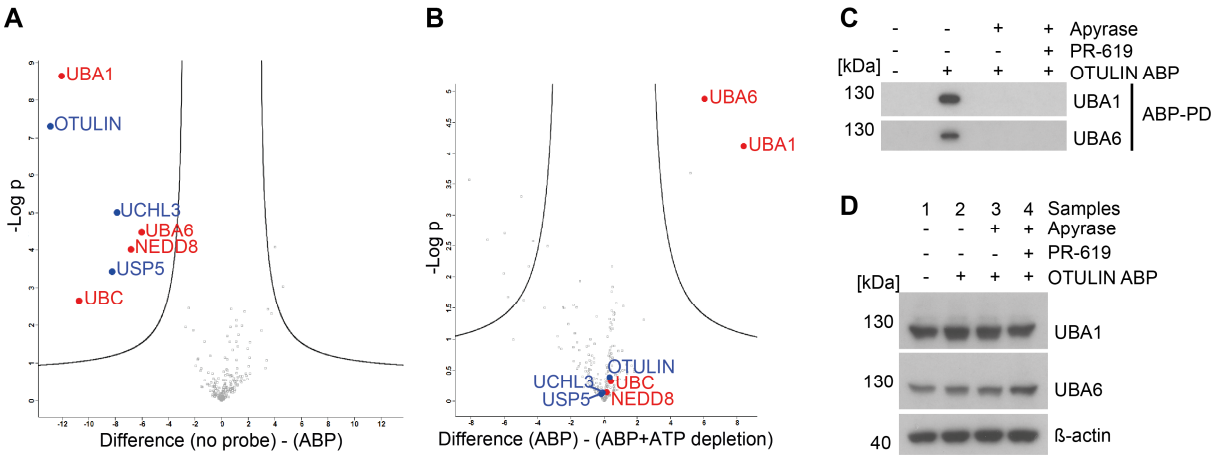

Figure 4-11: The E1 enzymes UBA1 and UBA6 bind to the ABP in an ATP-dependent manner.
A) Volcano plot illustrating the enrichment of identified proteins after ABP-PD under highly stringent conditions (DUBs – blue, others – red; sample 1 vs. 2). Curves depict significant enrichment or depletion, respectively. Illustration provided by A. Fernandez (Benedikt M. Kessler group, University of Oxford).
B) Volcano plot illustrating loss of E1 enzyme binding to OTULIN ABP upon ATP depletion (sample 2 vs. 3). Curves depict significant enrichment or depletion, respectively. Illustration provided by A. Fernandez (Benedikt M. Kessler group, University of Oxford).
C) See Figure 4-10F.
D) See Figure 4-10E.

4.1.8 E1-dependent auto-conjugation of the OTULIN ABP

After the MS analysis, the assumption that the ATP-dependent Ub chain assembly by the probe is not based on inhibiton of OTULIN and USP5, but instead, on ABP activation and conjugation by E1 enzymes, should be verified. For that purpose, the ability of the non-inhibitory and cleavage-resistant diUb mutant His-Ub^{G76A}-Ub (see Figure 4-6C) to also induce chain formation in extracts was investigated.

Indeed, the G76A mutant still induced Ub chain formation in a dose-dependent manner, which could be detected with anti-Met1-Ub antibody (Figure 4-12A). To prove that uncleavable diUbs like His-Ub^{G76A}-Ub and bio-Ub^{G76Dha}-Ub are embedded into Ub chains, cell extracts were incubated with ABP in order to induce polyUb chain formation and afterwards cleaned again from the ABP and ABP-adducts using streptavidin beads (Figure 4-12B). After the biotin-PD, the free ABP and the formed Ub chains were completely depleted from the supernatant, suggesting that ABP is covalently incorporated into polyUb chains.

To determine the linkage type of the Ub chains formed by ABP incubation and incorporation, the technique of Ubiquitin Chain Restriction Analysis (UbiCREST) was applied (Hospenthal et al., 2015). In this assay, the polyUb chains of interest are incubated with commercially available linkage-specific DUBs and then checked for degradation. In this case, HEK293

extracts were first incubated with OTULIN ABP (30 min, 30°C) and subsequently mixed with the recombinant DUBs for another 30 min.

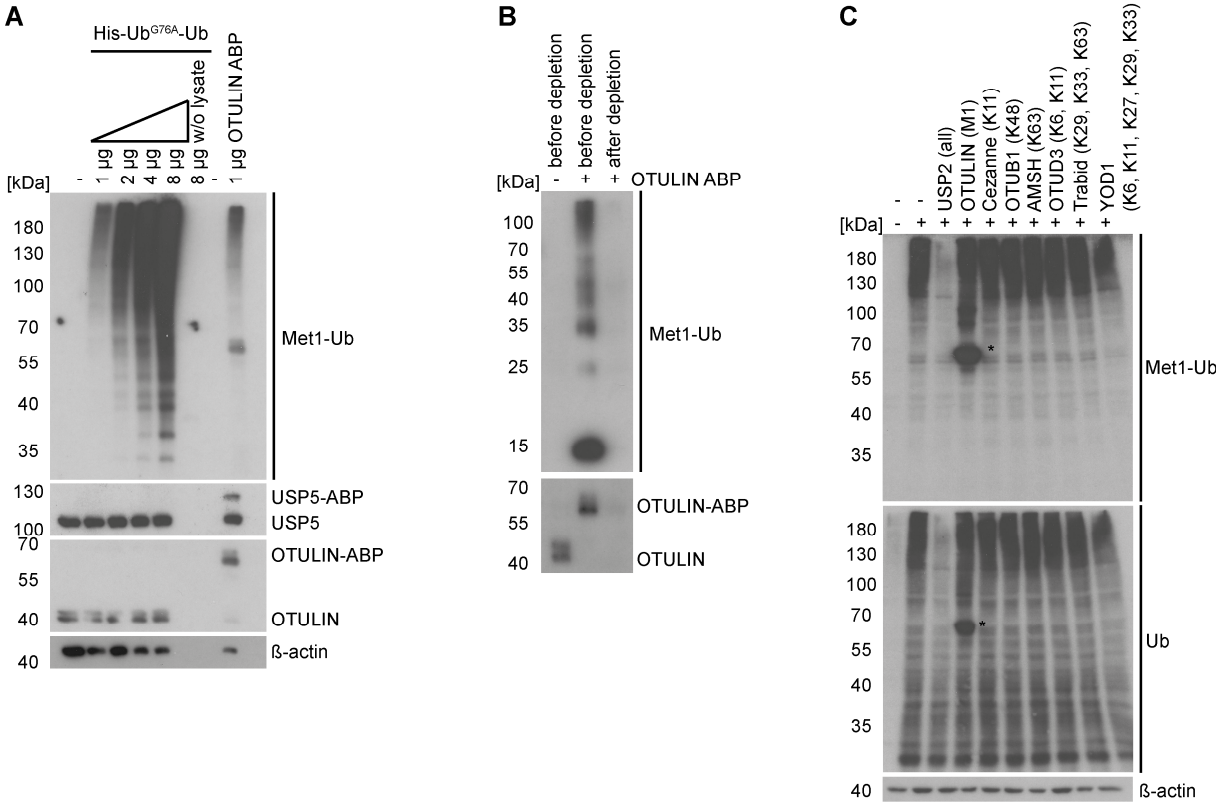

Figure 4-12: OTULIN ABP is incorporated into polyABP assemblies by E1 enzymes.
A) HEK293 cell extracts (6×10^5 cells/sample) were incubated with increasing amounts of His-Ub^{G76A}-Ub or with 1 µg OTULIN ABP (45 min, 30°C). Formation of Ub chains and OTULIN-ABP or USP5-ABP complexes was analyzed by WB.
B) Jurkat T cell extracts ($6x10^5$ cells/sample) were incubated with 1 µg OTULIN ABP (45 min, 30°C) and subjected to biotin-PD. Extracts were assessed for the presence of Ub chains before and after the PD by WB using anti-Met1-Ub antibody. Depletion of OTULIN-ABP complex is shown as control.
C) Linkage analysis of Ub chains formed in extracts of HEK293 cells following OTULIN ABP incubation (30 min, 30°C) by UbiCREST digestion. Treatment with linkage-specific DUBs was performed for another 30 min. Ub chains were analyzed by WB. Asterisk: OTULIN-ABP adduct.

WB analysis using anti-Met1-Ub and anti-Ub antibodies revealed that recombinant OTULIN was coupled and inhibited by OTULIN ABP (see asterisk), but even in excess, it failed to cleave the chains generated by ABP incubation (Figure 4-12C). Likewise, Lys11-specific Cezanne, Lys48-specific OTUB1 and Lys63-specific AMSH were not able to cleave the chains. Only the promiscuous DUB USP2, which cleaves all types of ubiquitin linkages, was able to completely remove the high-MW ubiquitin smear.

These data indicate that the chains are complex polyABP assemblies of bio-Ub^{G76Dha}-Ub, which are poorly accessible for linkage-specific DUBs. Furthermore, the data suggest that various lysine residues in the OTULIN ABP or in His-Ub^{G76A}-Ub can serve as attachment sites for the ubiquitination with activated diUbs. Head-to-tail linkages can be excluded, since the N-terminal tags block the access to the α-amino group of Met1 in the distal Ub moiety.

4.1.9 OTULIN ABP ΔG76: the first specific OTULIN ABP

USP5 preferentially cleaves unanchored Ub chains from the proximal end. Recognition and binding of the C-terminal di-Gly motif by a dedicated binding pocket in USP5 is essential for the hydrolysis reaction (Reyes-Turcu et al., 2006). In addition, the C-terminal Gly76 in the Ub molecule enables its recognition and activation by E1 enzymes in the ubiquitination process (Ciechanover et al., 1982). We decided to generate another OTULIN ABP, which lacks the Gly76 in the proximal Ub moiety (OTULIN ABP ΔG76), in order to eliminate the cross-reactivities of the ABP with USP5 and E1 enzymes.

This time, the precursor protein His-Ub^{G76C}-Ub(1-75) was recombinantly produced in *E. coli* and then sent to our collaboration partner Farid el Oualid (UbiQ), who converted the Cys76 in the distal Ub into electrophilic Dha by means of oxidative elimination (Figure 4-13A).

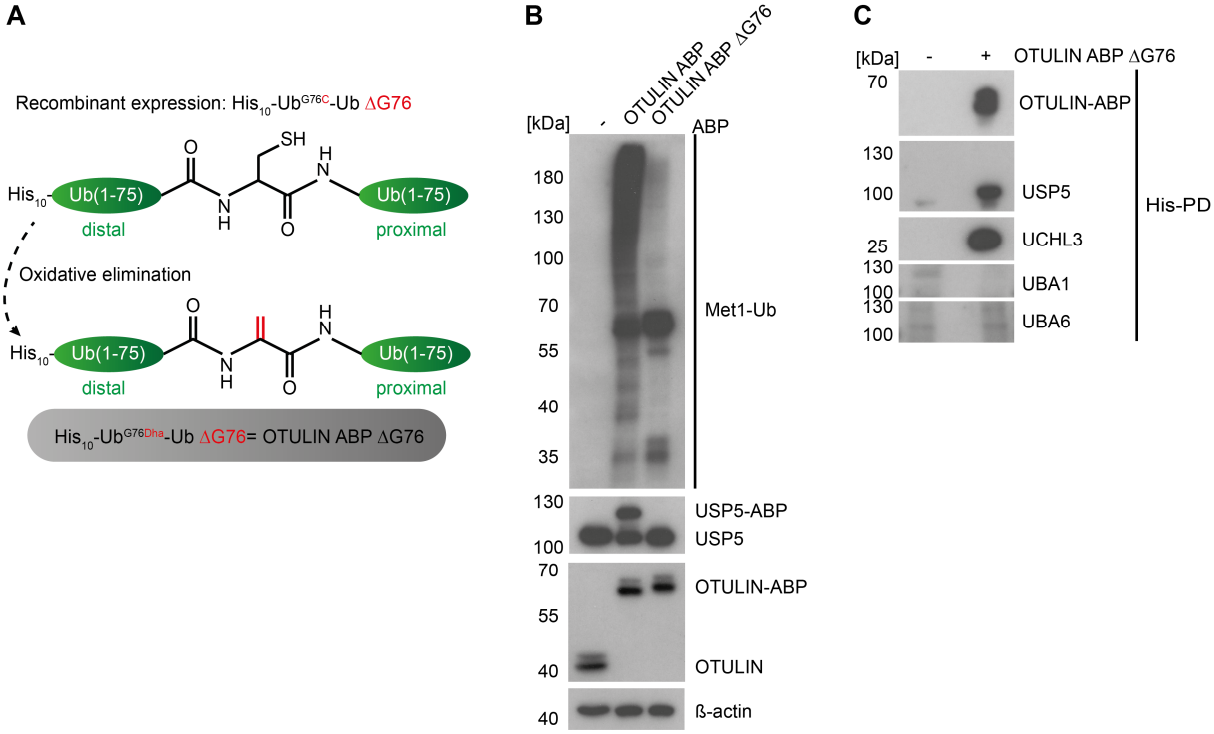

Figure 4-13: OTULIN ABP ΔG76 does not cross-react with USP5 and E1 enzymes.
A) Synthesis scheme of OTULIN ABP ΔG76.
B) HEK293 cell extracts (6x10^5 cells) were incubated with 1 µg OTULIN ABP or 1 µg OTULIN ABP ΔG76 (45 min, 30°C). Labeling of OTULIN and USP5 as well as Ub chain formation was analyzed by WB.
C) Jurkat T cell extracts (2x10^7 cells) were treated with 4 µg OTULIN ABP ΔG76 prior to His-PD. Interactions between the new probe and the indicated proteins were analyzed by WB.

Incubation of cell extracts with the new OTULIN ABP ΔG76 revealed that the probe still reacts with active OTULIN, however no longer with USP5 (Figure 4-13B). Deletion of the C-terminal Gly76 also abolished cross-reactivity with E1 enzymes (Figure 4-13C) and thus likewise prevented polyABP chain formation in cell extracts (Figure 4-13B). In a His-PD of the probe, not only the OTULIN-ABP ΔG76 complex, but also USP5 and UCHL3, could be enriched (Figure 4-13C). This confirms the conclusion from the MS analysis that the DUBs

USP5 and UCHL3, due to their high binding affinity towards diUb, strongly and non-covalently interact with the OTULIN ABP. Altogether, these results prove that the OTULIN ABP ΔG76 is the first specific OTULIN ABP.

4.1.10 Substrate-bound OTULIN interacts with LUBAC

It has previously been demonstrated that OTULIN interacts with LUBAC via HOIP (Elliott et al., 2014; Schaeffer et al., 2014). We wanted to verify this interaction by means of the newly developed and highly selective OTULIN ABP. For this purpose, various human cell lines were lysed and subjected to ABP-PDs. In order to detect non-covalently bound OTULIN interactors, PD was performed under mild co-immunoprecipitation (co-IP) conditions without SDS.

The OTULIN-ABP complex was precipitated from any extract (Figure 4-14). Further, the entire LUBAC composed of HOIP, HOIL-1 and SHARPIN was enriched from any cell line along with substrate-bound OTULIN. This indicates that the OTULIN ABP enables detection of OTULIN-associated protein complexes. Not only direct binding partners of OTULIN, like HOIP, but also indirect interactors like HOIL-1 and SHARPIN can be precipitated with the OTULIN-ABP complex.

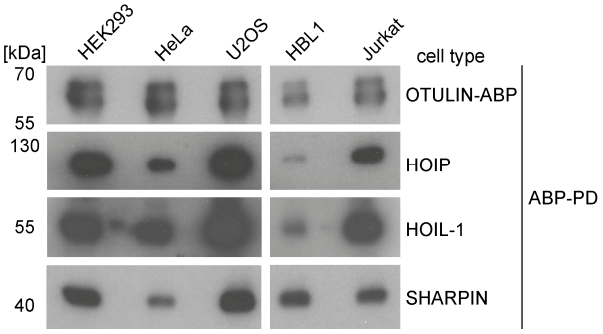

Figure 4-14: LUBAC associates with substrate-bound OTULIN.
ABP-PD under mild conditions from extracts of different human cell lines ($2x10^7$ cells/sample, 4 µg OTULIN ABP). Interaction of the OTULIN-ABP complex with LUBAC components was examined by WB.

4.1.11 Neither OTULIN activity nor the OTULIN-LUBAC interaction are affected by TNFα stimulation

The generation of Met1-linked Ub chains is involved in TNFR-dependent activation of NF-κB (Sasaki and Iwai, 2015). Therefore we wanted to determine whether OTULIN activity is altered upon TNFα stimulation. Stimulation of Jurkat T cells with TNFα for up to 90 min resulted in NF-κB activation, evident from IκBα phosphorylation and degradation (Figure 4-15A). However, OTULIN-ABP complex formation in the extracts did not change, indicating that OTULIN activity remains constant following TNFα stimulation.

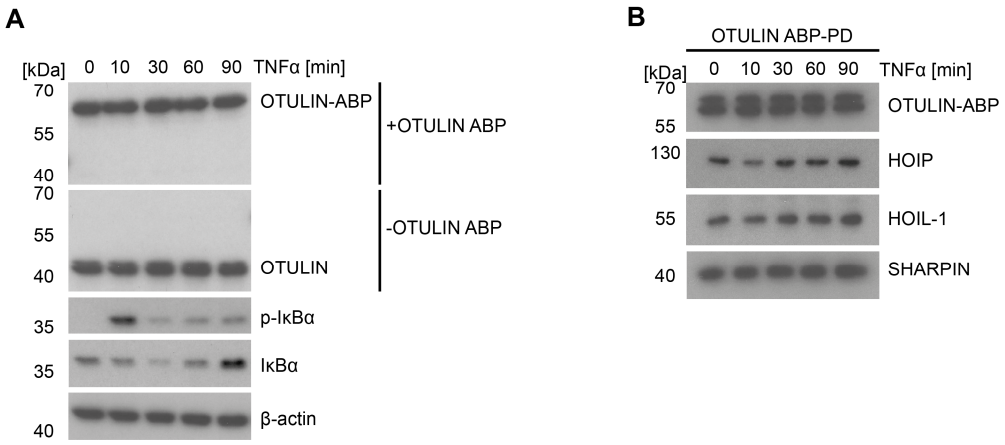

Figure 4-15: TNFα stimulation has no impact on OTULIN activity or the OTULIN-LUBAC interaction.
A) Jurkat T cells were stimulated with TNFα (20 ng/ml). Lysates ($2.5x10^5$ cells/sample) were incubated with 1 µg OTULIN ABP and analyzed for changes in OTULIN activity by WB.
B) ABP-PD (co-IP conditions) from Jurkat T cell extracts following stimulation with TNFα (20 ng/ml; $2x10^7$ cells/sample; 4 µg OTULIN ABP). Interaction of the OTULIN-ABP complex with LUBAC components was evaluated by WB.

Next, we wondered whether the OTULIN-LUBAC interaction changes in Jurkat T cells upon stimulation with TNFα. Due to constant acitivity of OTULIN after TNFα treatment (Figure 4-15A), equal amounts of the OTULIN-ABP complex were pulled down in the ABP-PD (Figure 4-15B). Likewise, the amounts of co-precipitated OTULIN-associated LUBAC components HOIP, HOIL-1 and SHARPIN did not alter significantly, suggesting that the OTULIN-LUBAC interaction is neither attenuated nor strengthened by TNFα stimulation.

4.1.12 The majority of cellular LUBAC is not associated with OTULIN

To get an impression of how much of the cellular LUBAC is associated with OTULIN in unstimulated Jurkat T cells, protein amounts of OTULIN, HOIP, HOIL-1 and SHARPIN in the extracts prior to (input) and after the ABP-PD (supernatant) were compared (Figure 4-16A). Although the OTULIN-ABP complex could be almost completely precipitated from the lysate, a considerable proportion of LUBAC components remained in the supernatant.

To determine this proportion more precisely, protein levels of HOIP, HOIL-1, SHARPIN and OTULIN were quantified in the input (total LUBAC amount) and in the supernatant ('free', OTULIN-ABP unbound LUBAC). To this end, the respective protein band intensities were measured using ImageJ software and normalized to β-actin in six independent experiments. The ratio of quantified proteins between the supernatant and input was calculated to obtain relative amounts of free, OTULIN-ABP unbound proteins. Whereas the ABP-PD removed more than 80% of active OTULIN from the extracts, less than 25% of each LUBAC subunit was co-precipitated (Figure 4-16B).

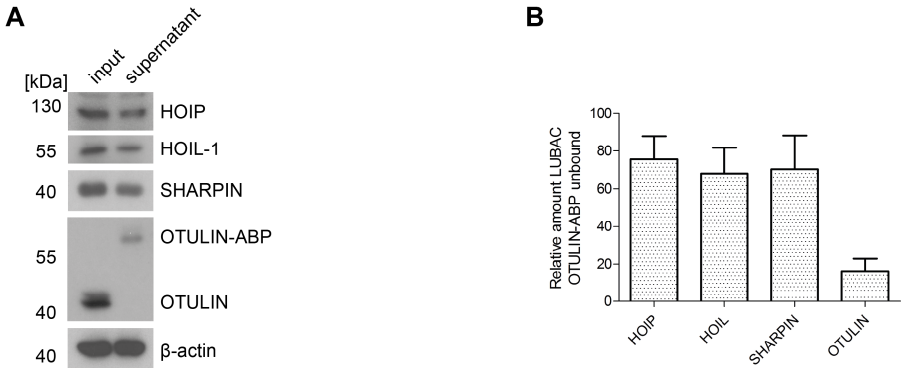

Figure 4-16: The majority of cellular LUBAC is not OTULIN-associated.
A) Protein amounts of OTULIN, HOIP, HOIL-1 and SHARPIN in Jurkat T cell extracts were assessed by WB, prior to (input), and following ABP-PD (supernatant).
B) Levels of LUBAC subunits and OTULIN in Jurkat T cell extracts were assessed by WB, prior to (input), and following ABP-PD (supernatant), and quantified using ImageJ software. The quantified relative amounts of 'free', OTULIN-ABP unbound proteins are depicted. Data represent the mean ± SD of six independent experiments.

These data suggest that the majority of the LUBAC complex (>75%) is not associated with substrate-bound OTULIN. Accordingly, the majority of cellular OTULIN is most likely also not in complex with LUBAC, what raised the question, which other proteins interact with OTULIN. Since the OTULIN ABP is an excellent tool to deplete OTULIN almost entirely from cell extracts and thus to monitor OTULIN-associated protein complexes, we addressed the question of further OTULIN interactors with the ABP.

4.2 Identification of SNX27 as a novel OTULIN interactor

4.2.1 Identification of OTULIN interactors by LC-MS/MS

Following the generation and characterization of the highly selective OTULIN ABP (section 4.1), we used it to identify potential novel OTULIN interactors by LC-MS/MS. For this purpose, Jurkat T cell extracts were initially treated with apyrase to prevent the ATP-dependent formation of polyABP assemblies (see sections 4.1.5 and 4.1.8). One sample was incubated with ABP to identify interactors of ABP-bound OTULIN (sample 2), whereas no probe was added to the control sample (sample 1). PR-619 was added to another control sample to inhibit OTULIN activity and thus prevent the OTULIN-ABP complex formation (sample 3). After the PD, beads were washed under mild co-IP conditions to avoid loss of non-covalently bound OTULIN interactors. For statistical significance, the ABP-PDs were performed in quadruplicate and the PD eluates were sent again to Adan Fernandez and Sarah Bonham (Benedikt M. Kessler group, University of Oxford) for trypsin digestion, LC-MS/MS and data analysis.

The comparison between the samples with and without probe shows the significant enrichment of the OTULIN ABP interactome (Figure 4-17A) comprising of covalent and

non-covalent ABP binders. In addition to the proteins that had been identified in the previous PDs under highly stringent conditions (see 4.1.7 and Figure 4-11A), seven more proteins were identified by LC-MS/MS analysis. Some of them have been directly linked with the Ub system (BRAP, HOIP, USP3 and VCP), whereas others have not been primarily associated with Ub regulation (HDAC6, SNX27 and WRNIP1). PR-619 treatment resulted not only in the significant removal of OTULIN from the ABP, but also in the significant loss of HOIP and SNX27 binding (Figure 4-17B). The expected OTULIN-dependent ABP binding of HOIP, as known OTULIN interactor, indicated that SNX27 could also be a potential OTULIN binding partner.

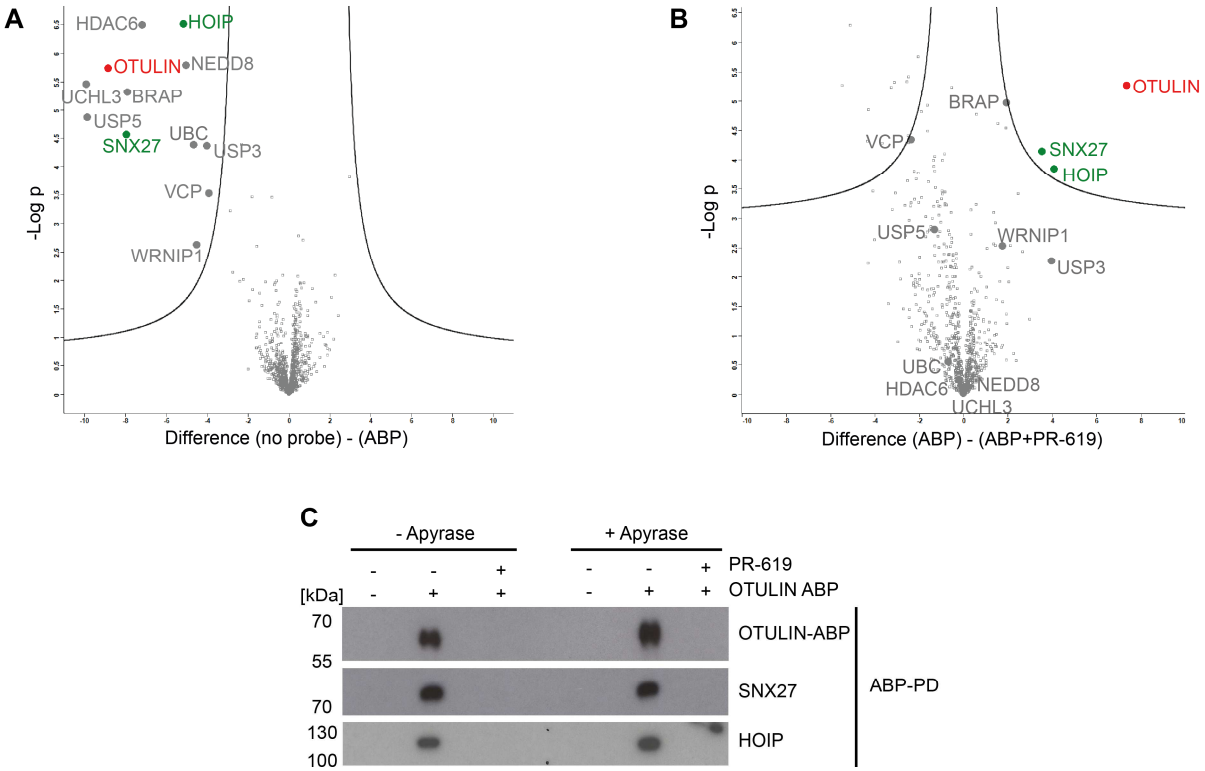

Figure 4-17: Identification of SNX27 as potential OTULIN interactor by LC-MS/MS.
A) Volcano plot illustrating the enrichment of identified proteins after ABP-PD under co-IP conditions (-ABP vs +ABP). Curves depict significant enrichment or depletion, respectively. Illustration provided by A. Fernandez (Benedikt M. Kessler group, University of Oxford).
B) Volcano plot illustrating loss of HOIP and SNX27 binding to OTULIN ABP upon OTULIN depletion by PR-619 (ABP vs. ABP+PR-619). Curves depict significant enrichment or depletion, respectively. Illustration provided by A. Fernandez (Benedikt M. Kessler group, University of Oxford).
C) ABP-PDs were performed under the same conditions as for LC-MS/MS analysis (extracts from $2x10^7$ Jurkat T cells) or without apyrase treatment and analyzed by WB to verify the MS results.

To verify the MS results, ABP-PDs were repeated under the same conditions as for LC-MS/MS and analyzed by WB. The validation experiment confirmed the enrichment of HOIP and SNX27 along with the OTULIN-ABP complex (Figure 4-17C). Moreover, ABP binding and enrichment was lost upon OTULIN inhibition by PR-619. Protein enrichment and depletion by PR-619, respectively, could be detected independently from ATP depletion by apyrase, suggesting that polyABP assembly formation does not affect the observed

interactions. Altogether, the OTULIN-ABP complex-dependent enrichment of SNX27 gave a first hint that it might be a potential OTULIN interactor.

4.2.2 SNX27 interacts with OTULIN independently from HOIP

To verify the putative interaction between OTULIN and SNX27, OTULIN-deficient Jurkat T cells were generated using the CRISPR/Cas9 technology. To this end, a single guide RNA (sgRNA) targeted at exon 2 of the *OTULIN* gene was designed and transfected into cells along with Cas9 to induce a double-strand break (DSB) in the genomic DNA (Figure 4-18A). In mammalian cells, DSBs are mainly repaired by the non-homologous end joining (NHEJ) pathway, generating nucleotide insertions or deletions at the respective sites. These indels can lead to insertions or deletions of amino acids or to frameshift mutations creating a premature stop codon within the open reading frame of the gene of interest. After expansion of single-cell clones, all clones were initially checked for the OTULIN protein expression by WB analysis (Figure 4-18B). In some clones, OTULIN expression was as high as in the parental cells or slightly reduced (clone #12, Figure 4-18B). In extracts of the clones #3, #6 and #11, no OTULIN could be detected (Figure 4-18B). Genomic DNA of these identified KO clones was amplified by PCR around the targeted site, in order to track changes on the DNA level. That way, all KOs were verified (data not shown).

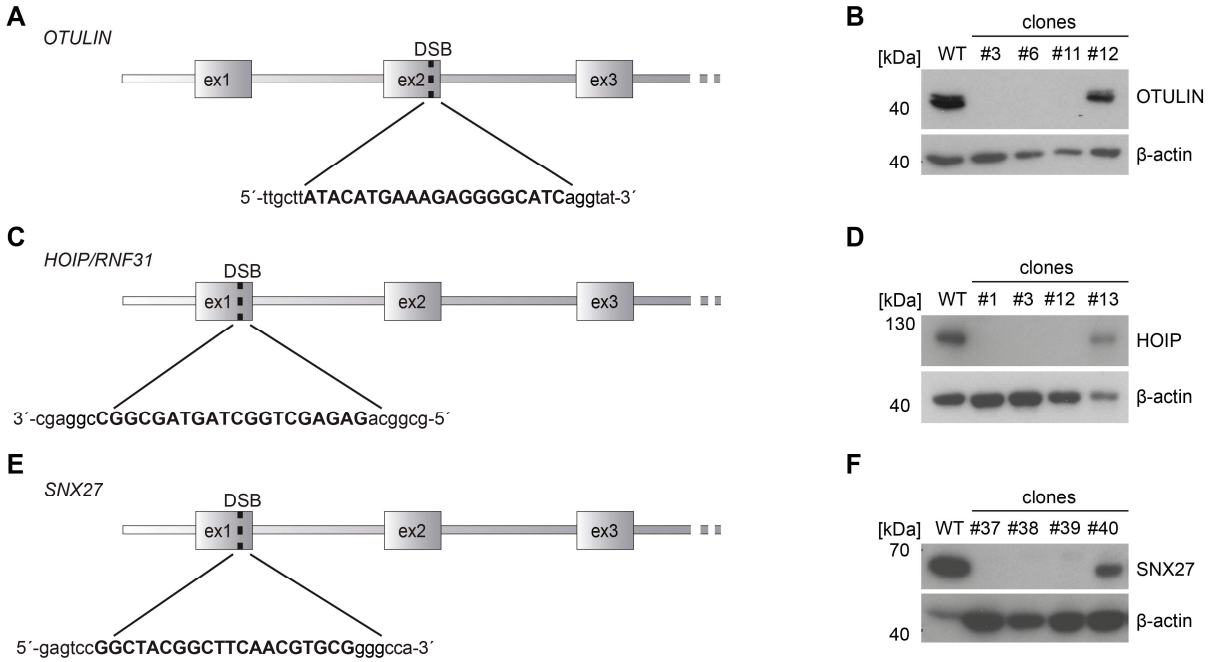

Figure 4-18: Generation of OTULIN-, HOIP- and SNX27-deficient Jurkat T cells by CRISPR/Cas9.
A), C) and E) Schematic representations of the *OTULIN* (A), *RNF31* (C) and *SNX27* (E) genes. Targeted sequences by sgRNAs, in exon 2 and exon 1, respectively, are depicted in bold type.
B), D) and F) Exemplary WBs of the KO screenings. Cell clones were analyzed for OTULIN (B), HOIP (D) or SNX27 (F) expression by WB and compared to the expression in parental Jurkat T cells.

To facilitate further studies, HOIP- and SNX27-deficient Jurkat T cell lines were also generated. For HOIP KO cells the sgRNA was targeted at exon 1 of the *HOIP/RNF31* gene (Figure 4-18C) in accordance with the previously published HOIP KO in Jurkat T cells (Yang et al., 2016). For the SNX27 KO, a sgRNA was designed that is targeted at exon 1 of the *SNX27* gene (Figure 4-18E). Several clones were obtained that are deficient in either HOIP or SNX27 expression (Figure 4-18D and F). Again, all KOs were verified on genomic level (data not shown).

To verify the putative interaction between OTULIN and SNX27, extracts of parental and OTULIN-deficient Jurkat T cells were incubated with OTULIN ABP and subsequently subjected to ABP-PDs. While HOIP and SNX27 were pulled down together with the OTULIN-ABP complex from WT cell extracts, both could not be enriched from OTULIN-deficient lysates without the formation and pull-down of the OTULIN-ABP adduct (Figure 4-19A). This proves that SNX27 binding to the ABP is OTULIN-dependent.

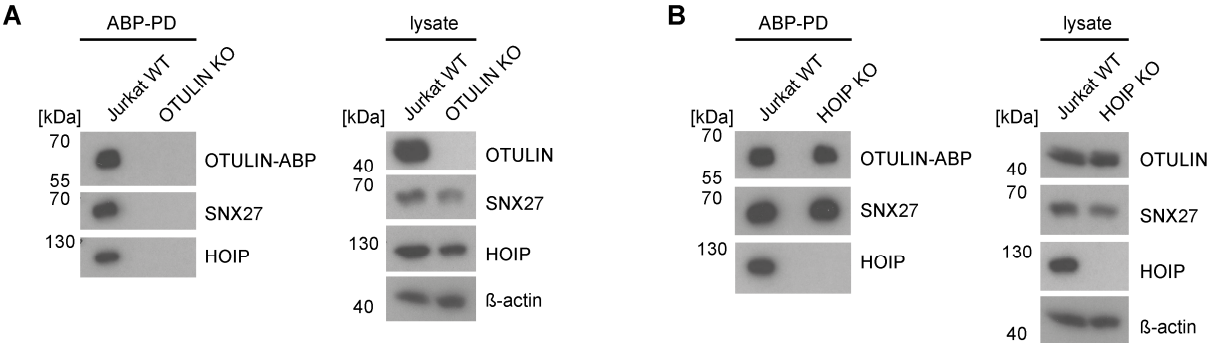

Figure 4-19: ABP binding of SNX27 is OTULIN-dependent.
A) ABP-PD was performed from extracts of $2x10^7$ parental and OTULIN KO Jurkat T cells. Enrichment of HOIP and SNX27 in PDs was analyzed by WB.
B) ABP-PD was performed from extracts of $2x10^7$ parental and HOIP KO Jurkat T cells. SNX27 enrichment in PDs was assessed by WB.

To exclude that OTULIN association of SNX27 proceeds indirectly via HOIP, ABP-PDs from HOIP-deficient and parental cell extracts were perfomed. HOIP was not present in the OTULIN-ABP complex in HOIP KO extracts (Figure 4-19B). Nevertheless, SNX27 binding to OTULIN-ABP could still be detected, suggesting that this interaction is independent of HOIP. Thus, experiments with the generated KO cell lines indicated that SNX27 is an OTULIN interactor, which binds OTULIN independently from HOIP.

4.2.3 ABP-independent MS approach confirms OTULIN-SNX27 interaction

Infection of cells with lentiviruses enables integration of DNA constructs in the genome and their stable expression. This technique was used to reconstitute OTULIN-deficient Jurkat T cells with N-terminally StrepII-StrepII-Flag-tagged (SSF-)OTULIN or with the SSF-tag (mock).

Transduction efficiency was assessed by co-expression of the cell surface marker ΔCD2 (see also section 7.2.6) through flow cytometry. More than 95% of the cells were infected (Figure 4-20A). Moreover, the protein amount of stably expressed OTULIN was checked by WB and compared to the expression of endogenous OTULIN in the parental cell line (Figure 4-20B). Reconstituted cells expressed OTULIN, even though at slightly reduced levels compared to Jurkat T cells.

Subsequently, Strep-PDs from extracts of the mock- and SSF-OTULIN-reconstituted cells were performed in triplicate and sent to Adan Fernandez and Sarah Bonham for LC-MS/MS analysis (Benedikt M. Kessler group, University of Oxford). We compared the enriched interactome in samples of mock and OTULIN-reconstituted cells and observed that SNX27 was again highly enriched in the presence of OTULIN (Figure 4-20C). The identified interaction of SSF-OTULIN and SNX27 was also verified by WB analysis (Figure 4-20D). HOIP was not identified, which might be due to the fact that the N-terminal SSF-tag of OTULIN impairs HOIP binding at the OTULIN N-terminus.

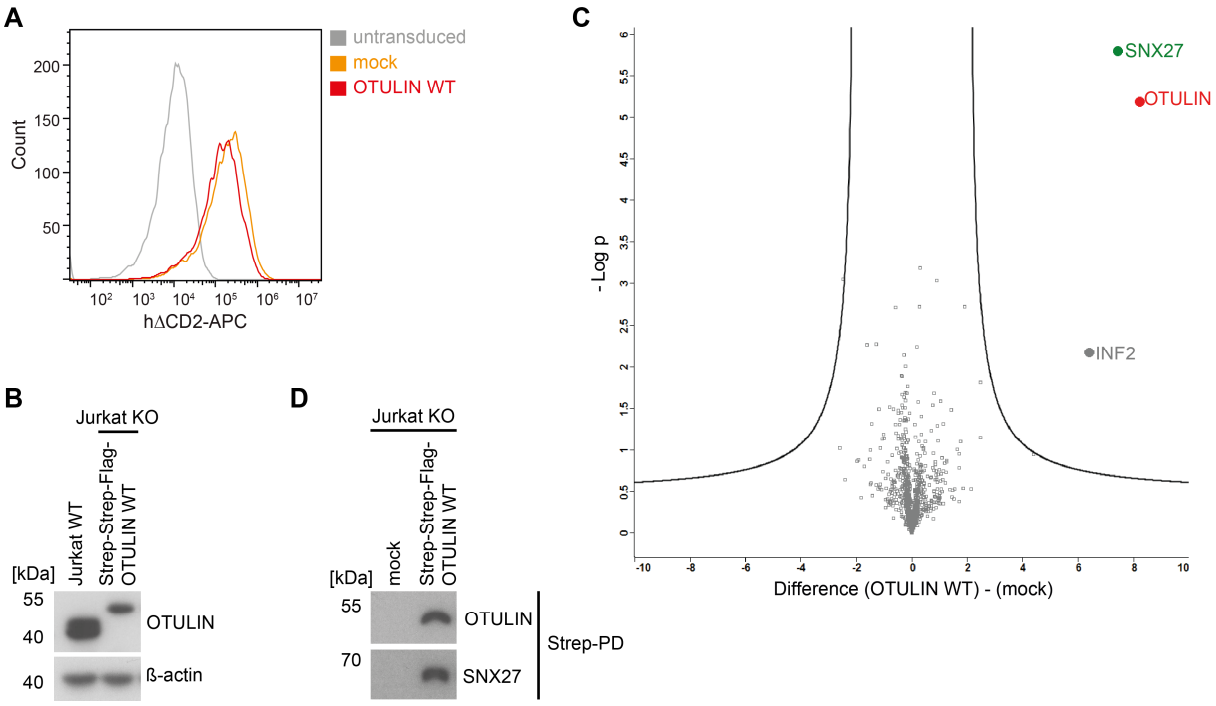

Figure 4-20: OTULIN interacts with SNX27 in reconstituted KO cells.
A) Transduction efficiency was determined by co-expression of the cell surface marker ΔCD2 by flow cytometry. Negative control: untransduced OTULIN-deficient Jurkat T cells.
B) SSF-OTULIN expression of lentivirally reconstituted cells was checked by WB and compared to endogenous OTULIN expression in Jurkat WT cells.
C) Volcano plot demonstrating the significant enrichment of identified proteins after Strep-PD from extracts of SSF-OTULIN or mock expressing reconstituted OTULIN-deficient Jurkat T cells. Curves depict significant enrichment or depletion, respectively. Illustration provided by A. Fernandez (Benedikt M. Kessler group, University of Oxford).
D) Verification of the OTULIN-SNX27 interaction by WB analysis of the Strep-PDs.

This second and OTULIN ABP-independent approach for the identification of OTULIN interactors revealed that the OTULIN-SNX27 interaction in Jurkat T cells is also detected by direct OTULIN precipitation.

4.2.4 Human and murine OTULIN-SNX27 interaction is not cell type-specific

To ascertain whether the OTULIN-SNX27 interaction is T cell-specific, immunoprecipitations (IPs) of OTULIN or SNX27 were performed from extracts of different cell lines and tested for co-IP of the respective binding partner (Figure 4-21). OTULIN could be isolated efficiently from human and murine cell extracts using anti-OTULIN antibody (Figure 4-21A and B). As expected, SNX27 co-precipitated with OTULIN from Jurkat extracts (Figure 4-21A). In the isotype control, both OTULIN and SNX27 were not pulled down, proving specificity of the IP.

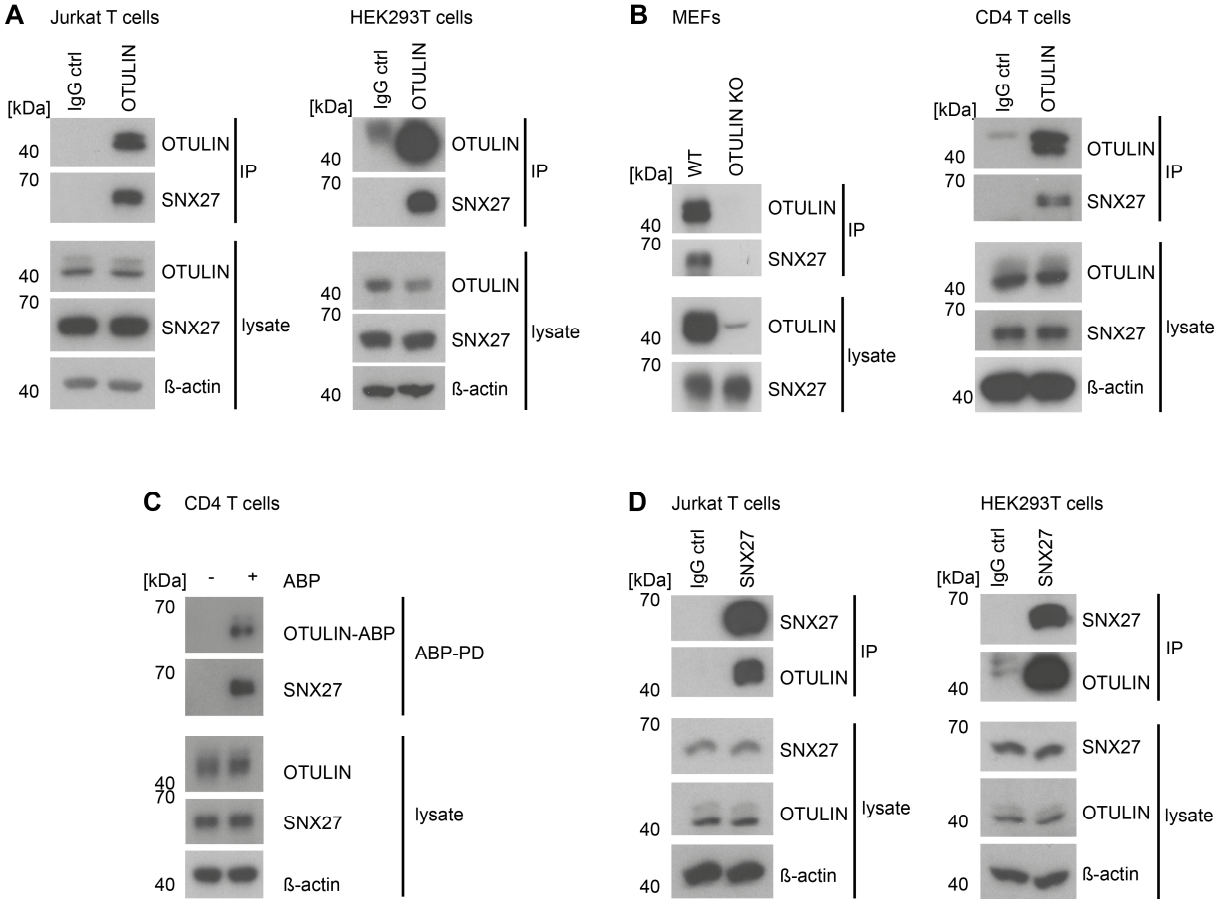

Figure 4-21: OTULIN interacts with SNX27 in different human and murine cell lines.
A) OTULIN-IP from extracts of $5x10^7$ Jurkat and HEK293T cells. As isotype control, rabbit IgG antibody was used. OTULIN enrichment and co-IP of SNX27 were analyzed by WB.
B) OTULIN-IP was performed as in A) from extracts of OTULIN KO MEFs / ctrl MEFs ($2.5x10^7$ cells) or isloated murine primary CD4 T cells ($5x10^7$ cells).
C) ABP-PD from murine primary CD4 T cell extracts ($2x10^7$ cells/sample; 2 µg OTULIN ABP). Interaction of the murine OTULIN-ABP complex with SNX27 was assessed by WB.
D) SNX27-IP from extracts of $5x10^7$ Jurkat and HEK293T cells. As isotype control, mouse IgG antibody was used. SNX27 enrichment and co-IP of OTULIN were analyzed by WB.

SNX27 also co-precipitated with OTULIN from extracts of HEK293T cells (Figure 4-21A), mouse embryonic fibroblasts (MEFs) and murine primary CD4 T cells (Figure 4-21B). Additionally, SNX27 was pulled out of the primary CD4 T cell lysates together with active OTULIN through an OTULIN ABP-PD (Figure 4-21C). Vice versa, SNX27 could also be efficiently enriched from Jurkat and HEK293T cell extracts by IP using anti-SNX27 antibody and OTULIN co-precipitated with SNX27 (Figure 4-21D). These results reveal that the OTULIN-SNX27 interaction exists in several human and murine cell lines as well as in primary cells.

4.2.5 OTULIN interacts with the SNX27 PDZ domain via a canonical PDZbm

SNX27 is involved in the fast transport of internalized cargos, like cell surface receptors and transmembrane transporters, back to the plasma membrane (Gallon and Cullen, 2015). The recycled cargos and other cytosolic proteins have been shown to bind the PDZ domain of SNX27 via a C-terminal class I PDZ-binding motif (PDZbm) with the consensus sequence X-[Thr/Ser]-X-Φ (X - any aa, Φ - aa with a bulky hydrophobic residue) (Gallon and Cullen, 2015; Lunn et al., 2007). An alignment of OTULIN amino acid sequences of different tetrapods indicated that a putative class I PDZbm also exists in the OTULIN C-terminus (Figure 4-22A). In human OTULIN this motif is formed by the last four amino acids, Glu-Thr-Ser-Leu (ETSL, aa 349-352).

To map the interaction sites of OTULIN and SNX27, different 3xFlag-tagged (Flag-)OTULIN mutants were generated by site-directed mutagenesis: One construct encoded C-terminally truncated OTULIN (aa 1-348, OTULIN ΔETSL), lacking the putative PDZbm. Other constructs encoded catalytically inactive OTULIN (C129A), the Ub-binding mutant (W96A), the HOIP-binding mutant (Y56F), or the OTU domain of OTULIN only ($OTULIN_{cat,}$ aa 80-352) (Figure 4-22A). All constructs were transiently overexpressed along with GFP-SNX27 in HEK293 cells and immunoprecipitated after lysis using anti-Flag antibody (Figure 4-22B). WB analysis demonstrated that all proteins were expressed at equivalent levels. As expected GFP-SNX27 was co-immunoprecipitated with OTULIN WT. The Y56F mutation in the OTULIN N-terminus, which abrogates HOIP binding to OTULIN (Elliott et al., 2014), did not impair the association of SNX27. The fact that both the OTU domain ($OTULIN_{cat}$) and catalytically inactive OTULIN (C129A) strongly interacted with SNX27, indicated that neither the N-terminus (aa 1-79) of OTULIN nor its catalytic activity are required for binding. It appears that only slightly less SNX27 bound the Ub-binding mutant W96A. However, it is well established that mutations at the site of Trp96 perturb the OTU domain structure (Rivkin, 2013), which might also affect SNX27 binding.

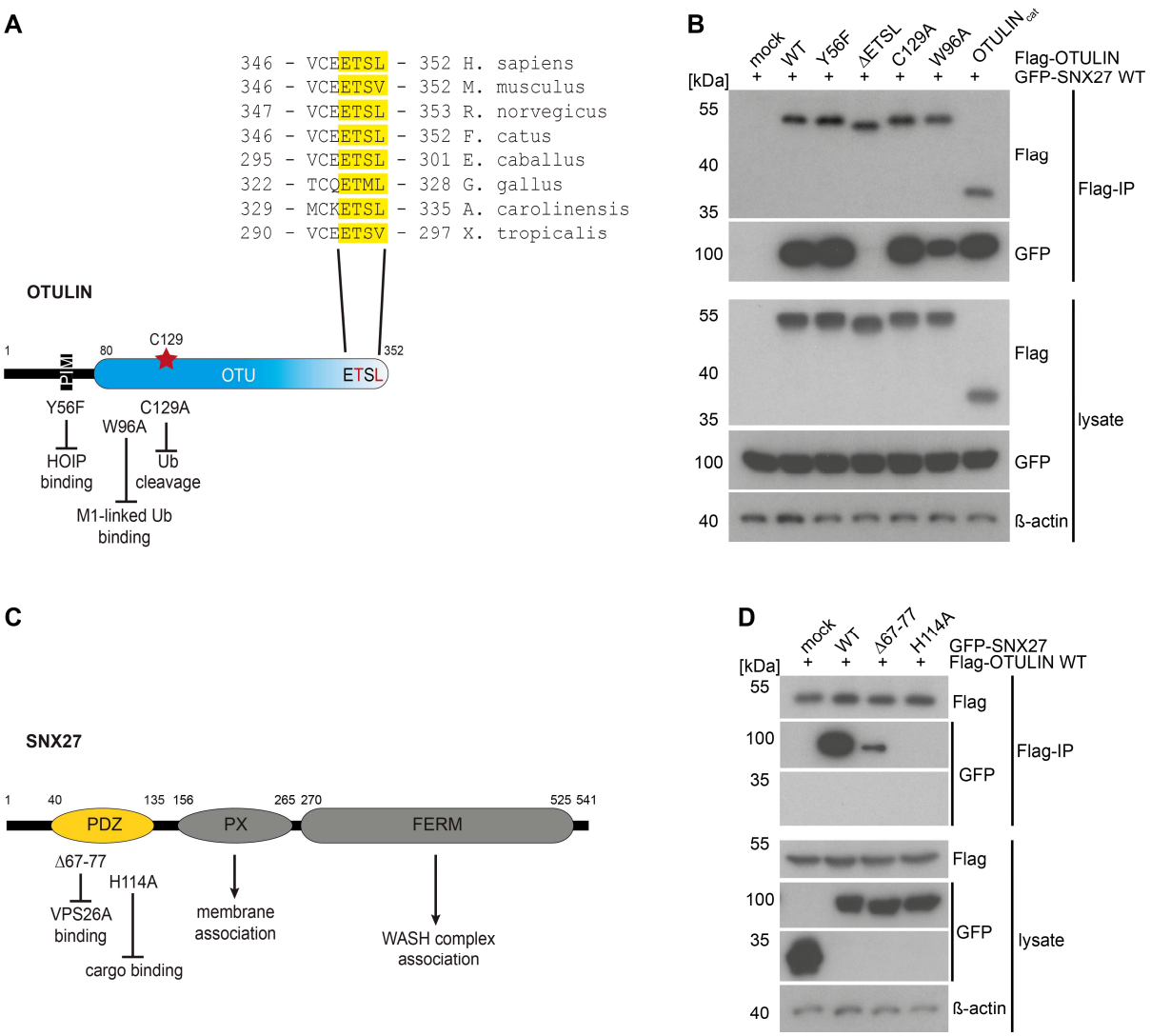

Figure 4-22: Canonical PDZ-PDZbm interaction mediates the SNX27-OTULIN association.
A) Schematic of OTULIN with a sequence alignment of OTULIN homologs of different tetrapods, revealing the existence of a conserved putative class I PDZbm. Protein sequences were retrieved from the Ensembl database, release 94 (Zerbino et al., 2018).
B) HEK293 cells were co-transfected with different Flag-OTULIN constructs and GFP-SNX27 as indicated. After lysis, co-IPs were performed using anti-Flag antibody and tested for the OTULIN-SNX27 interaction by WB.
C) Schematic representation of SNX27.
D) Experiment was performed as in B) after co-overexpression of different GFP-SNX27 constructs and Flag-OTULIN in HEK293 cells.

A complete loss of the SNX27 interaction was only achieved by deletion of the putative PDZbm in OTULIN ΔETSL (Figure 4-22B). This proves that OTULIN indeed contains a C-terminal PDZbm that is indispensable for the interaction with SNX27.

SNX27 is the only sorting nexin that has a PDZ domain. Via this PDZ domain (Figure 4-22C), SNX27 binds, on the one hand, cargos and, on the other hand, the retromer complex composed of VPS26, VPS35 and VPS29. It has previously been demonstrated that a mutation of His114 to Ala prevents binding to cargos and that a partial deletion of the β3-β4 loop (Δ67-77) destroys the retromer interaction (Gallon et al., 2014; Lauffer et al., 2010). To

confirm the PDZ-PDZbm interaction between SNX27 and OTULIN, GFP-SNX27 WT and these mutants were overexpressed together with Flag-OTULIN WT in HEK293 cells and subjected to Flag co-IPs (Figure 4-22D). While again a strong interaction between the WT proteins could be detected, this interaction was abolished by the H114A mutation in SNX27. Deletion of the β3-β4 hairpin loop (Δ67-77) also attenuated SNX27 binding to OTULIN, which indicates that additional surfaces besides the PDZ-PDZbm interface may be involved in SNX27-OTULIN binding.
These data reveal that the binding of SNX27 to OTULIN is mediated by a canonical PDZ-PDZbm interaction, as is the case with classical cargos, and potentially by an additional interface.

To obtain more insights into the association of SNX27 and OTULIN, our collaboration partner Paul Elliott (MRC, Cambridge; University of Oxford) determined the structure of the catalytically inactive OTU domain of OTULIN ($OTULIN_{cat}$ C129A) in complex with the PDZ domain of SNX27 ($SNX27_{PDZ}$, aa 40-135) by X-ray crystallography at 2 Å resolution (Figure 4-23A and B). Electron density corresponding to the PDZbm could be unambiguously assigned for the entire C-terminus of OTULIN. Indeed, this C-terminus provides the main interaction surface for the PDZ domain of SNX27 (Figure 4-23A). The major part of $OTULIN_{cat}$ including the catalytic site is not located in close proximity to $SNX27_{PDZ}$, explaining why the binding to SNX27 could be identified by means of the active site-directed diUb probe.
A close-up view of the PDZ-PDZbm interface (Figure 4-23B) revealed that the OTULIN PDZbm is bound in a canonical orientation identically to the previously described SNX27-binding peptides of cargos like diacylglycerol kinase ζ (DGKζ) (Clairfeuille et al., 2016). SNX27 His114, which was shown to be essential for cargo binding (Lauffer et al., 2010), forms hydrogen bonds to the peptide backbone of the OTULIN PDZbm and also to OTULIN Thr350, explaining the strict necessity of this interaction for complex assembly (Figure 4-23B).
Additionally, Paul Elliott (MRC, Cambridge; University of Oxford) performed isothermal calorimetry (ITC) experiments and measured a K_D of 1.1 ± 0.035 µM for the OTULIN PDZbm peptide (Ac-VRVCEETSL) and $SNX27_{PDZ}$ (Figure 4-23C). So far, the PDZbm peptides of DGKζ and PHLPP1 (PH Domain and Leucine Rich Repeat Protein Phosphatase 1) display the highest affinities for $SNX27_{PDZ}$ with a K_D of approximately 2 µM (Clairfeuille et al., 2016). This reveals that the affinity of the OTULIN PDZbm peptide for $SNX27_{PDZ}$ is approximately twice as high as the affinity of any other previously analyzed cargo peptide. With a K_D of 0.031 ± 0.014 µM, the determined binding affinity of the entire $OTULIN_{cat}$ for $SNX27_{PDZ}$ was

more than 30 times higher than the affinity of the isolated C-terminal peptide (Figure 4-23C) and the highest ever reported affinity for a SNX27 PDZ domain interaction (Clairfeuille et al., 2016). This indicated once again that there might be a potential second interface between OTULIN and SNX27. No binding could be detected in ITC studies between $SNX27_{PDZ}$ and $OTULIN_{cat}$ ΔETSL, confirming the finding from the co-IP studies that the PDZbm controls the association of OTULIN with SNX27 (see Figure 4-22B).

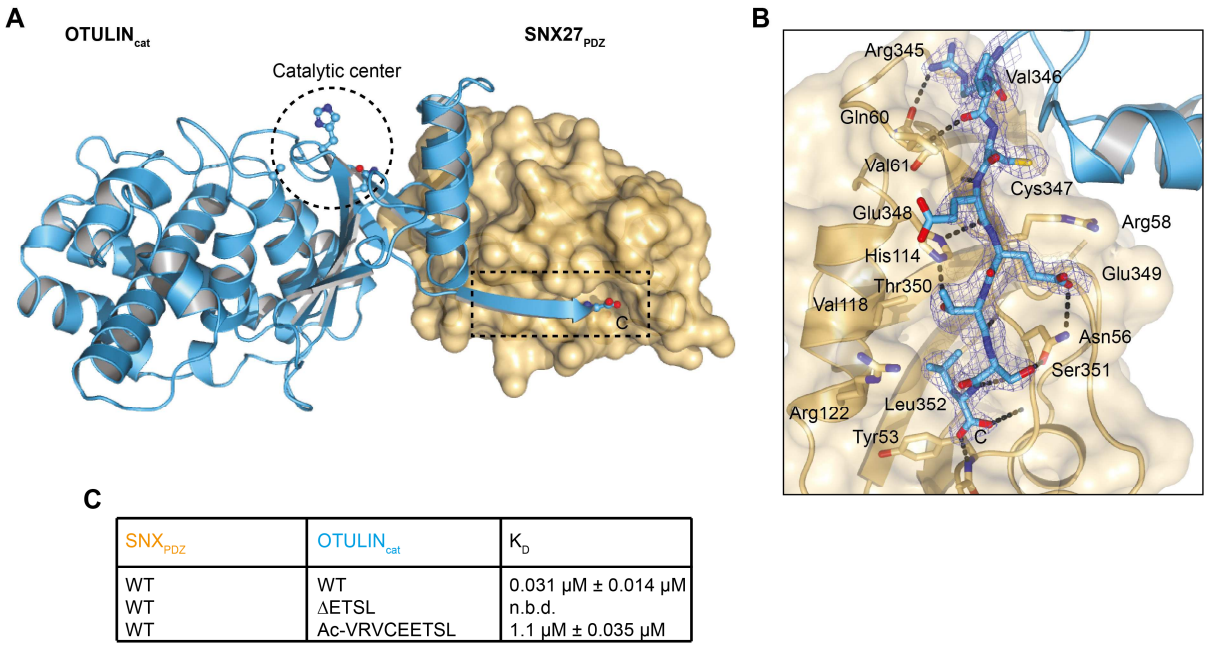

C

SNX_{PDZ}	$OTULIN_{cat}$	K_D
WT	WT	0.031 µM ± 0.014 µM
WT	ΔETSL	n.b.d.
WT	Ac-VRVCEETSL	1.1 µM ± 0.035 µM

Figure 4-23: Structural analysis of the OTULIN-SNX27 complex.
A) Structure of the OTULIN-SNX27 complex. SNX_{PDZ} (aa 40-135) is rendered in surface representation (yellow) with $OTULIN_{cat}$ (aa 80–352, blue) depicted as ribbon. Circle: catalytic center, rectangle: PDZ-PDZbm interaction site.
B) Close-up view of the PDZ-PDZbm interface. C-terminal OTULIN peptide (aa 345-352) is rendered in stick representation (blue) on $SNX27_{PDZ}$ (yellow).
C) Binding affinities of $OTULIN_{cat}$ or the C-terminal PDZbm peptide and $SNX27_{PDZ}$ determined by ITC.
Illustrations and ITC data are provided by P. Elliott (MRC, Cambridge; University of Oxford).

4.2.6 Second interface mediates the high-affinity interaction between OTULIN and SNX27

Besides the canonical PDZ-PDZbm interaction, Paul Elliott (MRC, Cambridge; University of Oxford) identified a second OTULIN-SNX27 interface (Figure 4-24A), which involves parts of the SNX27 β3-β4 loop (aa 67-79). Deletion of this loop, which is unique for the SNX27 PDZ domain, and which is required for VPS26A binding (Gallon et al., 2014), impaired OTULIN binding in previous experiments (see Figure 4-22D). The second interface comprises hydrogen bonds between the side chain carboxyl groups of OTULIN Glu85, Asp87 and Asp90, and Arg68 and Arg100 in SNX27 (Figure 4-24A). Additional important hydrogen bonds were established between OTULIN Glu209 and the amide backbone of SNX27 Gly64. Single mutations of OTULIN Asp87 or Glu85 to Arg decreased the binding affinity of OTULIN

for SNX27 in ITC studies approximately 10- to 30-fold (Figure 4-24B). Single mutations of SNX27 Gly64 or Arg100 to Glu likewise reduced binding affinities tenfold. A combination of both mutations in either $SNX27_{PDZ}$ or $OTULIN_{cat}$ resulted in K_D values of 1.09 ± 0.007 µM or 2.07 ± 0.12 µM, respectively (Figure 4-24B). These values closely resemble the binding affinity of the isolated OTULIN PDZbm peptide for $SNX27_{PDZ}$ (K_D of 1.1 ± 0.035 µM; see Figure 4-23C). This suggests that the second OTULIN-SNX27 interface mainly contributes to the high-affinity interaction of the two proteins.

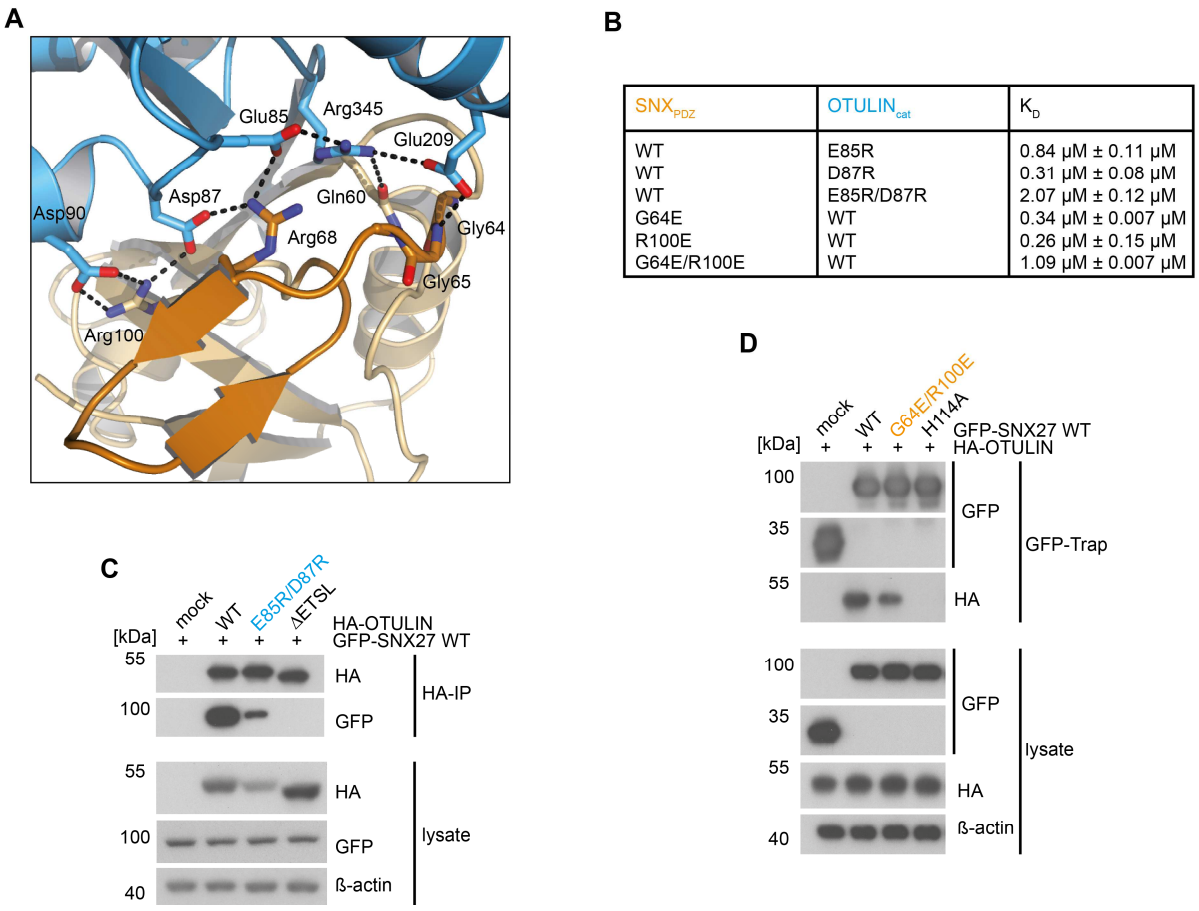

Figure 4-24: Second non-canonical interface.
A) Close-up view of the second OTULIN-SNX27 interface (OTULIN – blue, SNX27 – orange). Relevant residues are shown in stick format, dashed lines indicate hydrogen bonds. Illustration provided by P. Elliott (MRC, Cambridge; University of Oxford).
B) Summary of binding affinities of $SNX27_{PDZ}$ and $OTULIN_{cat}$ mutants determined by ITC (P.Elliott, MRC, Cambridge; University of Oxford). Mutations were designed based on the structure of the second interface.
C) and D) Extracts of HEK293 cells expressing different HA-OTULIN or GFP-SNX27 constructs (as indicated) were subjected to immunoprecipitations. Differences in OTULIN-SNX27 association were determined by WB.

Co-IP experiments confirmed that the overexpressed OTULIN E85R/D87R mutant bound considerably more weakly to GFP-SNX27 WT in comparison to WT OTULIN (Figure 4-24C). However, since the PDZ-PDZbm complex could still be formed, only deletion of the PDZbm in OTULIN resulted in the complete loss of the interaction. In GFP-Traps, less HA-OTULIN was co-precipitated by overexpressed GFP-SNX27 G64E/R100E than by WT SNX27 (Figure 4-24D). Again, complete abrogation of the OTULIN-SNX27 interaction was only achieved by

mutation of SNX27 at the canonical cargo-binding site (H114A). Altogether, these results reveal that the canonical PDZbm-PDZ interaction is essential for binding of OTULIN to SNX27 and that a second non-canonical interface considerably contributes to strengthening the interaction.

4.3 OTULIN counteracts SNX27-dependent cargo recycling

4.3.1 OTULIN competes with the VPS26 subunit of the retromer for binding to SNX27

ABP-PDs of active OTULIN as well as Strep-PDs of OTULIN from cell extracts of OTULIN-reconstituted cells led to the identification of SNX27 as OTULIN interaction partner (see sections 4.2.1 and 4.2.3). However, association of OTULIN with components of the retromer complex (VPS26, VPS35) or the WASH complex (WASH1) were not detected in any experiment although these proteins are known SNX27 interactors (Gallon and Cullen, 2015). The studies of the second non-canonical OTULIN-SNX27 interface moreover demonstrated that OTULIN interacts with SNX27 very closely to the β3-β4 loop, and forms hydrogen bonds, for example, with Gly64 before the loop and Arg68 within the loop (see section 4.2.6). However, SNX27 Arg68 is also implicated in binding of VPS26A (Gallon et al., 2014), suggesting that the interaction surfaces of OTULIN and VPS26A with SNX27 partially overlap and that a simultaneous binding of all three proteins is unlikely (Figure 4-25A).

To check whether a ternary OTULIN-SNX27-VPS26A complex could form in cells, different HA-OTULIN constructs were expressed together with Flag-VPS26A and GFP-SNX27 in HEK293 cells. GFP-SNX27 interacted with Flag-VPS26A just as with HA-OTULIN after the respective double transfection (Figure 4-25B). Upon simultaneous expression of all three constructs, however, SNX27 lost the binding to VPS26A and only interacted with OTULIN. This effect was independent of OTULIN´s deubiquitinating activity (C129A) but dependent on the canonical interaction between SNX27 and OTULIN. By deleting the OTULIN PDZbm (OTULIN ΔETSL), the OTULIN-SNX27 interaction was abrogated and the effect on VPS26-SNX27 binding was reversed. In line with this, association of the endogenous retromer components VPS26 and VPS35 with overexpressed SNX27 was diminished upon co-overexpression OTULIN WT and C129A, whereas OTULIN ΔETSL did not impair the interaction (Figure 4-25C).

These results indicate that binding of OTULIN and VPS26 to SNX27 are mutually exclusive, and that OTULIN competes with VPS26 for complex formation with SNX27. This implicates that OTULIN cannot be a cargo of the SNX27-retromer complex, although it binds to SNX27 in a similar manner to known cargos.

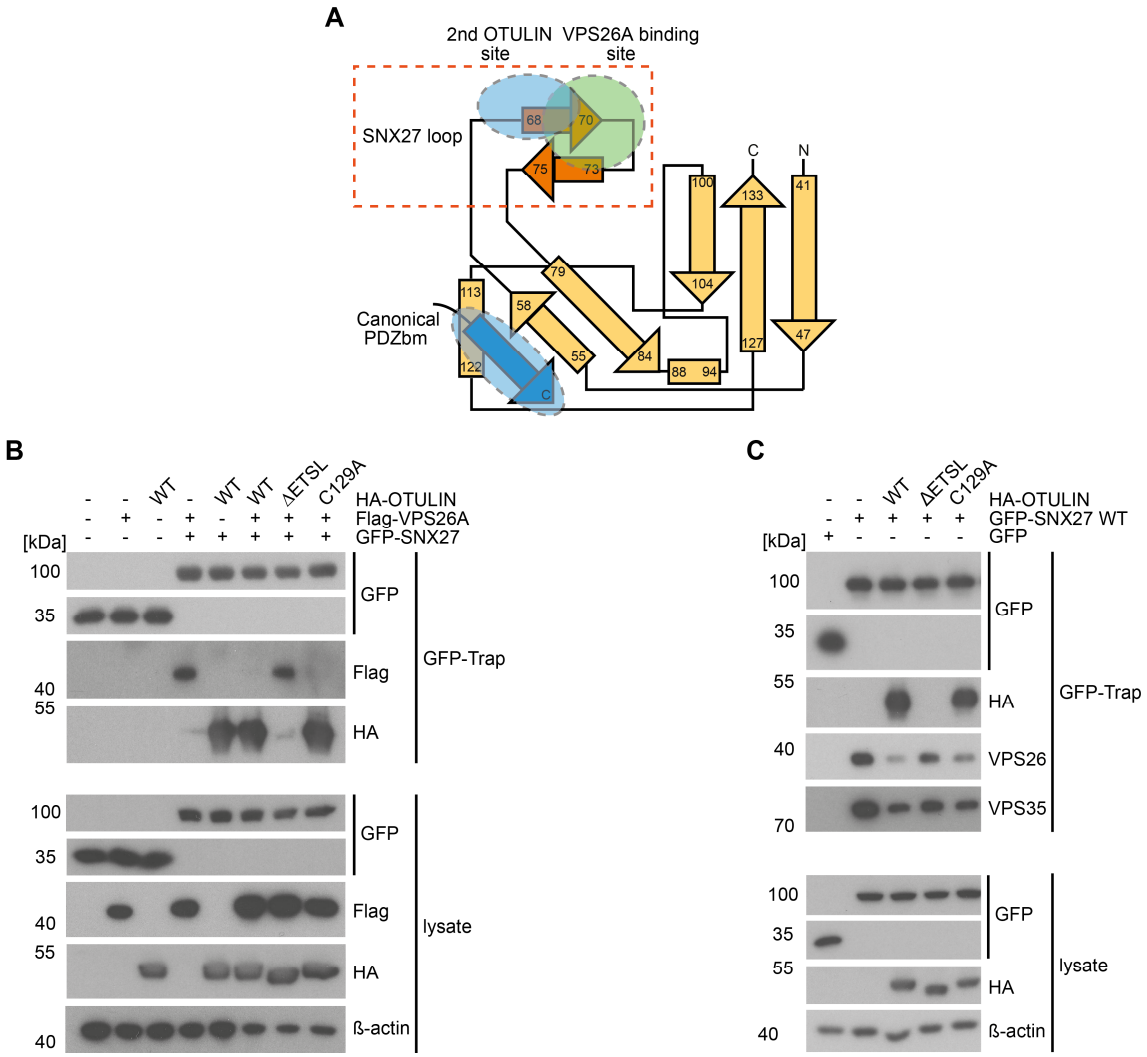

Figure 4-25: Binding of OTULIN and VPS26 to SNX27 is mutually exclusive.
A) Topology diagram of $SNX27_{PDZ}$. The OTULIN PDZbm and other class I PDZbms bind to the canonical cargo-binding site in SNX27. VPS26A and OTULIN (second interface) binding sites at the β3-β4 loop partially overlap. Illustration provided by P. Elliott (MRC, Cambridge; University of Oxford).
B) HEK293 cells were co-transfected with GFP-SNX27, Flag-VPS26A and HA-OTULIN constructs as indicated. After cell lysis, GFP-SNX27 was immunoprecipitated by GFP-Traps and tested for interactions with VPS26A and OTULIN by WB.
C) Experiment was performed as in B) without overexpressing VPS26A. Binding of endogenous VPS26 and VPS35 to GFP-SNX27 was monitored by WB.

4.3.2 OTULIN removes SNX27 from early endosomes

To determine the cellular localization of OTULIN-SNX27 complexes, RFP-OTULIN and GFP-SNX27 were overexpressed in U2OS cells and subjected to confocal fluorescence microscopy. As it has been previously reported (Cai et al., 2011; Rincon et al., 2007), GFP-SNX27 co-localized with the protein EEA1 and is thus mainly associated with early endosomes (Figure 4-26A). Upon co-overexpression of RFP-OTULIN, however, GFP-SNX27 lost its distinct association with early endosomes and became evenly distributed throughout the cytoplasm where it co-localized with OTULIN (Figure 4-26B).

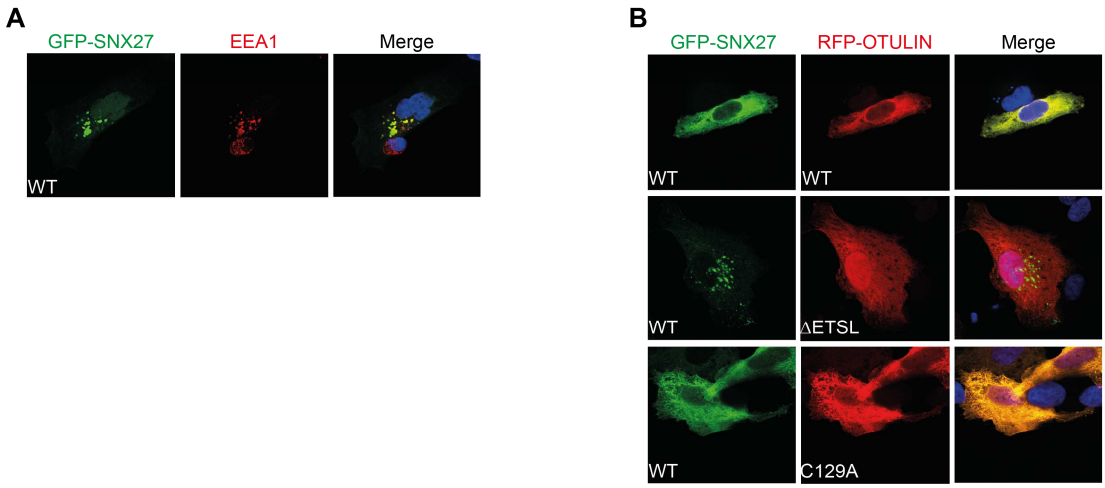

Figure 4-26: OTULIN removes SNX27 from early endosomes.
A) GFP-SNX27 was expressed in U2OS cells. Cells were immunostained for EEA1 (red) and co-localization of SNX27 with EEA1 was analyzed by confocal fluorescence microscopy.
B) RFP-OTULIN WT, ΔETSL or C129A was expressed together with GFP-SNX27 in U2OS cells and localization was analyzed by confocal fluorescence microscopy.

Catalytically inactive OTULIN affected the cellular distribution of SNX27 in a similar manner. Again, deletion of the PDZbm in OTULIN ΔETSL prevented detachment of SNX27 from the early endosomes and the even distribution of SNX27 throughout the cytoplasm. Thus, OTULIN is able to remove SNX27 from the early endosomal sorting compartment.

4.3.3 Formation of a ternary HOIP-OTULIN-SNX27 complex

As OTULIN interacts with HOIP via its N-terminal PIM (Elliott et al., 2014; Schaeffer et al., 2014) and with SNX27 through its C-terminal PDZbm, we wanted to know whether a ternary complex may form. To answer this question, GFP-SNX27, HA-HOIP and different Flag-OTULIN constructs were co-expressed in HEK293 cells. GFP-SNX27 was immunoprecipitated from extracts by GFP-Traps and its association to HOIP and OTULIN, respectively, was assessed by WB. Upon co-expression of all three proteins, a ternary HOIP-OTULIN-SNX27 complex could be detected (Figure 4-27). Expression of the SNX27-binding mutant (ΔETSL) or the HOIP-binding mutant (Y56F) of OTULIN prevented the formation of a complex, confirming that OTULIN bridges the indirect interaction between SNX27 and HOIP. A very weak interaction between HA-HOIP and GFP-SNX27 was already detectable without overexpression of OTULIN, most likely mediated by endogenous OTULIN.
Thus, the two binding sites of SNX27 and HOIP in the OTULIN molecule might enable ternary complex formation in cells as a result of their physical distance.

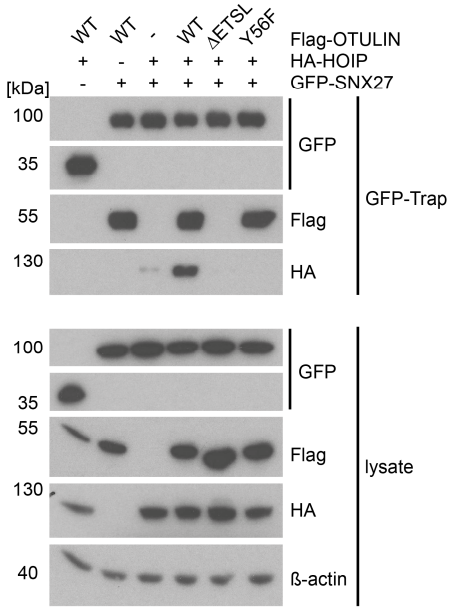

Figure 4-27: OTULIN can simultaneously interact with SNX27 and HOIP.
HEK293 cells were co-transfected with GFP-SNX27, HA-HOIP and different Flag-OTULIN constructs as indicated. After lysis, GFP-SNX27 was immunoprecipitated by GFP-Traps and analyzed for its association with OTULIN and HOIP by WB.

4.3.4 The endogenous OTULIN-SNX27 complex is predominantly not LUBAC-associated

Knowing that a ternary HOIP-OTULIN-SNX27 complex can basically exist in cells (section 4.3.3), we wanted to determine whether an endogenous ternary complex consisting of HOIP, OTULIN and SNX27 could be formed. To this end, extracts of Jurkat T cells were separated by analytical size exclusion chromatography (Figure 4-28A). As it has been previously observed (Elliott et al., 2014), only a very small proportion of OTULIN co-migrated with HOIP, which eluted in fractions 4-7 at an apparent MW of approximately 400-670 kDa (Figure 4-28A). SNX27 also did not co-migrate with HOIP for the most part, suggesting that, if at all, an endogenous ternary complex exists at low levels. Interestingly, SNX27 also barely co-eluted with the two retromer components VPS26 and VPS35, which eluted in fractions 8-11, corresponding to an apparent MW of approximately ~130-400 kDa. Importantly, the majority of cellular SNX27 eluted together with OTULIN in fractions 12-14 at an apparent MW of ~44-130 kDa. Thus, peak elution profiles of OTULIN (~42 kDa) and SNX27 (~61 kDa) closely resemble a complex with a molecular mass of ~100 kDa. This would be the expected size for an OTULIN-SNX27 complex consisting of two monomers as seen in the crystal structure.

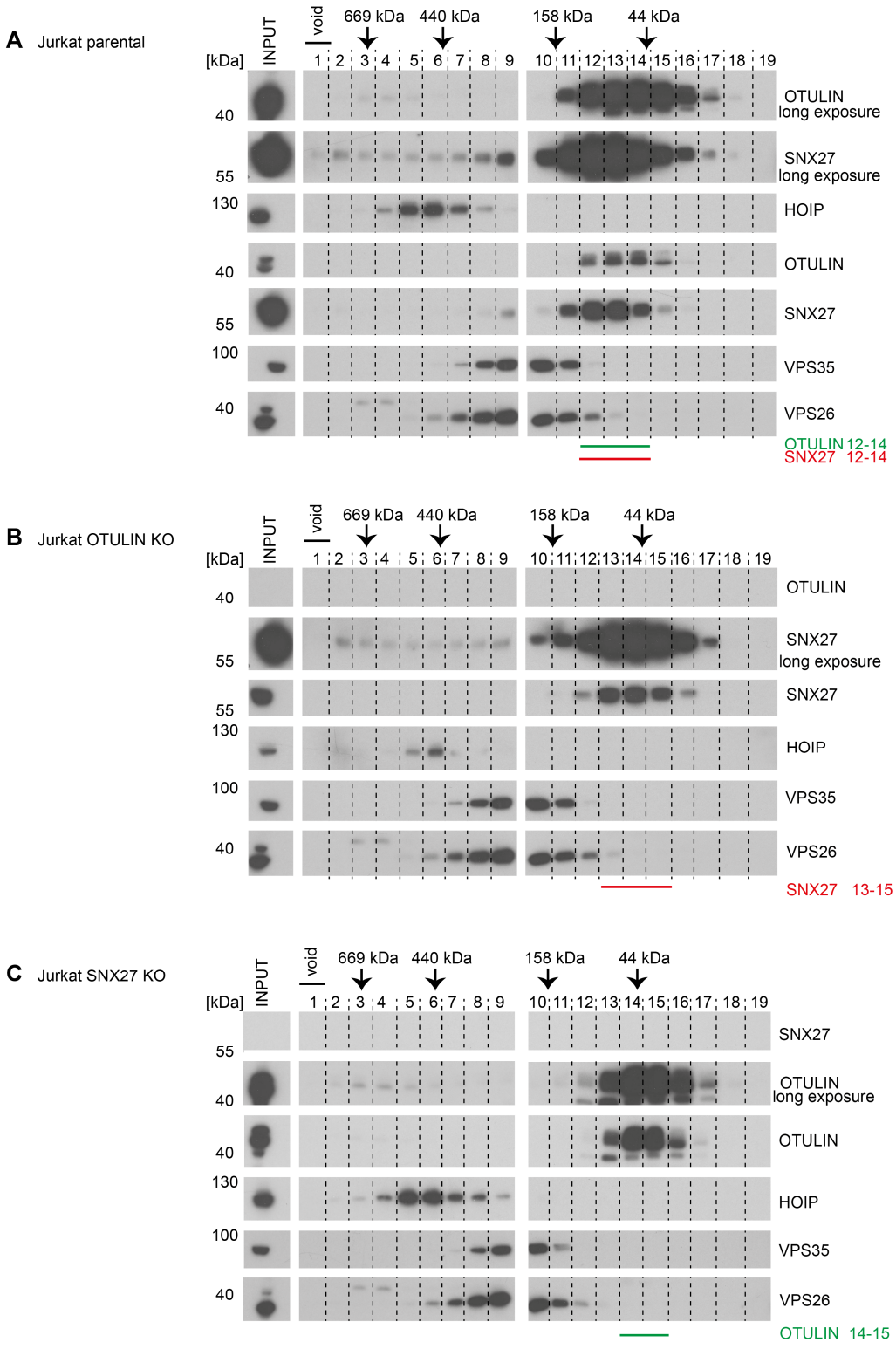

Figure 4-28: Gel filtration analysis of parental and KO Jurkat T cell extracts.
Extracts from parental (A), OTULIN-deficient (B) or SNX27-deficient (C) Jurkat T cells were fractionated by analytical size exclusion chromatography. Elution profiles of the indicated proteins were determined by WB.

To confirm these results, gel filtration analysis of extracts from OTULIN- or SNX27-deficient Jurkat T cells was performed (Figure 4-28B and C). Elution peaks of OTULIN and SNX27

shifted to a lower MW by 1 or 2 fractions. OTULIN eluted in the absence of SNX27, in fractions 14 and 15 at an apparent MW of about 44 kDa (Figure 4-28C). SNX27 migrated without OTULIN in fractions 13-15 (Figure 4-28B). These shifts approximately correspond to the expected elution profile of OTULIN and SNX27 monomers. Although OTULIN competes with the retromer for SNX27 binding (Figure 4-25), SNX27 was not increasingly detected in the retromer-containing fractions following OTULIN depletion (Figure 4-28B). Further, neither the elution profile of HOIP nor the elution profile of the retromer components shifted in extracts of KO Jurkat T cells.

Thus, analytical size exclusion chromatography experiments indicated that endogenous OTULIN and SNX27 form a stable complex that is mainly not associated with the LUBAC or the retromer complex.

4.3.5 SNX27 does not have an impact on the regulation of Met1-Ub

To investigate whether SNX27 affects the homeostatic control of the Met1-Ub machinery by OTULIN, extracts of different KO clones were analyzed for HOIP levels and basal Met1-Ub levels (Figure 4-29). To this end, OTULIN- and SNX27-deficient HEK293 cells were additionally generated analogous to the Jurkat KO cell lines (section 4.2.2, Figure 4-18).

As it has been previously described (Damgaard et al., 2016), depletion of OTULIN led to downregulation of HOIP in Jurkats, as well as in HEK293 cells (Figure 4-29A and B). By contrast, HOIP levels were not reduced in SNX27-deficient cells. SNX27-deficient HEK293 clones even displayed slightly increased HOIP expression, but this effect could not be observed in SNX27 KO Jurkat T cells.

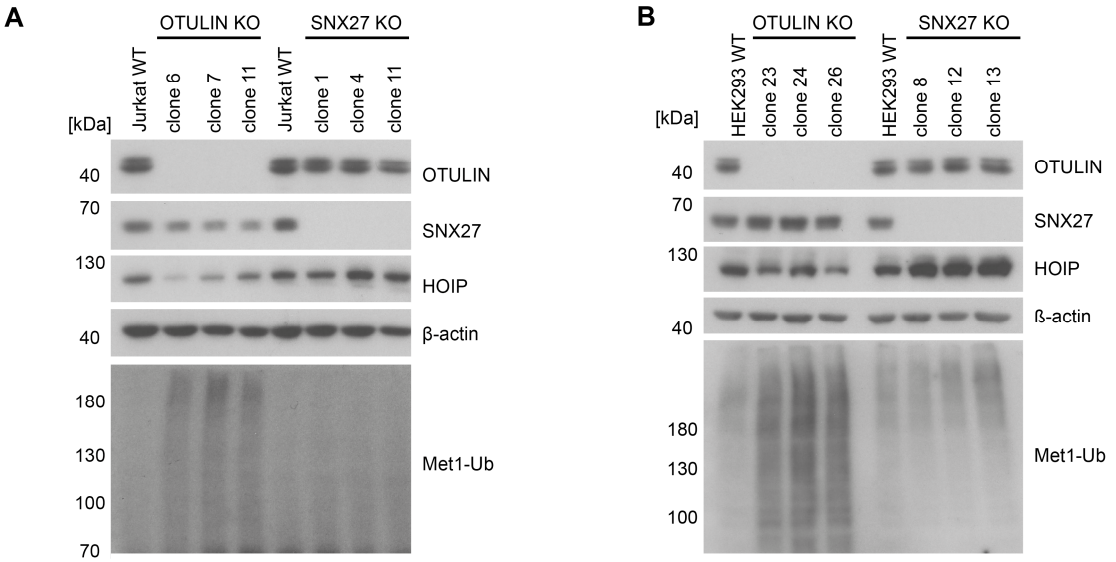

Figure 4-29: SNX27 deficiency does not result in accumulation of Met1-Ub.
Extracts of parental, OTULIN-deficient and SNX27-deficient Jurkat T cells (A) or HEK293 cells (B), respectively, were analyzed for Met1-Ub and HOIP expression by WB.

In OTULIN-deficient Jurkat T cells, SNX27 expression was reduced, but again this effect could not be detected in OTULIN KO HEK293 clones. These data suggest that the expression of SNX27 is tightly regulated and, depending on the cell type, closely related to the OTULIN expression.
In line with the homeostatic control of cellular Met1-Ub levels by OTULIN, OTULIN-deficient clones from both cell lines displayed an accumulation of linear Ub (Figure 4-29). SNX27 KO clones, however, did not show changes in Met1-Ub levels, indicating that the OTULIN-SNX27 interaction does not play a role in the regulation of Met1-Ub cellular availability.

4.3.6 NF-κB, MAPK and Wnt signaling are not severly affected in OTULIN- and SNX27-deficient Jurkat T cells

Since OTULIN has been implicated in the negative regulation of NF-κB signaling by cleaving Met1-Ub (Damgaard et al., 2016; Keusekotten et al., 2013), we wanted to assess how the absence of OTULIN in OTULIN-deficient Jurkat T cells affects NF-κB activation after stimulation with the pro-inflammatory cytokine TNFα (Figure 4-30A), as well as following CD3/28 co-stimulation (Figure 4-30C).
Stimulation of the parental cell line with TNFα for up to 30 min resulted in NF-κB activation, evident from IκBα phosphorylation and degradation. NF-κB activation was not significantly altered in all OTULIN KO clones (Figure 4-30A). Moreover, neither the reduction of SNX27 (clone 8) nor the complete absence of SNX27 (clones 14, 19, 20) had an impact on NF-κB activation in Jurkat T cells in response to TNFα (Figure 4-30B).
CD3/CD28 co-stimulation of the parental cell line for up to 30 min induced likewise phosphorylation and degradation of IκBα (Figure 4-30C and D). Besides, the MAPK signaling pathway was also activated, evident from ERK phosphorylation. Again, no significant changes in IκBα phosphorylation and degradation or ERK phosphorylation could be observed in OTULIN-deficient Jurkat T cell clones (Figure 4-30C). It has been previously described that SNX27 may be a negative regulator of ERK phosphorylation following TCR/CD28 stimulation in Jurkat T cells (Rincon et al., 2011). However, no significant alterations in ERK phosphorylation became apparent in our SNX27 KO clones in response to CD3/CD28 co-stimulation (Figure 4-30D). IκBα phosphorylation and degradation were also not significantly altered in SNX27-deficient cells.

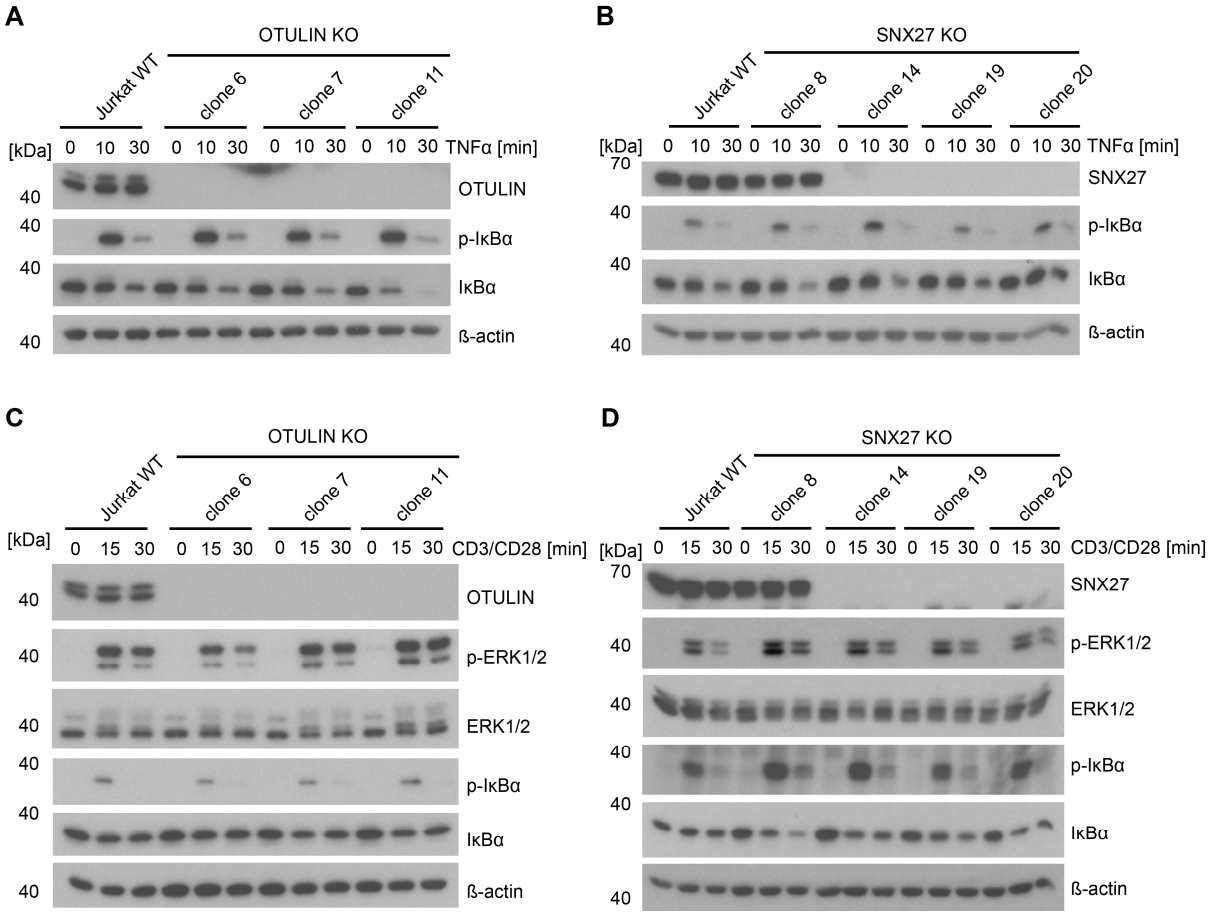

Figure 4-30: Neither NF-κB nor MAPK signaling are affected in OTULIN- and SNX27-deficient in Jurkat T cells.
A & B) OTULIN-deficient (A) or SNX27-deficient (B) Jurkat T cells were stimulated with recombinant TNFα (20 ng/ml) for the indicated times. Extracts were analyzed for NF-κB activation by WB using antibodies against p-IκBα and IκBα.
C & D) OTULIN-deficient (C) or SNX27-deficient (D) Jurkat T cells were stimulated with anti-CD3 and anti-CD28 antibodies for the indicated times. Extracts were analyzed for T cell activation by WB using the indicated antibodies.

OTULIN and SNX27 have been associated with the regulation of canonical Wnt signaling (Rivkin, 2013; Sun et al., 2016; Takiuchi et al., 2014). To study whether loss of OTULIN or SNX27 in Jurkat T cells has an impact on β-catenin stabilization, cells were stimulated with recombinant Wnt3a protein (Figure 4-31). In the parental cell line, stabilization of β-catenin increased steadily within the four-hour stimulation. This stabilization, however, was not reduced, delayed, enhanced, or accelerated in OTULIN- (Figure 4-31A) or SNX27-deficient cells (Figure 4-31B).

Altogether, lack of OTULIN or SNX27 in Jurkat T cells did not have a significant impact on NF-κB signaling following stimulation with TNFα and following CD3/CD28 co-stimulation, respectively. OTULIN and SNX27 KO clones also did not significantly affect β-catenin stabilization following Wnt3a stimulation.

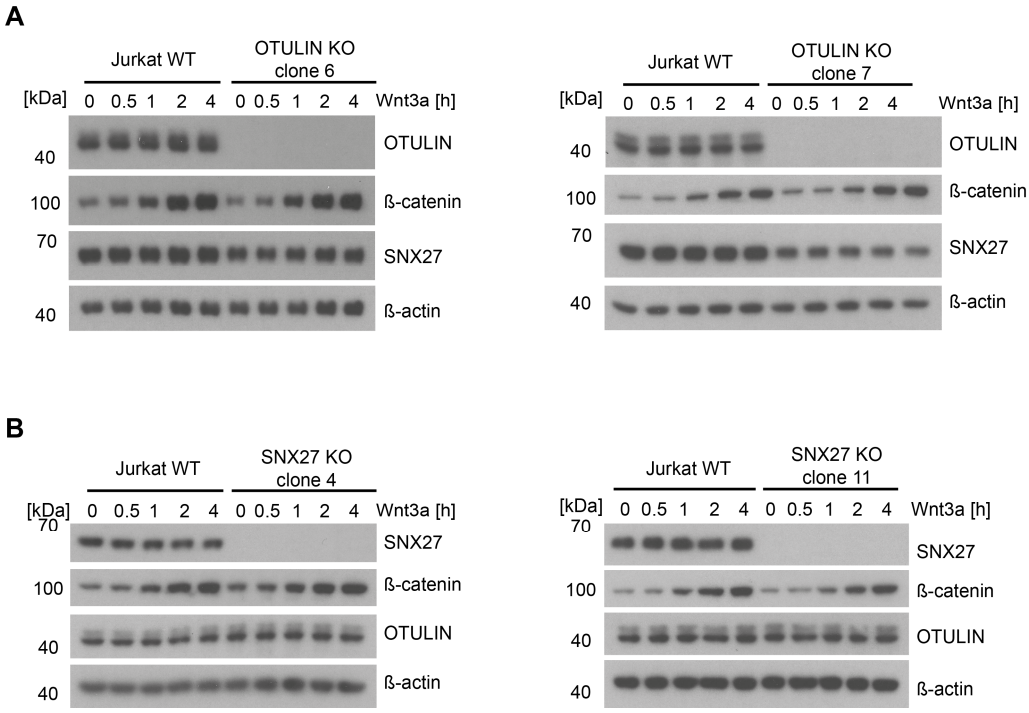

Figure 4-31: β-catenin stabilization is not affected by OTULIN or SNX27 deficiency.
OTULIN-deficient (A), SNX27-deficient (B) or the parental Jurkat T cells were stimulated with recombinant Wnt3a (20 ng/ml) for up to 4 hrs. Activation of the canonical Wnt signaling pathway was monitored by β-catenin stabilization on WBs.

4.3.7 OTULIN counteracts binding of cargos to SNX27

Since OTULIN binds the SNX27 PDZ domain at the same site as PDZbm-containing cargos (see section 4.2.5), we wanted to analyze whether OTULIN interferes with cargo loading of SNX27. To this end, first the attachment of known cargos (Steinberg et al., 2013) to overexpressed GFP-SNX27 was determined in HEK293 cells by GFP-Traps. The previously identified cargos, ATP7A, MRP4, DGKζ, GLUT1 and STEAP3, co-precipitated together with GFP-SNX27 (Figure 4-32A). Cargo binding was either prevented or severly diminished by mutating His114 in the canonical PDZbm binding pocket.

Upon co-expression of HA-OTULIN, not only the SNX27-retromer interaction, but also association of SNX27 to PDZbm-containing cargos like ATP7A, MRP4, DGKζ, GLUT1 and STEAP3, were reduced (Figure 4-32B). Prevention of the OTULIN-SNX27 interaction by deletion of the PDZbm in OTULIN abolished this effect. Interestingly, catalytically inactive OTULIN C129A still counteracted cargo binding to SNX27, however, it was less effective than OTULIN WT (Figure 4-32B). Since catalytically inactive OTULIN is a strong Ub binder (Keusekotten et al., 2013), we wanted to exclude that this Ub binding impairs the ability of OTULIN to counter cargo binding to SNX27. Indeed, the C129A/L259E mutant, which is catalytically dead and fails to bind Met1-Ub (Keusekotten et al., 2013), could restrict cargo binding to SNX27 to the same extent as WT OTULIN (Figure 4-32B).

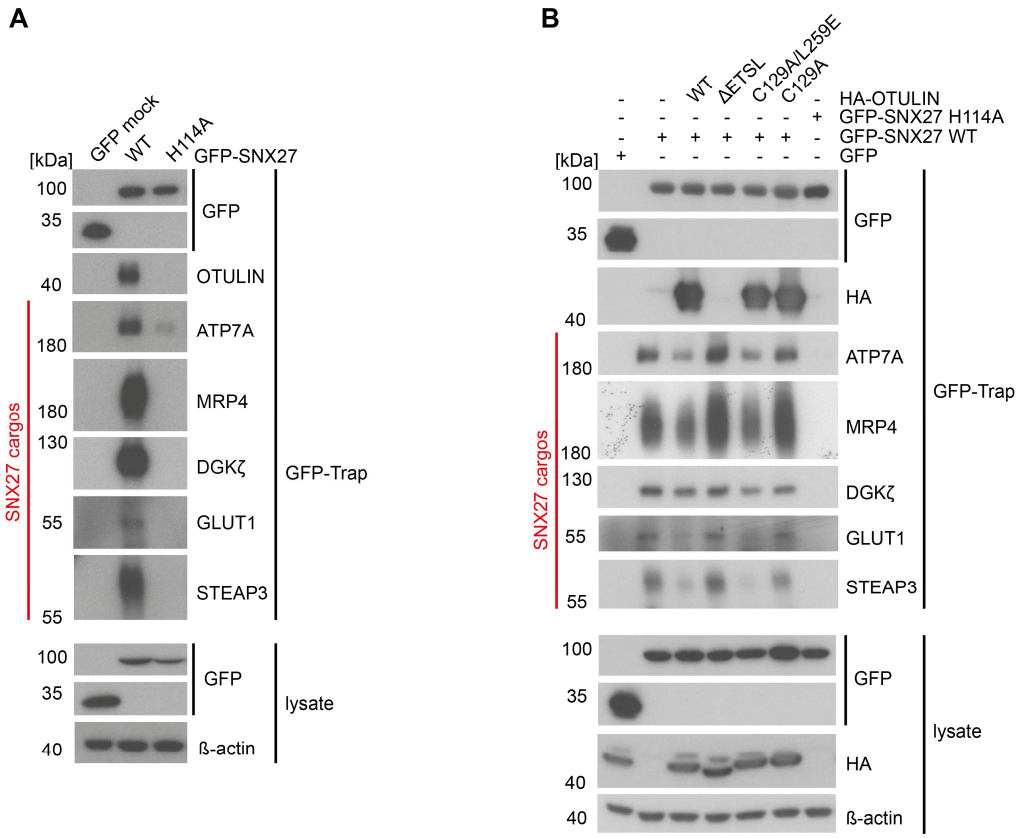

Figure 4-32: OTULIN competes with cargos for SNX27 binding.
A) Different GFP-SNX27 constructs were overexpressed in HEK293 cells and immunoprecipitated by GFP-Traps following cell lysis. Association of SNX27 with cargos was assessed by WB analysis.
B) Experiment was performed as in A) after overexpression of GFP-SNX27 and different HA-OTULIN constructs.

4.3.8 OTULIN limits cell surface recycling of GLUT1

Since endosome-to-plasma membrane transport of the glucose transporter GLUT1 is SNX27-retromer-dependent (Steinberg et al., 2013), and since OTULIN competes with GLUT1 for SNX27 binding (Figure 4-32B), we finally wanted to assess whether OTULIN affects GLUT1 recycling.

To this end, we overexpressed OTULIN or OTULIN ΔETSL in U2OS cells together with the co-expressed surface marker ΔCD2 and determined GLUT1 levels on the cell surface of transfected (ΔCD2 positive) cells by flow cytometry (Figure 4-33). First, cells were gated based on low and high expression of ΔCD2 (Figure 4-33A). In low expressing cells, no changes in GLUT1 surface expression were observed (Figure 4-33B). In high expressing cells, however, OTULIN reduced the surface expression of GLUT1 to approximately 65% (Figure 4-33C). This indicates that OTULIN restricts SNX27-mediated endosome-to-plasma membrane trafficking of GLUT1 by binding to SNX27 and displacing GLUT1. Again, deletion of the PDZbm in OTULIN reversed the downregulation of the GLUT1 surface expression (Figure 4-33C) and resulted in GLUT1 amounts comparable with the amounts on mock-

transfected cells. This proves that the OTULIN-SNX27 interaction is critical for counteracting SNX27-mediated GLUT1 recycling.

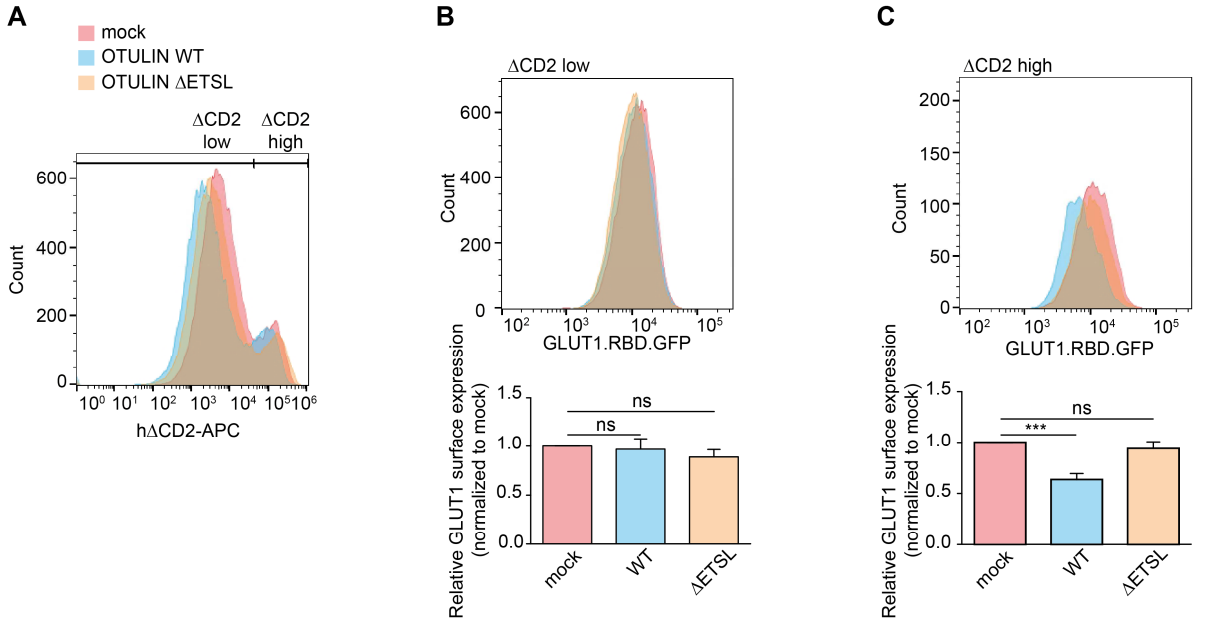

Figure 4-33: OTULIN limits GLUT1 recycling.
A) Mock, OTULIN and OTULIN ΔETSL expressing U2OS cells were determined by flow cytometry by co-expression of the surface marker ΔCD2. Gates were set on low and high ΔCD2 expressing cells.
B and C) GLUT1 surface expression of low (B) and high (C) ΔCD2 expressing cells (upper panels). The quantified relative GLUT1 surface expression (normalized to mock) is depicted in the lower bar graphs. Data represent the mean ± SD of three independent experiments. ***p<0.001; n.s. - not significant; unpaired t-test.

5. Discussion

5.1 Generation and characterization of active site-directed probes for OTULIN

5.1.1 OTULIN ABPs covalently label active OTULIN

To date, no DUB ABP has been generated that closely resembles native Met1-linked diUb and labels Met1-specific active OTULIN. In this study, the first substrate-based active site-directed probes were generated that covalently label the Met1-specific DUB OTULIN. As a supplement to previously developed probes that are based on all seven Lys-linked diUbs (Mulder et al., 2014), the Met1-diUb based probes, bio-Ub^{G76Dha}-Ub (OTULIN ABP) and His$_{10}$-Ub^{G76Dha}-Ub ΔG76 (OTULIN ABP ΔG76), complete the toolkit of linkage-specific DUB ABPs.

In a previous attempt to develop a Met1-diUb based probe, the introduction of a large, flexible electrophile resulted in loss of specificity and thus OTULIN was not labeled (McGouran et al., 2013). Therefore we decided to use the small non-canonical amino acid Dha as reactive group in order to better mimic the structure and chemical features of the peptide bond in linear diUb. With reference to the crystal structure of catalytically inactive OTULIN in complex with Met1-diUb (Figure 5-1A), we assumed that the position of Gly76 in the distal Ub might be accessible for a nucleophilic attack by the catalytic Cys (Keusekotten et al., 2013). Accordingly, we substituted this Gly76 with Dha in the OTULIN ABPs.

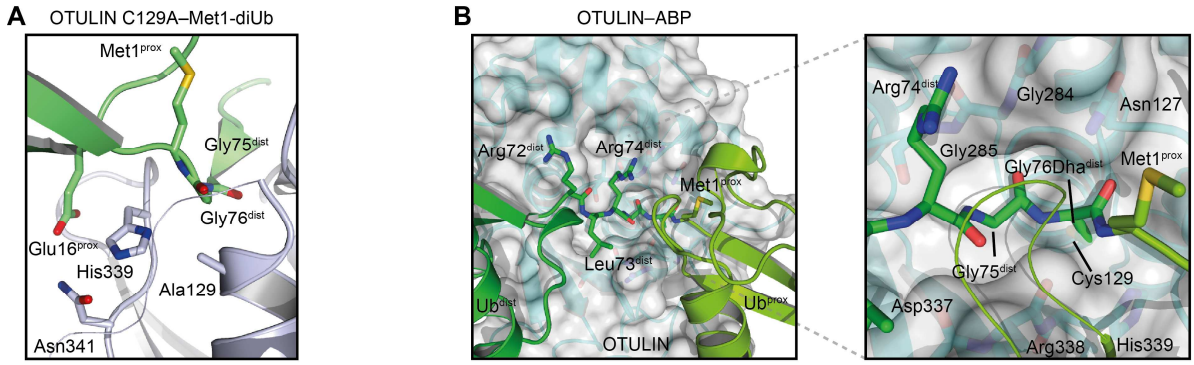

Figure 5-1: Bio-Ub^{G76Dha}-Ub is attacked by the nucleophilic Cys129 of OTULIN.
A) Structure of OTULIN$_{cat}$ C129A (grey) in complex with Met1-diUb (green) (PDB ID: 3ZNZ) (Keusekotten et al., 2013). A close-up view of the catalytic pocket of OTULIN is depicted. Relevant residues are shown in stick format. Gly76^{dist} points towards the catalytic site, which does not apply to Met1^{prox}.
B) Surface representation of OTULIN$_{cat}$ (white) in complex with OTULIN ABP (green cartoon) (PDB ID: 5OE7) (Weber et al., 2017). A close-up view of the catalytic site of OTULIN is depicted. OTULIN residues that form the substrate channel are shown in stick representation.
Illustrations provided by P. Elliott (MRC, Cambridge; University of Oxford) (Weber et al., 2017).

Moreover, the crystal structure reveals that the proximal Met1 side chain does not point toward the catalytic Cys (Figure 5-1A). This explains why the replacement of Met1 by Dha in a recently generated probe did not result in covalent coupling to OTULIN but instead in its cleavage by OTULIN (Haj-Yahya et al., 2014).

By determining the structure of OTULIN in complex with the OTULIN ABP, we confirmed that the electrophilic Dha76 in the distal Ub moiety reacts with the catalytic Cys129 in active OTULIN (Figure 4-4). The close structural resemblance of the OTULIN-ABP and OTULIN-Met1-diUb complexes emphasizes the unique Met1-specificity of OTULIN that is based on both Met1-Ub specific binding sites and the substrate-assisted cleavage reaction (Keusekotten et al., 2013).
Mutation of the distal Gly76 in linear diUb to alanine strikingly reduced binding affinity to OTULIN and thus prevented cleavage by OTULIN (Figure 4-6C and D). In line with this, it was shown earlier that OTULIN fails to hydrolyze Ser76-Met1 linkages (Keusekotten et al., 2013). A close-up view of the active site of OTULIN bound to the OTULIN ABP indicates that there is very little space and that the accommodation of an alanine at the Gly76 position might be difficult (Figure 5-1A and B). As the Dha, despite its apparently lower binding affinity, still reacts with the active Cys, we conclude that the coupling reaction between OTULIN and the ABP is mainly driven by the electrophile and less by the affinity.

5.1.2 OTULIN ABPs label OTULIN with high selectivity

The most remarkable feature of the OTULIN ABP is its high selectivity for OTULIN, which was determined in direct *in vitro* DUB assays as well as in global MS analysis (sections 4.1.3 - 4.1.6). Interestingly, the Met1-Ub cleaving DUBs USP2, USP21 and CYLD did not react with the OTULIN ABP (Figure 4-6A). For the promiscuous DUBs USP2 and USP21, which cleave all types of Ub chains, this might be the result of their low reactivity towards Met1-Ub (Bremm et al., 2010; Faesen et al., 2011; Komander et al., 2009b; Virdee et al., 2010; Ye et al., 2011). CYLD efficiently disassembles Met1- and Lys63-linked Ub chains (Sato et al., 2015), but was still not labeled by the OTULIN ABP. A structural comparison of the OTULIN-ABP complex and the non-covalent zebrafish CYLD (C596S)-Met1-diUb complex (Sato et al., 2015) may provide an explanation (Figure 5-1B and Figure 5-2): In the active site of CYLD, Lys756, Ser800 and Asp794 form a very narrow channel that surrounds the distal Ub tail and the Gly76-Met1 linkage (Sato et al., 2015). It is likely that the OTULIN ABP does not fit into this channel due to the slightly bigger Dha residue at the distal Gly76 position and can therefore not be attacked by the catalytic Cys.

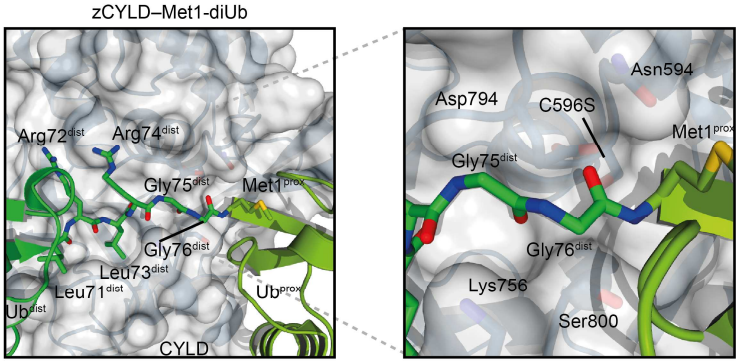

Figure 5-2: Close-up view of the CYLD catalytic pocket in complex with Met1-diUb.
Surface representation of zebrafish CYLD (zCYLD) (aa 578-951, C596S, white) in complex with Met1-diUb (green cartoon) (PDB ID: 3WXE) (Sato et al., 2015). A close-up view of the catalytic site of CYLD is depicted. CYLD residues that form a tight substrate channel around the Gly76-Met1 peptide bond are shown in stick format.
Illustration provided by P. Elliott (MRC, Cambridge; University of Oxford) (Weber et al., 2017).

Amino acid residues interacting with the Ub C-terminus are well conserved in other USPs such as USP2, USP7, USP14 and USP21 (Hu et al., 2002; Hu et al., 2005; Renatus et al., 2006; Ye et al., 2011). In line with this, USP21 and CYLD failed to hydrolyze Ub^{G76A}-Ub (Figure 4-6C), suggesting that the distal Gly76 is crucial for binding to and cleavage by USPs.

The only, albeit weak, DUB cross-reactivity of the OTULIN ABP was toward recombinant and endogenous USP5 (Figure 4-5A and Figure 4-8A). In cells, USP5 recognizes and binds the C-terminal di-Gly motif in free unanchored Ub chains via its ZnF UBP domain and disassembles them from the proximal end (Reyes-Turcu et al., 2006; Reyes-Turcu et al., 2008). Apparently, USP5 is in the same way allosterically activated by the C-terminal di-Gly motif in the OTULIN ABP and thus attacks the active site-directed probe. This cross-reactivity could be eliminated by generating the OTULIN ABP ΔG76, which lacks the Gly76 in the proximal Ub (Figure 4-13B).
Covalent USP5-ABP adducts, which are only formed by a small amount of cellular USP5, were exclusively detected by direct staining but not in biotin-ABP pull-downs. One possible explanation for this could be that the biotin-tag of USP5-bound ABP is not accessible for streptavidin beads due to structural constraints of the catalytic pocket.
USP5 was also identified together with UCHL3 and OTULIN in the selectivity analysis of the OTULIN ABP by LC-MS/MS (Figure 4-10C). After treatment with the broad-ranging DUB inhibitor PR-619, only ABP binding of OTULIN was lost, although USP5 and UCHL3 are likewise affected by the inhibitor (Altun et al., 2011). This indicates that USP5 and UCHL3 predominantly non-covalently interact with the ABP, which might be due to their high cellular abundance (Clague et al., 2015). Indeed, USP5 is one of the most abundant DUBs in HeLa and Swiss3T3 cells (Clague et al., 2015). In addition, it has been demonstrated that UCHL3

non-covalently associates with Ub dimers *in vitro* and in cells without cleaving them (Setsuie et al., 2009).

So far, all DUB ABPs that are based on Lys-linked diUb target a broad range of DUBs in cell extracts and do not exhibit specificity towards one particular enzyme (Li et al., 2014; Mulder et al., 2014). This mainly results from the large number of USP DUBs that rather unspecifically hydrolyze different types of Ub chains (Faesen et al., 2011; Komander et al., 2009a; Ritorto et al., 2014). In contrast, the OTULIN ABP ΔG76 is the first specific active site-directed probe that reacts with one single DUB. Highly selective labeling of OTULIN by means of the two new OTULIN ABPs emphasizes its unique ability to specifically recognize and efficiently cleave Met1-Ub (Keusekotten et al., 2013).

5.1.3 ABP coupling to E1 enzymes triggers formation of polyABP assemblies

Interestingly, incubation of cell extracts with OTULIN ABP led to the ATP-dependent formation of linear polyUb assemblies, which could be detected with anti-Met1-Ub antibody (Figure 4-9). Moreover, ATP-dependent binding of the E1 enzymes UBA1 and UBA6 to the ABP was determined in the proteome-wide selectivity analysis (Figure 4-11). This finding suggests that the accumulation of linear polyUb adducts is not caused by the ABP-induced inhibition of OTULIN and the unrestricted synthesis of Met1-Ub, as observed in knock-in mice that express catalytically inactive OTULIN (Heger et al., 2018). The data rather indicate that the OTULIN ABP is assembled into polyABP adducts by enzymes of the ubiquitination cascade. In line with this, the uncleavable and non-inhibitory diUb mutant His-Ub^{G76A}-Ub was also incorporated into high molecular polyUb assemblies, detectable with anti-Met1-Ub antibody (Figure 4-12A). As the diUb N-termini are occupied by affinity tags, internal lysine residues must serve as docking sites for other diUb molecules. And since only USP2, which can cleave all Ub linkages, was able to completely degrade the polyABP assemblies (Figure 4-12C), different lysines seem to function as attachment sites for the formation of branched Ub chains.

Currently, it is unclear whether the finding of the *in vitro* synthesis of such branched artificial chains is physiologically relevant. However, unanchored ubiquitin dimers and chains exist in cells and thus might be used for polyubiquitin conjugation (Chen and Pickart, 1990; Martinez-Fonts and Matouschek, 2016; Strachan et al., 2012). For the generation of diUb-based DUB ABPs it should be noted that deletion of Gly76 in the proximal Ub prevents cross-reactivity with E1 enzymes (Figure 4-13C).

5.1.4 Potential applications for the OTULIN ABP

Recently, the OTU DUB Cezanne was crystallized in complex with a Lys11-linked diUb-based ABP (Mevissen et al., 2016). By means of this substrate-bound structure, both the reason for the Lys11-specificity of Cezanne and conformational changes of the S1´ binding site during the catalytic cycle were revealed, demonstrating the benefit of utilizing selective ABPs in functional analyses of DUBs (Mevissen et al., 2016).

In this study, further potential applications for the highly selective OTULIN ABP were validated. The OTULIN ABP can be used in order to analyze OTULIN activity in cell extracts. Upon treatment of cell extracts with OTULIN ABP, all OTULIN reacted with the probe (Figure 4-7A and Figure 4-8A). This indicates that in these cells, all OTULIN is active or rather becomes activated by binding of Met1-Ub to the Met1-Ub specific binding sites, which enables substrate-assisted catalysis (Keusekotten et al., 2013). TNFα stimulation did not lead to a decrease in OTULIN activity (Figure 4-15A). As it yet might well be that OTULIN activity is down-regulated in response to other stimuli or in other cell lines, the OTULIN ABP will be helpful for such investigations.

By means of the biotin-labeled OTULIN ABP, substrate-bound OTULIN was almost entirely depleted from extracts. Thus, its association with protein complexes can also be analyzed (Figure 4-15B and Figure 4-16). Equivalent levels (<25%) of all LUBAC components interacted with substrate-bound OTULIN in ABP-PDs. Accordingly, the majority (>75%) of LUBAC is not stably associated with substrate-bound OTULIN. Certainly, affinity of LUBAC for OTULIN might vary depending on whether OTULIN is present in a substrate-bound or -unbound state. However, gel filtration experiments also revealed that the majority of cellular OTULIN does not form a complex with the catalytic LUBAC subunit HOIP (Figure 4-28A). This finding is in accord with a recent study, in which it was shown that the majority of LUBAC does not interact with OTULIN (Elliott et al., 2014). It was suggested that phosphorylation of the PIM in OTULIN prevents the OTULIN-LUBAC interaction and thus might represent a potential regulatory mechanism of the interaction (Elliott et al., 2014; Schaeffer et al., 2014). TNFα does not seem to have an effect on such regulation, since the amount of LUBAC associated with substrate-bound OTULIN in ABP-PDs did not change by TNFα stimulation (Figure 4-15B). This observation and the fact that LUBAC-SPATA2-CYLD but not LUBAC-OTULIN complexes are recruited to the TNFR complex in order to counteract LUBAC activity after receptor engagement suggest that two distinct LUBAC-DUB complexes exist that are regulated independently of each other (Elliott et al., 2016; Kupka et al., 2016a; Schlicher et al., 2016; Wagner et al., 2016).

5.2 OTULIN regulates the SNX27-retromer function

5.2.1 High-affinity interaction between OTULIN and SNX27

In this study, SNX27 was identified as OTULIN interactor by means of the newly developed OTULIN ABP and LC-MS/MS analysis (Figure 4-17). The OTULIN-SNX27 interaction is not cell type-specific, detectable in both human and murine cells (Figure 4-21) and not dependent on either the catalytic activity of OTULIN (Figure 4-22B) or HOIP binding to OTULIN (Figure 4-19B).

In common with typical SNX27 cargos (Gallon and Cullen, 2015; Steinberg et al., 2013), OTULIN directly binds to the canonical cargo-binding site in the SNX27 PDZ domain via a C-terminal class I PDZbm, which is indispensable for the interaction and highly conserved among tetrapods (Figure 4-22 and Figure 4-23). Interestingly, the affinity of the OTULIN PDZbm peptide (K_D ~1.1 µM) is at least twofold higher compared to all measured affinities of $SNX27_{PDZ}$-binding PDZbm peptides (Figure 5-3). So far, the peptides of DGKζ and PLHPP1 have displayed the highest affinity for SNX27 with K_D values of approximately 2 µM, whereas, for example, the peptide of LRRC3B (K_D ~73 µM) has an approximately 66-fold lower affinity than the OTULIN peptide (Figure 5-3) (Clairfeuille et al., 2016).

PDZbm peptide	K_D [µM]	Source
ß2-AR	>200	Clairfeuille et al., 2016
DGKζ	2.0 ± 0.1	Clairfeuille et al., 2016
PTHR	6.3 ± 0.1	Clairfeuille et al., 2016
GluN1	>200	Clairfeuille et al., 2016
GluN2B	>200	Clairfeuille et al., 2016
5-$HT_{4(a)}$R	8.8 ± 0.6	Clairfeuille et al., 2016
CFTR	5.1 ± 0.2	Clairfeuille et al., 2016
KIDINS220	6.5 ± 0.4	Clairfeuille et al., 2016
LRRC3B	73 ± 6	Clairfeuille et al., 2016
PHLPP1	2.1	Clairfeuille et al., 2016
PHLPP2	4.8	Clairfeuille et al., 2016
PTEN	37	Shinde et al., 2017
Kir3.3	17 ± 1.2	Gallon et al., 2014
GLUT1	154 ± 11	Gallon et al., 2014

Figure 5-3: Summary of ITC data for the association of $SNX27_{PDZ}$ with PDZbm peptides.
(Clairfeuille et al., 2016; Gallon et al., 2014; Shinde and Maddika, 2017)

In structural analyses it was shown that amino acid residues upstream of the P-5 position in the DGKζ PDZbm peptide do not contribute to binding of the SNX27 PDZ domain (Clairfeuille et al., 2016). In contrast, our structural analysis of the $OTULIN_{cat}$-$SNX27_{PDZ}$ complex revealed that also Val346 (P-6) and Arg354 (P-7) in the OTULIN C-terminus form hydrogen bonds with residues in SNX27 (Figure 4-23B). This might explain why the SNX27 affinity of the OTULIN PDZbm peptide is higher than the affinity of the DGKζ PDZbm peptide.

To date, all structural and biophysical data of SNX27-cargo interactions have been based on studies with PDZbm peptides of cargos (Clairfeuille et al., 2016; Gallon et al., 2014). The

crystal structure of the $OTULIN_{cat}$-$SNX27_{PDZ}$ complex reveals for the first time, how an entire PDZbm-containing protein domain binds to SNX27 (Figure 4-23A). Interestingly, the affinity of $OTULIN_{cat}$ for $SNX27_{PDZ}$ is with a K_D value of ~31 nM about 35 times higher than the affinity of the C-terminal OTULIN peptide and the highest of all ever measured affinities of SNX_{PDZ} interactors (Clairfeuille et al., 2016). The high affinity can be explained by a second interface between OTULIN and SNX27, which was determined by means of the crystal structure (Figure 4-23 and Figure 4-24). This second interaction surface is spatially separated from the canonical PDZ-PDZbm interface and involves parts of the β3-β4 loop in SNX27 and conserved amino acids in the OTU domain of OTULIN that are not contributing to its hydrolase activity (Keusekotten et al., 2013). Accordingly, the OTULIN substrate Met1-diUb could be modeled onto the $OTULIN_{cat}$-$SNX27_{PDZ}$ structure without having any impact on the interfaces between OTULIN and SNX27 (Figure 5-4). This is in line with the fact that SNX27 was identified as interactor of OTULIN in complex with the substrate-like ABP. Mutations in the second interface, both on the SNX27 and on the OTULIN side, reduced the affinity to that of the PDZbm peptide (Figure 4-24B). This indicates that the second interface considerably strengthens the OTULIN-SNX27 interaction, which is primarily mediated by the attachment of the PDZbm to the PDZ domain.

Analogous to this, it was shown that a second interface between PlexinB2 and the PDZ domain of RhoGEF also increases binding affinity at least by tenfold to a K_D of 2 µM (Pascoe et al., 2015). These findings imply that the existence of a second interaction surface might be a general concept to regulate binding affinities and possibly, selectivities of PDZ interactors.

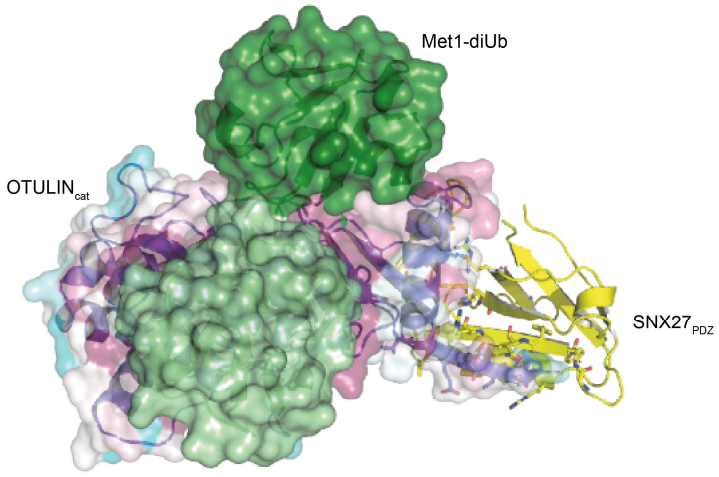

Figure 5-4: Met1-diUb and SNX27 can simultaneously bind to OTULIN.
$OTULIN_{cat}$ (aa 80–352) is rendered in surface representation with SNX_{PDZ} (aa 40-135) depicted as ribbon (yellow). Met1-linked diUb (green) is modeled onto the complex by superimposition of the $OTULIN_{cat}$-Met1-diUb structure (PDB: 3ZNZ) (Keusekotten et al., 2013). Illustration provided by P. Elliott (MRC, Cambridge; University of Oxford).

5.2.2 OTULIN binds the SNX27 PDZ domain with high selectivity

Consistent with the *in vitro* ITC data, mutations in the canonical or non-canonical interfaces resulted in loss or attenuation of the OTULIN-SNX27 interaction in cells (Figure 4-22 and Figure 4-24). The cellular OTULIN-SNX27 complex was detected in OTULIN ABP-PDs, co-immunoprecipitations and confocal fluorescence microscopy. OTULIN was also recently identified in a mass spectrometric analysis of the GFP-SNX27 interactome, but the interaction was not validated or further investigated (Tello-Lafoz et al., 2017).

In the human proteome, more than 150 proteins exist that contain at least one PDZ domain (Ivarsson, 2012). In a previous report, it has been suggested that OTULIN interacts with several PDZ domain-containing proteins via its PDZbm (Rivkin, 2013). In our LC-MS/MS analysis, however, we identified SNX27 as the only PDZ domain-containing protein in the OTULIN interactome across two independent experiments. Since the β3-β4 loop is a unique feature of the SNX27 PDZ domain (Gallon et al., 2014) and since it is involved in the non-canonical OTULIN-SNX27 interaction, this might explain the observed selectivity of OTULIN for SNX27. It is probable that other PDZ domains would fail to bind OTULIN due to the lack of the β3-β4 loop and other structural differences.

At present, more than 400 structures of PDZ domains, either alone or in complex with binding partners, have been determined (Laskowski et al., 2018). Future structural and biophysical studies with OTULIN and other PDZ domains are necessary to better understand the high selectivity of OTULIN for SNX27.

5.2.3 SNX27 does not affect OTULIN and LUBAC functions

So far, all cellular functions of OTULIN have been attributed to its catalytic activity as a deubiquitinating enzyme for Met1-Ub. OTULIN-deficient HEK293 and Jurkat T cells generated in this study showed increased Met1-Ub levels and reduced HOIP amounts in comparison with parental cells (Figure 4-29). Other research groups have also observed that depletion of OTULIN, but not CYLD, leads to a massive accumulation of linear Ub chains under unstimulated conditions and that OTULIN deficiency in T and B cells results in loss of LUBAC components (Damgaard et al., 2016; Draber et al., 2015). These observations emphasize the important role of OTULIN in the homeostatic control of Met1-Ub and the LUBAC stabilization (Damgaard et al., 2016; Draber et al., 2015).

In spite of the fact that Met1-Ub and SNX27 can simultaneously bind to OTULIN (Figure 5-4), $SNX27_{PDZ}$ had no impact on the proteolytic cleavage of Met1-linked tetraUb chains by $OTULIN_{cat}$ *in vitro* (Paul Elliott, unpublished data). Moreover, we neither detected increased Met1-Ub levels nor reduced HOIP amounts in SNX27 KO HEK293 or Jurkat T cells,

suggesting that SNX27 is not required for the homeostatic regulation of Met1-Ub or for LUBAC stabilization by OTULIN.

OTULIN interacts with HOIP via its N-terminal PIM, which is distant from the C-terminal PDZbm (Elliott et al., 2014; Schaeffer et al., 2014). Co-immunoprecipitations following overexpression of HOIP, OTULIN and SNX27 demonstrated that a ternary complex can form, in which OTULIN mediates the interaction between HOIP and SNX27 (Figure 4-27). The study of endogenous complexes by gel filtration analysis, however, revealed that the cellular OTULIN-SNX27 complex is not associated with LUBAC (Figure 4-28). Besides, the majority of OTULIN does also not form a complex with the LUBAC component HOIP, which is in line with a recently published gel filtration analysis (Elliott et al., 2014). It might be that the interaction is impaired by phosphorylation of the PIM in OTULIN, as suggested by Elliott et al. (Elliott et al., 2014), or that the OTULIN-HOIP interaction is very unstable and hardly detectable by size exclusion chromatography. However, it is important to emphasize that the association with SNX27 does not seem to prevent OTULIN binding to HOIP since the elution peak of OTULIN does not shift to HOIP-containing fractions in SNX27-deficient cell extracts as well. So far, the role of a ternary complex, which may form under physiological conditions is unclear and could be investigated in the future. While it cannot be excluded that LUBAC affects the recycling function of the SNX27-retromer complex, the OTULIN-SNX27 interaction can certainly not contribute to this, as OTULIN counters formation of the SNX27-retromer complex (see section 5.2.4).

The absence of OTULIN in Jurkat T cells had no significant impact on NF-κB activation following TNFα stimulation and CD3/CD28 co-stimulation, respectively, implying that OTULIN is not an essential regulator of Met1-Ub in NF-κB and MAPK signaling (Figure 4-30). Likewise, data from other research groups indicate that CYLD is instead the central DUB that restricts Met1-Ub and also Lys63-Ub in signaling complexes after stimulation (Draber et al., 2015; Harhaj and Dixit, 2012; Hrdinka et al., 2016; Kupka et al., 2016b). CYLD is also recruited by LUBAC to the receptor-associated signaling complexes upon TNFR1 or NOD2 engagement, whereas minimal or no OTULIN is detected in activated signaling complexes (Draber et al., 2015; Elliott et al., 2016; Kupka et al., 2016a; Schlicher et al., 2016; Wagner et al., 2016). It should be noted that effects of OTULIN deficiency can vary in different cell types. While loss of OTULIN in T and B cells results in LUBAC destabilization, as mentioned above, in myeloid cells knockout of OTULIN triggers spontaneous Met1-Ub formation and NF-κB activation (Damgaard et al., 2016). Thus, the OTULIN-LUBAC interaction might be differentially regulated depending on the cell type.

OTULIN has also been associated with canonical Wnt signaling during embryogenesis (Rivkin, 2013). Moreover, OTULIN counteracts LUBAC-mediated suppression of Wnt signaling in reporter assays (Rivkin, 2013; Takiuchi et al., 2014). We could not determine any significant changes in the stabilization of β-catenin upon treatment of OTULIN KO Jurkat T cells with recombinant Wnt3a, indicating that OTULIN is at least not required for β-catenin stabilization after Wnt3a stimulation (Figure 4-31).

It has been previously proposed that SNX27 may be a negative regulator of ERK phosphorylation following TCR/CD28 stimulation in Jurkat T cells (Rincon et al., 2011). SNX27 has further been associated with the regulation of canonical Wnt signaling as it interacts with Frizzled receptor Fzd7 (Sun et al., 2016). The absence of SNX27 in Jurkat T cells did, however, just as the absence of OTULIN, not significantly affect TNF, TCR/CD28 and Wnt signaling (Figure 4-30 and Figure 4-31). Altogether, these data reveal that the interaction between OTULIN and SNX27 has no effect on NF-κB, MAPK and Wnt signaling in Jurkat T cells.

5.2.4 OTULIN is not a cargo of the SNX27-retromer

The formation of the endosomal SNX27-retromer complex is important for the fast endosome-to-plasma membrane recycling of SNX27-associated cargos (Gallon and Cullen, 2015). The retromer component VPS26 binds to the β3-β4 loop in the SNX27 PDZ domain (Gallon et al., 2014), which also interacts with OTULIN (Figure 4-24).

Superimposition of the $SNX27_{PDZ}$-$OTULIN_{cat}$ and $SNX27_{PDZ}$-VPS26A complexes revealed that binding sites of OTULIN and VPS26A partially overlap (Figure 4-24 and Figure 4-25A). The resulting clash excludes the possibility that OTULIN and VPS26 simultaneously bind to SNX27. Due to its high affinity for SNX27, OTULIN rather competes with retromer for binding to SNX27 (Figure 4-25). Confocal fluorescence microscopy moreover revealed that OTULIN, which is not located on early endosomes, counteracts endosomal association of SNX27 (Figure 4-26).

To analyze the distribution of SNX27 and OTULIN in cellular complexes, analytical size exclusion chromatography with extracts from parental, OTULIN KO and SNX27 KO Jurkat T cells was performed (Figure 4-28). It became apparent that the majority of endogenous OTULIN and SNX27 exists in a stable complex with 1:1 stoichiometry, which is consistent with the results from the crystal structure analysis of the OTULIN-SNX27 complex. Despite its essential role in retromer-mediated cargo transport to the plasma membrane (Steinberg et al., 2013), the majority of SNX27 was surprisingly not detected together with the retromer complex but with OTULIN. Even though preparation of the cell extracts might favor cytosolic,

not membrane-associated protein complexes, our data suggest that only a small proportion of endogenous SNX27 interacts with the retromer. This explains why the SNX27–retromer interaction has so far only been shown in immunoprecipitations after overexpression of at least one component (Gallon et al., 2014; Steinberg et al., 2013) and why the endogenous interaction has never been detected. It is important to emphasize that the OTULIN-SNX27 complex was not detected together with the retromer complex in our gel filtration analysis.
Altogether, structural analysis, immunoprecipitations, fluorescence microscopy and comparative analytical size exclusion chromatography provided evidence that OTULIN cannot be a cargo of the SNX27-retromer complex since OTULIN prevents formation of the SNX27-retromer complex.

5.2.5 OTULIN counteracts cargo recycling by the SNX27-retromer

Much is known about the structure of the recombinant SNX27-VPS26-VPS35-VPS29 complex (Gallon and Cullen, 2015; Kovtun et al., 2018). However, it is entirely ambiguous, how and when the cellular SNX27-retromer complex assembles on the endosomes, how cargos are selectively recruited, and how the transport complex is disassembled again at the plasma membrane. The fact that the endogenous interaction has never been detected in immunoprecipitations indicates that the interaction might occur at low frequency or that the regulation of the interaction might be very dynamic. Our data suggest that OTULIN regulates and tightly controls the assembly of the SNX27-retromer by binding and thus retaining a majority of endogenous SNX27. Furthermore, OTULIN might also be responsible for the disassembly of cargo-bound SNX27-retromer complexes once they have reached the plasma membrane.

OTULIN not only competes with the retromer complex for binding to SNX27, but also hinders classical cargos from interacting with SNX27 by binding to the canonical cargo-binding site (Figure 4-32). Consequently, OTULIN impairs the recycling of cargos by the SNX27-retromer complex, as it has been shown for the glucose transporter GLUT1 (Figure 4-33 and Figure 5-5). While catalytic activity of OTULIN is crucial for controlling the cellular Met1-Ub concentration, regulation of the SNX27-retromer proceeds independently from the hydrolase activity (Figure 5-5).
Currently, the spatiotemporal regulation of the SNX27-retromer by OTULIN is unclear and requires further investigation. Recently, it was shown that phosphorylation of C-terminal peptides with PDZbm have the ability to increase or decrease peptide affinities for PDZ domains (Sundell et al., 2018). Analogous to this, phosphorylation of some cargo peptides

augments their binding to SNX27 (Clairfeuille et al., 2016). Thus, phosphorylation in the OTULIN PDZbm, for example at the positions P-2 (Thr350) and P-1 (Ser351), might also influence the OTULIN-SNX27 interaction, represent a potential regulatory mechanism for the interaction, and alter the balance of OTULIN and cargo binding to SNX27. In addition, it was reported that in ITC experiments the affinity of SNX27 for the PDZbm-containing peptides of Kir3.3 and GLUT1 is enhanced upon VPS26A binding, suggesting that the SNX27-retromer interaction may facilitate cargo binding (Gallon et al., 2014).

Remarkably, loss of OTULIN is insufficient to detect a higher amount of SNX27 in the retromer-containing fractions in gel filtration experiments (Figure 4-28B). Thus, further events are necessary to form the SNX27-retromer or the complex is not stable enough for analysis by means of size exclusion chromatography.

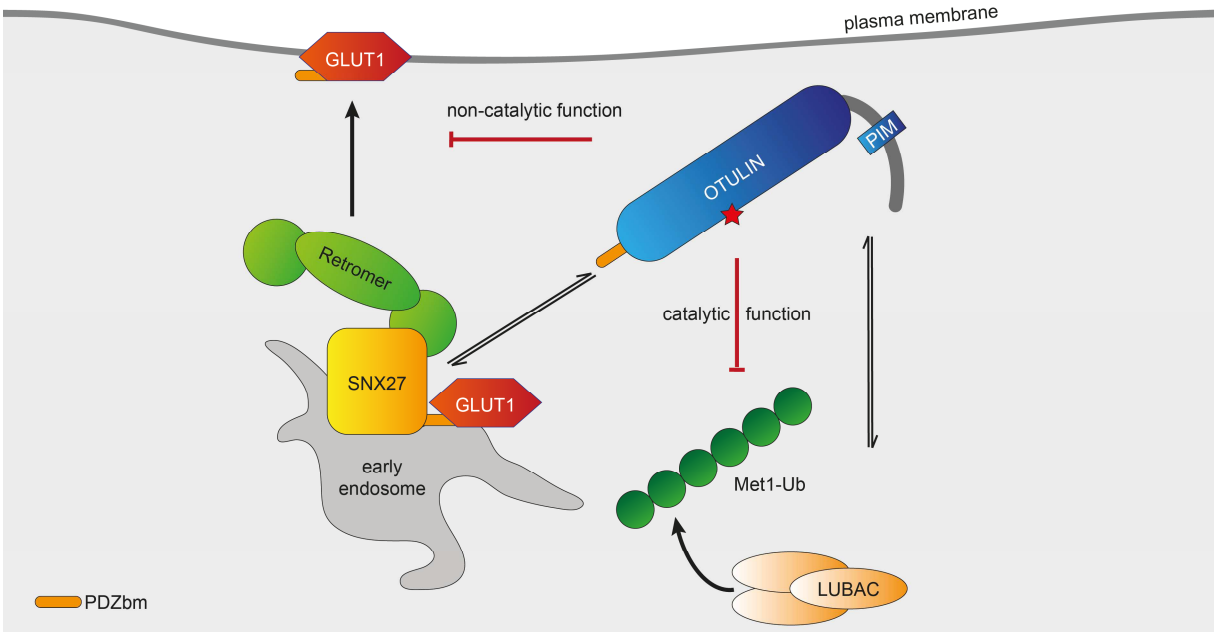

Figure 5-5: Model for the dual role of OTULIN.
Via the degradation of Met1-linked Ub chains synthesized by LUBAC, OTULIN regulates the Met1-Ub concentration in the cell and thus acts as homeostatic control factor. By contrast, catalytic activity of OTULIN is not required for the interaction with SNX27. The interaction is mediated by the canonical PDZbm-PDZ interface and a second non-canonical interface. OTULIN binding to SNX27 suppresses formation of the cargo-SNX27-retromer complex and thus counteracts endosomal sorting and fast recycling of plasma membrane proteins, such as GLUT1.

Analogous to the role of OTULIN, it was recently suggested that the phosphatase PTEN impairs assembly of the SNX27-retromer complex and thus counteracts SNX27-retromer mediated GLUT1 recycling (Shinde and Maddika, 2017). With a K_D of 37 µM the affinity of the PDZbm-containing PTEN peptide is approximately 33 times lower than the affinity of the OTULIN peptide and also very low for an interaction partner that competes with the retromer and cargos for binding to SNX27. The study does not contain structural data of the PTEN-SNX27 complex, but still it reveals that besides OTULIN, additional proteins might exist that regulate or control the function of the SNX27-retromer.

The impairment of the deubiquitinase activity of OTULIN is associated with severe phenotypes. In humans, hypomorphic germline mutations in the *OTULIN* gene reduced the stability of OTULIN (L272P) and its affinity for Met1-Ub, causing a severe disease called OTULIN-related auto-inflammatory syndrome (ORAS) or otulipenia (Damgaard et al., 2016; Zhou et al., 2016). In mice, both the loss of Otulin and a mutation in the Met1-Ub specific binding site (W96R) are embryonically lethal (Damgaard et al., 2016; Rivkin, 2013). Inducible Otulin deletion and the expression of catalytically inactive Otulin (C129A) in adult mice result in spontaneous, fatal auto-inflammation and lethal weight loss within five days (Damgaard et al., 2016; Heger et al., 2018). SNX27-deficient mice suffer from growth retardation and die within three weeks after birth (Cai et al., 2011). To unravel the physiological consequences of the OTULIN-SNX27 interaction, *in vivo* studies will be necessary. However, the serious consequences of an OTULIN or SNX27 deficiency make it impossible to investigate the physiological role of the OTULIN-SNX27 interaction in currently available mouse models.

5.3 Conclusion and perspectives

In this study, we generated the first diUb-based ABPs for the Met1-specific DUB OTULIN. Direct DUB assays and structural analysis of the OTULIN-ABP complex revealed that active OTULIN reacts with the probe via its catalytic Cys and is thus covalently and irreversibly bound. By global LC-MS/MS analysis of ABP-bound proteins, a high selectivity of the OTULIN ABP could be determined. Minimal cross-reactivities with USP5 and E1 enzymes could be prevented by deleting Gly76 in the proximal Ub moiety of the ABP. Thus, OTULIN ABP ΔG76 is the first completely specifc ABP for OTULIN. The OTULIN ABP does not only enable us to analyze OTULIN activity in cell extracts of unstimulated or stimulated cells, but also to efficiently enrich active OTULIN along with its associated interactors from lysates.
The OTULIN ABP might be used in the future to determine cell type-specific differences in OTULIN activity and to analyze influences of different stimuli on OTULIN activity. By the efficient pull-down of OTULIN by means of the ABP, the association with LUBAC may also be investigated more precisely. Thus, conclusions could be drawn about the cell type-specific regulation of the Met1-Ub machinery. These insights would be important for explaining distinct phenotypic effects of OTULIN depletion in lymphocytes and myeloid cells (Damgaard et al., 2016). Additionally, the OTULIN ABP might be helpful for localizing active OTULIN in intact cells via fluorescence microscopy.

By ABP-PDs in combination with LC-MS/MS, we could identify SNX27 as new OTULIN interactor. The OTULIN-SNX27 interaction could be verified by means of ABP-PDs, confocal

microscopy, analytical size exclusion chromatography and co-IPs in various human and murine cell lines. It could be demonstrated by structural, biophysical and cellular analyses that the interaction is independent of the catalytic activity of OTULIN, and relies on direct binding of a highly conserved C-terminal PDZbm in OTULIN to the canonical cargo-binding site in the PDZ domain of SNX27. The identification of a second interface could additionally explain the high affinity of the two proteins.

Binding studies and functional analyses revealed that the OTULIN-SNX27 association prevents the retromer subunit VPS26A and cargos from binding to SNX27 and that OTULIN removes SNX27 from the early endosomes. Consequently, OTULIN is not a cargo of SNX27, but counteracts fast cargo recycling mediated by the SNX27-retromer. Thus it regulates surface expression of plasma membrane proteins, as it was shown for GLUT1.

Taken together, we identified in this study a novel biological function of OTULIN that is important for the maintenance of the cellular homeostasis. While OTULIN controls the cellular Met1-Ub concentration through its deubiquitinase activity, it regulates SNX27/retromer-mediated endosomal sorting of plasma membrane proteins independently from its catalytic activity, by binding to SNX27.

In a next step, the question should be addressed, how the OTULIN-SNX27 interaction is regulated. To this end, it will be necessary to check interfaces between OTULIN and SNX27 for post-translational modifications by mass spectrometric analysis. Structural, biophysical and cellular studies will be useful to find out whether potential modifications strengthen or weaken the interaction. Since phosphorylation of C-terminal cargo peptides as well as binding of VPS26 to SNX27 can have a bearing on the affinity of cargos for SNX27, it will be important to study the OTULIN-SNX27 interaction in the context of the SNX27-retromer assembly.

The fatal consequences of a loss of OTULIN´s catalytic function make it impossible to study the physiological role of the OTULIN-SNX27 interaction in currently available mouse models. Therefore, the generation of an appropriate mouse model would be of particular importance. Considering the structural information on the OTULIN-SNX27 interaction from this work, the generation of a knock-in mouse line expressing a truncated version of OTULIN that lacks the C-terminal PDZbm would be useful. Alternatively, point mutations in the second interface might help to elucidate the physiological relevance of the high affinity and selectivity of OTULIN for SNX27. The apparently very stable OTULIN-SNX27 complex suggests that the interaction might also play additional, completely new roles besides the regulation of cargo recycling.

6. Materials

6.1 Instruments and equipment

Instrument / equipment	Source
Agarose gel chambers	NeoLab, Heidelberg
Autoclave – VX-95	Systec, Linden
Bacterial culture flasks/tubes	Schott, Zwiesel; BD, Heidelberg
Cell culture flasks/plates	BD, Heidelberg; Nunc, Wiesbaden
Cell scraper	Sarstedt, Newton, USA
Cell viability analyzer - ViCell-XR	Beckman Coulter, Krefeld
Centrifuge Beckman Avanti J-26 XP	Beckman Coulter, Krefeld
Centrifuges - 5810R, 5417R, 5471C, 5804	Eppendorf, Hamburg
CO_2 incubators	Binder, Tuttlingen
Cryo tubes	Greiner Bio-One, Frickenhausen
Developer - Optimax	Protec, Oberstenfeld
Electroporation cuvettes - Gene Pulser	Bio-Rad, München
Electroporator - Gene Pulser Xcell System	Bio-Rad, München
Eppendorf tubes	Eppendorf, Hamburg
FACS Attune Acoustic Focusing Cytometer	Thermo Fisher Scientific, Waltham, USA
FACS tubes	BD, Heidelberg
Falcon tubes	BD, Heidelberg
Filter pipette tips - TipOne	StarLab, Hamburg
Freezers and Fridges	Liebherr, Ochsenhausen
Gel Documentation System - Intas Gel iX Imager	Intas, Göttingen
Gel filtration column – Superdex200 10/300	GE Healthcare, München
Heat blocks	Techne, Burlington, USA
Ice machine – Scotsman AF20	Scotsman Ice Systems, Vernon Hills, USA
Incubator shaker – I 26	New Brunswick Scientific, Hamburg
Incubators	Sartorius, Göttingen; Heraeus, Hanau
LC columns – StrepTrap HP, HisTrap HP, HiTrap Desalting	GE Healthcare, München
LC system - ÄKTA Purifier System	GE Healthcare, München
Magnetic stirrer	NeoLab, Heidelberg
Micro scales, scale	Kern & Sohn, Balingen
Microscopes	Leica, Wetzlar
Microwave	SHARP, Hamburg
Petri dishes	Greiner Bio-One, Frickenhausen
pH meter - inoLab pH7110	WTW, Weilheim
Pipette tips	Eppendorf, Hamburg
Pipettes - Reference	Eppendorf, Hamburg
Pipetting aid - accu-jet pro	Brand, Wertheim
Power supplies - EV202, EV243	Consort, Turnhout, Belgium
Precision scale – New Classic MS	Mettler Toledo, Gießen
Rotator – Intelli-Mixer	NeoLab, Heidelberg
SDS-PAGE gel chambers	Roth, Karlsruhe
Serological pipettes - Cellstar	Greiner Bio-One, Frickenhausen
Shaker - Polymax 1040	Heidolph Instruments, Schwabach
Spectral photometer - Biophotometer	Eppendorf, Hamburg
Syringes	Braun, Melsungen
Thermocycler – Mastercycler gradient	Eppendorf, Hamburg
Thermomixer comfort	Eppendorf, Hamburg

Instrument / equipment	Source
Tissue culture hoods Safeflow 1.2	Nunc, Wiesbaden
Ultracentrifuge – Optima MAX	Beckman Coulter, Krefeld
Ultra-pure water system - Milli-Q Plus	Merck Millipore, Darmstadt
Ultrasonic Device - UP200S	Hielscher Ultrasonics GmbH, Teltow
UV cuvettes micro	Brand, Wertheim
UV-Vis Spectrophotometer - NanoDrop 2000	Thermo Fisher Scientific, Waltham, USA
Vortexer	Heidolph Instruments, Schwabach
Western blotting detection – Amersham Hyperfilm TM ECL	GE Healthcare, München
Western blotting transfer – PVDF-membrane, 0.45 µm	Merck Millipore, Darmstadt
Western blotting transfer - Semi-dry blotter	Peqlab, Erlangen
Western blotting transfer – Whatman paper	Roth, Karlsruhe

6.2 Chemicals

6.2.1 General chemicals

Chemical	Source
Acrylamide/Bisacrylamide	Roth, Karlsruhe
Agarose	Biozym, Hessisch Oldendorf
Ammonium persulfate (APS)	Bio-Rad, München
Ampicillin	Roth, Karlsruhe
Anhydrotetracycline hydrochloride (AHT)	IBA, Göttingen
Boric acid	Roth, Karlsruhe
Bovine serum albumin (BSA)	Sigma-Aldrich, Taufkirchen
Calcium chloride ($CaCl_2$)	Roth, Karlsruhe
Chloramphenicol	Roth, Karlsruhe
Chloroquine-diphosphate	Sigma-Aldrich, Taufkirchen
Coomassie-based PageBlue Protein Staining Solution	Thermo Fisher Scientific, Waltham, USA
cOmplete – Protease Inhibitor Cocktail	Roche, Mannheim
cOmplete Tablets, Mini, EDTA-free	Roche, Mannheim
Dimethyl sulfoxide (DMSO)	Roth, Karlsruhe
Dithiothreitol (DTT)	Sigma-Aldrich, Taufkirchen
DNA 1kb plus ladder	Thermo Fisher Scientific, Waltham, USA
dNTP-Mix	Thermo Fisher Scientific, Waltham, USA
Donkey serum	Jackson ImmunoResearch, Cambridgeshire, UK
DPBS (w/o $MgCl_2$ and $CaCl_2$)	Thermo Fisher Scientific, Waltham, USA
Ethanol (EtOH, p. a.)	Merck, Darmstadt
Ethidium bromide (EtBr)	Roth, Karlsruhe
Ethylenediaminetetraacetic acid (EDTA)	Roth, Karlsruhe
Gel Loading Dye, Purple (6x)	NEB, Frankfurt
GFP-Trap	Chromotek, Martinsried
GLUT1.RBD.GFP	Pelobiotech, Planegg
Glycerol	Roth, Karlsruhe
Glycine	Roth, Karlsruhe
HEPES	Roth, Karlsruhe
Hoechst33342	Thermo Fisher Scientific, Waltham, USA
Human recombinant TNFα	Biomol, Hamburg
Imidazole	Roth, Karlsruhe
Isopropyl alcohol (p.a.)	Merck, Darmstadt
Isopropyl β-D-1-thiogalactopyranoside (IPTG)	Thermo Fisher Scientific, Waltham, USA

Chemical	Source
Kanamycin	Roth, Karlsruhe
LB-Agar (Luria/Miller)	Roth, Karlsruhe
LB-Medium (Luria/Miller)	Roth, Karlsruhe
Methanol (MeOH, p.a.)	Merck, Darmstadt
Milk powder	Roth, Karlsruhe
Monopotassium phosphate (KH_2PO_4)	Roth, Karlsruhe
Nonidet P40 substitute (NP-40)	Sigma-Aldrich, Taufkirchen
PageRuler Prestained Protein Ladder	Thermo Fisher Scientific, Waltham, USA
Pierce High Capacity Streptavidin Agarose	Thermo Fisher Scientific, Waltham, USA
Polybrene	Sigma-Aldrich, Taufkirchen
Poly-L-lysine solution (P4832)	Sigma-Aldrich, Taufkirchen
Potassium chloride (KCl)	Roth, Karlsruhe
PR-619	Merck, Darmstadt
Protein-G-Sepharose (PGS) 4B	Thermo Fisher Scientific, Waltham, USA
Protino Ni-NTA Agarose	Macherey-Nagel, Düren
Roti-Histofix 4%	Roth, Karlsruhe
Roti-Load 1 - 4x SDS sample buffer	Roth, Karlsruhe
S.O.C. Medium	Thermo Fisher Scientific, Waltham, USA
Sodium chloride (NaCl)	Roth, Karlsruhe
Sodium dodecyl sulfate (SDS)	Roth, Karlsruhe
Sodium fluoride	Sigma-Aldrich, Taufkirchen
Sodium hydrogen phosphate (Na_2HPO_4)	Roth, Karlsruhe
Sodium vanadate	Roth, Karlsruhe
Strep Elution Buffer (10x)	IBA, Göttingen
Strep Regeneration Buffer (10x)	IBA, Göttingen
Strep-Tactin Sepharose	IBA, Göttingen
TAE buffer (50x)	Omnilab, Bremen
Tetramethylethylenediamine (TEMED)	Roth, Karlsruhe
Tris(hydroxymethyl)-aminomethan (Tris)	Roth, Karlsruhe
TritonX-100	Roth, Karlsruhe
Trypan blue	Thermo Fisher Scientific, Waltham, USA
Tween-20	Roth, Karlsruhe
Western blotting detection (ECL substrate) 20x LumiGlo and 20x Peroxide	Cell Signaling Technology, Frankfurt
X-tremeGENE HP Transfection Reagent	Roche, Mannheim
β-Glycerophosphate	Sigma-Aldrich, Taufkirchen

6.2.2 Cell culture media and supplements

Medium / supplement	Source
DMEM (Dulbecco's modified eagle medium)	Thermo Fisher Scientific, Waltham, USA
Fetal calf serum (FCS)	Thermo Fisher Scientific, Waltham, USA
Penicillin-Streptomycin (10,000 U/ml)	Thermo Fisher Scientific, Waltham, USA
RPMI (Roswell Park Memorial Institute) 1640	Thermo Fisher Scientific, Waltham, USA
Trypsin (0.05%)/EDTA	Thermo Fisher Scientific, Waltham, USA

6.3 Buffers and solutions

Buffer / solution	Composition
2x HBS (HEPES buffered saline)	50 mM HEPES (pH 7), 280 mM NaCl, 1.5 mM Na_2HPO_4
4x Stacking gel buffer	0.5 M Tris (pH 6.8)
5x Separation gel buffer	1.88 M Tris (pH 8.8)
Annealing buffer	10 mM Tris (pH 8), 50 mM NaCl, 1 mM EDTA
Blocking solution (Confocal microscopy)	0.1% Tween-20, 10% (v/v) FCS, 0.1% (w/v) BSA, 3% (v/v) donkey serum in PBS
Blocking solution (WB)	5% (w/v) milk powder in PBS-T
Blotting buffer	25 mM Tris (pH 8.3), 192 mM Glycine, 20% (v/v) MeOH
Cargo buffer	50 mM Tris (pH 7.4), 0.5% (v/v) NP-40, cOmplete – Protease Inhibitor Cocktail
Co-IP buffer	150 mM NaCl, 25 mM HEPES (pH 7.5), 0.2% (v/v) NP-40, 1 mM glycerol, 1 mM DTT, cOmplete protease inhibitors, 10 mM NaF, 8 mM β-glycerophosphate, 300 µM sodium vanadate
Desalting buffer	20 mM Tris (pH 8), 100 mM NaCl
DUB Reaction buffer	50 mM Tris (pH 7.5), 5 mM DTT, +/- 0.03% (w/v) BSA
FACS buffer	3% (v/v) FCS in PBS
High salt buffer	20 mM HEPES (pH 7.9), 350 mM NaCl, 20% (v/v) glycerol, 1 mM $MgCl_2$, 0.5 mM EDTA, 0.1 mM EGTA, 1% (v/v) NP-40, 1 mM DTT, cOmplete protease inhibitors, 10 mM NaF, 8 mM β-glycerophosphate, 300 µM sodium vanadate
His Binding buffer	100 mM Tris (pH 8), 150 mM NaCl, 30 mM imidazole Add just before use: EDTA-free cOmplete Mini protease inhibitors and 0.5 mg/ml lysozyme
His Lysis buffer (PD)	150 mM NaCl, 50 mM NaH_2PO_4 (pH 8), 0.2% NP-40, 10% glycerol, 10 mM imidazole, 1 mM DTT, 10 mM sodium fluoride, 8 mM β-glycerophosphate and 300 µM sodium vanadate
His Elution buffer	100 mM Tris (pH 8), 150 mM NaCl, 300 mM imidazole
His Washing buffer	100 mM Tris (pH 8), 150 mM NaCl, 30 mM imidazole
LB agar	40 g/l
LB medium	25 g/l
PBS (phosphate buffered saline)	137 mM NaCl, 2.7 mM KCl, 10 mM Na_2HPO_4, 1.7 mM KH_2PO_4
PBS-T	0.1% (v/v) Tween-20 in PBS
Permeabilization buffer	PBS, 0.1 M Glycine, 0.1% Triton X-100
RIPA buffer	250 mM NaCl, 1% (v/v) Triton-X, 0.5% (w/v) sodium deoxycholate, 0.1% (w/v) SDS, 10 mM Tris (pH 7.4), 1 mM DTT, cOmplete protease inhibitors, 10 mM NaF, 8 mM β-glycerophosphate, 300 µM sodium vanadate
SDS Electrophoresis buffer	25 mM Tris (pH 8.8), 192 mM Glycine, 0.1% (w/v) SDS
SEC buffer	20 mM Tris (pH 7.4), 150 mM NaCl, 2 mM DTT
SEC lysis buffer	25 mM HEPES (pH 7.5), 150 mM NaCl, 0.2% NP-40, 1 mM DTT, cOmplete protease inhibitors, 10 mM NaF, 8 mM β-glycerophosphate, 300 µM sodium vanadate
Separation gel	375 mM Tris (pH 8.8), 7.5-15% (v/v) Acrylamide, 0.1% (w/v) SDS, 0.1% (w/v) APS, 0.1% (v/v) TEMED
Stacking gel	125 mM Tris (pH 6.8), 3% (v/v) Acrylamide, 0.1% (w/v) SDS, 0.1% (w/v) APS, 0.1% (v/v) TEMED
Strep Lysis buffer	100 mM Tris (pH 8), 150 mM NaCl, 1 mM EDTA. Add just before use: cOmplete Mini protease inhibitors and 0.5 mg/ml lysozyme
Strep Washing buffer	100 mM Tris (pH 8), 150 mM NaCl, 1 mM EDTA
Strep-PD buffer A	PBS, 0.1% (w/v) BSA, 5% (v/v) glycerol, 0.1% Triton-X, cOmplete protease inhibitors

Buffer / solution	Composition
Strep-PD buffer B	PBS, 0.1% (w/v) BSA, 5% (v/v) glycerol, 0.5% Triton-X, cOmplete protease inhibitors
Stripping buffer	0.2 M glycine, 0.1% (w/v) SDS, 1% (v/v) Tween-20, pH 2.2

6.4 Kits

Kit	Source
Deconjugating Enzyme Set	R&D Systems, Minneapolis, USA
GLUT1.RBD.GFP	Pelobiotech, Planegg
NucleoSpin Gel and PCR Clean-up Kit	Macherey-Nagel, Düren
NucleoSpin Plasmid Mini Kit	Macherey-Nagel, Düren
Pierce Silver Stain Kit	Thermo Fisher Scientific, Waltham, USA
Plasmid Maxi Kit	Qiagen, Hilden
QIAamp DNA Mini Kit	Qiagen, Hilden
Rapid DNA Ligation Kit	Roche, Mannheim
Taq DNA Polymerase Kit	Qiagen, Hilden
UbiCREST Deubiquitinase Enzyme Set	R&D Systems, Minneapolis, USA

6.5 Enzymes

Enzymes	Source
Deconjugating Enzyme Set	R&D Systems, Minneapolis, USA
E. coli recombinant Apyrase	NEB, Frankfurt
Herculase II Polymerase	Agilent Technologies, Santa Clara, USA
Lysozyme	Roth, Karlsruhe
Rapid DNA Ligation Kit	Roche, Mannheim
Recombinant human GST-YOD1	Laboratory of D. Krappmann
Recombinant human His_6-CYLD Isoform 1	R&D Systems, Minneapolis, USA
Recombinant human $USP21_{cat}$	Laboratory of T. Sixma
Restriction enzymes and buffers	NEB, Frankfurt
T4 DNA Ligase	NEB, Frankfurt
Taq DNA Polymerase Kit	Qiagen, Hilden
UbiCREST Deubiquitinase Enzyme Set	R&D Systems, Minneapolis, USA

6.6 Oligonucleotides

6.6.1 Oligonucleotides for the generation of KO cell lines

Target	Sequence
OTULIN – exon 2	5‘-CACCGATACATGAAAGAGGGGCATC-3‘ and 5‘-AAACGATGCCCCTCTTTCATGTATC-3
SNX27 – exon 1	5´-CACCGGCTACGGCTTCAACGTGCG-3´ and 5´-AAACCGCACGTTGAAGCCGTAGCC-3´
HOIP – exon 1	5´-CACCGAGAGCTGGCTAGTAGCGGC-3´ and 5´-AAACGCCGCTACTAGCCAGCTCTC-3´

6.6.2 Oligonucleotides for the verification of KO cell lines

KO cell line	Sequence
OTULIN	5´ primer: 5´-GCCTTCAGAGCTACCTAGCAAATGAAG-3´ 3´ primer: 5´-GGAAATCAAGAACTGAGAGAGGACGG-3´
SNX27	5´ primer: 5´-ATTCATCCCTCAGCCCCTCA-3´ 3´ primer: 5´-GGCAGCCCACAAGGAGG-3´
HOIP	5´ primer: 5´-AGAGTGACCGTGGTCTGAGTGACCTGG-3´ 3´ primer: 5´-GTGGACAGGGTGTTGAGGTAGTTTCGG-3´

6.7 Plasmids

Vector	Information
pASK-IBA3(+)	IBA, Cat#2-1402-000; For bacterial expression of recombinant proteins
pASK-IBA3 OTULIN$_{cat}$-Strep WT	C-terminal Strep-tag II, OTULINcat = aa 80-352, NheI/HindIII
pASK-IBA3 OTULIN$_{cat}$-Strep C129A	C-terminal Strep-tag II, aa 80-352, NheI/HindIII
pASK-IBA3 OTULIN$_{cat}$-Strep W96A	C-terminal Strep-tag II, aa 80-352, NheI/HindIII
pASK-IBA3 His-Ub-Ub	N-terminal His$_{10}$-tag, XbaI/HindIII
pASK-IBA3 His-UbG76A-Ub	N-terminal His$_{10}$-tag, XbaI/HindIII
pASK-IBA3 His-UbG76C-UbΔG76	N-terminal His$_{10}$-tag, XbaI/HindIII
pEF Flag	Modified pEF4 backbone (Scharschmidt et al., 2004); 3xFlag-tag
pEF Flag-OTULIN WT	N-terminal 3xFlag-tag, BamHI/NotI
pEF Flag-OTULIN C129A	N-terminal 3xFlag-tag, BamHI/NotI
pEF Flag-OTULIN Y56F	N-terminal 3xFlag-tag, BamHI/NotI
pEF Flag-OTULIN ΔETSL	N-terminal 3xFlag-tag, BamHI/NotI
pEF Flag-OTULIN W96A	N-terminal 3xFlag-tag, BamHI/NotI
pEF Flag-OTULIN$_{cat}$	N-terminal 3xFlag-tag, aa 80-352, BamHI/NotI
pEF Flag-VPS26A	N-terminal 3xFlag-tag, BamHI/NotI
pEF Flag-OTUB1	Gift from K. Hadian; N-terminal 3xFlag-tag
pEF Flag-CYLD	Krappmann laboratory, K.Demski; N-terminal 3xFlag-tag, BamHI/NotI
pEF Flag-A20	Krappmann laboratory (Duwel et al., 2009); N-terminal 3xFlag-tag, EcoRI/NotI
pEF Flag-YOD1	Krappmann laboratory (Schimmack et al., 2017); N-terminal 3xFlag-tag, BamHI/NotI
pEF Flag-UCHL3	Krappmann laboratory, L. Glockner; N-terminal 3xFlag-tag, EcoRI/NotI
pEF HA	Modified pEF4 backbone; HA-tag
pEF HA-OTULIN WT	N-terminal HA-tag, BamHI/NotI
pEF HA-OTULIN ΔETSL	N-terminal HA-tag, BamHI/NotI
pEF HA-OTULIN C129A	N-terminal HA-tag, BamHI/NotI
pEF HA-OTULIN E85R/D87R	N-terminal HA-tag, BamHI/NotI
pEF HA-OTULIN C129A/L259E	N-terminal HA-tag, BamHI/NotI

Vector	Information
pSpCas9(BB)-2A-GFP (PX458)	Gift from Feng Zhang (Addgene#48138); For the generation of KO cell lines. Cas9 from *S. pyogenes* with 2A-EGFP, and cloning backbone for sgRNA
PX458 OTULIN KO	For the generation of OTULIN KO cells. Cas9 from *S. pyogenes* with 2A-EGFP and sgRNA
PX458 HOIP KO	For the generation of HOIP KO cells. Cas9 from *S. pyogenes* with 2A-EGFP and sgRNA
PX458 SNX27 KO	For the generation of SNX27 KO cells. Cas9 from *S. pyogenes* with 2A-EGFP and sgRNA
pHAGE-hΔCD2-T2A-SSF	Lentiviral vector; truncated human CD2-T2A-2xStrep-tag II-Flag (N-terminal)
pHAGE-hΔCD2-T2A-SSF-OTULIN WT	N-terminal 2xStrep II-Flag-tag, XbaI/SalI
pHAGE-hΔCD2-T2A-SSF-OTULIN ΔETSL	N-terminal 2xStrep II-Flag-tag, XbaI/SalI
pHAGE-hΔCD2-T2A-SSF-OTULIN C129A	N-terminal 2xStrep II-Flag-tag, XbaI/SalI
pMD2.G	Gift from D. Trono, Addgene#12259; VSV-G envelope expressing plasmid
psPAX2	Gift from D. Trono, Addgene#12260; Lentiviral packaging plasmid
pEGFP-C1	Clontech, N/A; GFP-tag
pEGFP-C1 GFP-SNX27 WT (Isoform 2)	Gift from P. Cullen (Gallon et al., 2014); N-terminal GFP-tag, HindIII/BamHI
pEGFP-C1 GFP-SNX27 H114A (Isoform 2)	Gift from P. Cullen; N-terminal GFP-tag, HindIII/BamHI
pEGFP-C1 GFP-SNX27 Δ67-77 (Isoform 2)	Gift from P. Cullen (Gallon et al., 2014); N-terminal GFP-tag, HindIII/BamHI
pEGFP-C1 GFP-SNX27 G64E/R100E	N-terminal GFP-tag, HindIII/BamHI
pcDNA3.1 (+)	Thermo Fisher Scientific, Cat# V79020
pcDNA3.1 RFP-OTULIN WT	N-terminal RFP-tag, NotI/XbaI
pcDNA3.1 RFP-OTULIN C129A	N-terminal RFP-tag, NotI/XbaI
pcDNA3.1 RFP-OTULIN ΔETSL	N-terminal RFP-tag, NotI/XbaI
pcDNA3.1 HA-HOIP	Gift from K. Winklhofer (Muller-Rischart et al., 2013); N-terminal HA-tag

6.8 *Escherichia coli* (*E. coli*) strains

Strain [Source]	Genotype	Advantage
One Shot TOP10 Chemically Competent *E. coli*	F$^-$ *mcr*A *Δ*(*mrr-hsd*RMS-*mcr*BC) Φ80*lac*ZΔM15 Δ*lac*X74 *rec*A1 *ara*D139 Δ(*ara-leu*)*7697 gal*U *gal*K *rps*L(Str^R) *end*A1 *nup*G	Stable replication of *high-copy* plasmids
One Shot Stbl3 Chemically Competent *E. coli*	F$^-$ *mcr*B *mrr hsd*S20 (r_B^-, m_B^-) *rec*A13 *sup*E44 *ara*-14 *gal*K2 *lac*Y1 *pro*A2 *rps*L20 (Str^R) *xyl*-5 λ$^-$ *leu mtl*-1	Reduced frequency of homologous recombination → cloning of the lentiviral vector
BL21-CodonPlus(DE3)-RIPL Competent *E. coli*	*E. coli* B F$^-$ *ompT hsdS* (r_B^- m_B^-) *dcm*$^+$ Tet^r gal λ (DE3) *endA* Hte [*argU proL* Cam^r] [*argU ileY leuW* Strep/Spec^r]	Additional copies of tRNA genes → specialized in production of recombinant proteins

6.9 Eukaryotic cell lines

Cell line	Information
Jurkat T cells	human T cell line, derived from acute T cell leukemia patient
HEK293 cells	human embryonic kidney cell line containing Adenovirus 5 DNA
HEK293T cells	HEK293 cells containing SV40 large T-antigen
U2OS	human osteosarcoma cell line
OTULIN$^{-/-}$ Jurkat T cells	human T cell line, generated by CRISPR/Cas9
SNX27$^{-/-}$ Jurkat T cells	human T cell line, generated by CRISPR/Cas9
HOIP$^{-/-}$ Jurkat T cells	human T cell line, generated by CRISPR/Cas9
MEF Otulin$^{-/-}$	Mouse embryonic fibroblasts, OTULIN KO, polyclonal, immortalized, gift from D. Komander (MRC, Cambridge)
MEF Otulin$^{+/+}$	Mouse embryonic fibroblasts, control cell line, polyclonal, immortalized, gift from D. Komander (MRC, Cambridge)

6.10 Recombinant proteins

Recombinant protein	Source	Identifier
Biotin-Ahx-Ub^{G76Dha}-Ub	UbiQ, Amsterdam, NL	Cat#UbiQ-121, (Weber et al., 2017)
Biotin-Ahx-Ub-PA	UbiQ, Amsterdam, NL	Cat#UbiQ-076
Deconjugating Enzyme Set	R&D Systems, Minneapolis, USA	Cat#K-E10B
His_{10}-Ub^{G76Dha}-Ub ΔG76	A. Weber; UbiQ, Amsterdam, NL	(Weber et al., 2017)
Recombinant human diUb chains (K48-linked)	R&D Systems, Minneapolis, USA	Cat#UC-200-100
Recombinant human GST-YOD1	Laboratory of D. Krappmann	(Schimmack et al., 2017)
Recombinant human His_6-CYLD Isoform 1	R&D Systems, Minneapolis, USA	Cat#E-556-050
Recombinant human TNF alpha	biomol, Hamburg	Cat#50435.50
Recombinant human $USP21_{cat}$	Gift from T. Sixma	(Faesen et al., 2011)
Recombinant human Wnt3a	R&D Systems, Minneapolis, USA	Cat#5036-WN-010
Recombinant M1-linked tetraUb chains	Enzo Life Sciences, Lörrach	Cat#BML-UW0785-0100
UbiCREST Deubiquitinase Enzyme Set	R&D Systems, Minneapolis, USA	Cat#K-400

6.11 Antibodies

6.11.1 Primary antibodies

Antibody	Dilution	Source	Identifier
Anti-normal mouse IgG	Isotype control in IPs	Santa Cruz Biotechnology, Heidelberg	Cat#sc-2025; RRID: AB_737182
Anti-normal rabbit IgG	Isotype control in IPs	Cell Signaling Technology, Frankfurt	Cat#2729; RRID: AB_2617119
Goat anti-biotin	1:3,000	Cell Signaling Technology, Frankfurt	Cat#7075; RRID: AB_330923
Goat polyclonal anti-Actin [I-19] HRP	1:2,000	Santa Cruz Biotechnology, Heidelberg	Cat#sc1616 HRP; RRID: N/A
Human monoclonal anti-M1-polyUb	1:2,500	Gift from V. Dixit	(Matsumoto et al., 2012); RRID: N/A
Mouse monoclonal anti-CYLD [E10]	1:1,000	Santa Cruz Biotechnology, Heidelberg	Cat#sc-74435; RRID: AB_1122022
Mouse monoclonal anti-ubiquitin [P4D1]	1:1,000	Santa Cruz Biotechnology, Heidelberg	Cat#sc-8017; RRID: AB_2315523
Mouse monoclonal anti-IκBα	1:1,000	Cell Signaling Technology, Frankfurt	Cat#4814; RRID: AB_390781
Mouse monoclonal anti-phospho-IκBα (Ser32/36) [5A5]	1:1,000	Cell Signaling Technology, Frankfurt	Cat#9246; RRID: AB_2151442
Mouse monoclonal anti-FLAG M2	1:10,000	Sigma-Aldrich, Taufkirchen	Cat#F3165; RRID: AB_259529
Mouse monoclonal anti-HOIP	1:5,000	R&D Systems, Minneapolis, USA	Cat#MAB8039: RRID: AB_10676585
Mouse monoclonal anti-SNX27 [1C6]	1:1,000	Abcam, Cambridge, UK	Cat#ab77799; RRID: AB_10673818
Mouse monoclonal anti-ATP7A [D9]	1:1,000	Santa Cruz Biotechnology, Heidelberg	Cat#sc-376467; RRID: AB_11150485
Mouse polyclonal anti-β-catenin	1:2,000	BD Biosciences, Franklin Lakes, USA	Cat#610153; RRID: AB_397554
Rabbit monoclonal anti-M1-polyUb	1:1,000	Merck Millipore, Darmstadt	Cat#MABS19; RRID:AB_2576212
Rabbit monoclonal anti-EEA1 [C45B10]	1:500	Cell Signaling Technology, Frankfurt	Cat#3288; RRID: AB_2096811
Rabbit monoclonal anti-VPS35 [EPR11501(B)]	1:10,000	Abcam, Cambridge, UK	Cat#ab157220; RRID: AB_2636885
Rabbit polyclonal anti-OTULIN	1:1,000	Cell Signaling Technology, Frankfurt	Cat#14127; RRID: AB_2576213
Rabbit polyclonal anti-OTUB1	1:1,000	Bethyl Laboratories, Montgomery, USA	Cat#A302-917A; RRID: AB_10663033
Rabbit polyclonal anti-USP5/IsoT	1:1,000	Bethyl Laboratories, Montgomery, USA	Cat#A301-542A; RRID: AB_1040028
Rabbit polyclonal anti-SHARPIN	1:1,000	Proteintech, Manchester, UK	Cat#14626-1-AP; RRID: AB_2187734
Rabbit polyclonal anti-GFP	1:1,000	Cell Signaling Technology, Frankfurt	Cat#2555; RRID: AB_390710

Antibody	Dilution	Source	Identifier
Rabbit polyclonal anti-SNX27	1:1,000	Gift from W. Hong	(Cai et al., 2011)
Rabbit polyclonal anti-VPS26	1:1,000	Abcam, Cambridge, UK	Cat#ab23892; RRID: AB_2215043
Rabbit polyclonal anti-DGKζ	1:1,000	Abcam, Cambridge, UK	Cat#ab105195; RRID: AB_10714139
Rabbit polyclonal anti-GLUT1	1:100	Abcam, Cambridge, UK	Cat#ab15309; RRID: AB_301844
Rabbit polyclonal anti-STEAP3	1:1,000	Proteintech, Manchester, UK	Cat#17186-1-AP; RRID: AB_2197841
Rabbit polyclonal anti-KIDINS220	1:1,000	Proteintech, Manchester, UK	Cat#21856-1-AP; RRID: AB_10836934
Rabbit polyclonal anti-Beta PIX	1:1,000	Merck Millipore, Darmstadt	Cat#07-1450-I; RRID: AB_1586904
Rat monoclonal anti-HA [3F1]	1:10,000	Core facility monoclonal antibodies HMGU	RRID: N/A
Rat monoclonal anti-HA [12CA5]	1:1,000	Core facility monoclonal antibodies HMGU	RRID: N/A
Rat monoclonal anti-MRP4 [M4I-10]	1:2,500	Abcam, Cambridge, UK	Cat#ab15602; RRID: AB_301991
Sheep polyclonal anti-HOIL-1/RBCK1	1:1,000	MRC PPU Reagents and Services, Dundee, UK	Cat#S105D; RRID: N/A

6.11.2 Secondary antibodies

Antibody	Dilution	Source	Identifier
Donkey polyclonal anti-human IgG	1:10,000	Jackson ImmunoResearch, Cambridgeshire, UK	Cat# 709-035-149; RRID: AB_2340495
Donkey polyclonal anti-mouse IgG	1:10,000	Jackson ImmunoResearch, Cambridgeshire, UK	Cat#715-035-150; RRID: AB_2340770
Donkey polyclonal anti-rabbit IgG	1:10,000	Jackson ImmunoResearch, Cambridgeshire, UK	Cat#711-035-152; RRID: AB_10015282
Donkey polyclonal anti-rabbit IgG-Cy5	1:500	Jackson ImmunoResearch, Cambridgeshire, UK	Cat#711-175-152; RRID: AB_2340607
Donkey polyclonal anti-rat IgG	1:10,000	Jackson ImmunoResearch, Cambridgeshire, UK	Cat#112-035-003; RRID: AB_2338128
Donkey polyclonal anti-sheep IgG	1:10,000	Jackson ImmunoResearch, Cambridgeshire, UK	Cat#713-035-003; RRID: AB_2340709

6.11.3 Stimulatory antibodies

Antibody	Dilution	Source	Identifier
Mouse monoclonal anti-human CD28 [CD28.2]	1 µg in 300 µl	BD Biosciences, Franklin Lakes, USA	Cat#555725; RRID: AB_396068
Mouse monoclonal anti-human CD3 [HIT3a]	0.3 µg in 300 µl	BD Biosciences, Franklin Lakes, USA	Cat# 555336; RRID: AB_395742

Antibody	Dilution	Source	Identifier
Rat monoclonal anti-mouse IgG1 [A85-1]	0.5 µg in 300 µl	BD Biosciences, Franklin Lakes, USA	Cat#553440; RRID: AB_394860
Rat monoclonal anti-mouse IgG2a [R19-15]]	0.5 µg in 300 µl	BD Biosciences, Franklin Lakes, USA	Cat#553387; RRID: AB_394825

6.11.4 FACS antibodies

Antibody	Dilution	Source	Identifier
Mouse monoclonal anti-CD2-APC [RPA-2.10]	1:400	Thermo Fisher Scientific, Waltham, USA	Cat# 17-0029-41; RRID: AB_10806970
Mouse monoclonal anti-human CD28-APC [CD28.2]	1:50	BD Biosciences, Franklin Lakes, USA	Cat#559770; RRID: AB_398666
Mouse monoclonal anti-human CD3-FITC [OKT3]	1:100	Thermo Fisher Scientific, Waltham, USA	Cat#11-0037-41; RRID: AB_2016601

6.12 Software

Software	Source
Adobe Illustrator CS6 (version 16)	Adobe Systems, San José, USA
Adobe Photoshop CS6 (version 16)	Adobe Systems, San José, USA
CLC Main Workbench (version 7.0.3)	Qiagen, Hilden
Endnote X9	Clarivate Analytics, Philadelphia, USA
FlowJo (version 10)	FlowJo LLC, Ashland, USA
GraphPad Prism (version 5.01)	GraphPad, San Diego, USA
Image J (1.50i)	Wayne Rasband, NIH, USA
Microsoft Office 2010	Microsoft Corp., Redmond, USA

7. Methods

7.1 Molecular biology methods

7.1.1 Polymerase chain reaction (PCR)

For the amplification of DNA sequences, samples were prepared as specified in the following scheme:

Component	Amount or volume
Template DNA	50 ng
5´ primer (25 µM)	0.5 µl
3´ primer (25 µM)	0.5 µl
dNTPs (10 mM each)	1.25 µl
5x Herculase buffer	10 µl
DNA polymerase (Herculase II)	0.75 µl
H_2O	Ad 50 µl

The following standard PCR program was used for the amplification:

Step	Temperature	Time	Cycles
Initialization	95°C	4 min	1
Denaturation	95°C	1 min	33
Annealing	lowest primer melting temperature – 5°C	40 s	
Elongation	72°C	30 s/kb	
Final elongation	72°C	7 min	1
Cooling	4°C	∞	1

PCR products were assessed for correct size on agarose gels and purified (section 7.1.4).

7.1.2 Site-directed mutagenesis

Mutants were generated by site-directed mutagenesis. In this PCR-based method, the desired mutation is introduced by a specifically designed primer, which contains the mutation. In a first PCR (megaprimer PCR), a fragment was generated that bears the mutation at one end and the flanking restriction site at the other end. This PCR product was then purified and used as megaprimer (5 - 15 µl) in a second PCR, together with a primer that contains the second restriction site. In the second PCR, the annealing temperature was reduced to 50°C. The final PCR product was examined by agarose gel electrophoresis and purified (section 7.1.4).

7.1.3 DNA restriction digestion

Amplified inserts and target vectors were digested using restriction enzymes and the appropriate buffers. The prepared reaction mixtures were incubated for at least 90 min at 37°C. Subsequently, samples were separated by agarose gel electrophoresis and DNA fragments of correct size were purified (section 7.1.4).

7.1.4 Agarose gel electrophoresis

PCR products and digested DNA samples were separated on the basis of size by agarose gel electrophoresis. Agarose gels were prepared by dissolving 1 - 2% (w/v) agarose in warm TAE buffer. For visualization of DNA molecules ethidium bromide was added to the solution. DNA samples were mixed with 6x DNA loading dye and loaded on the hardened gels. For sizing of DNA fragments, 5 µl 1 kb plus DNA ladder was loaded. Gels were run in TAE buffer at 80-120 V for approximately 1 h. Afterwards, DNA molecules were visualized by UV light and extracted from the gel using the "Nucleo-Spin Gel and PCR Clean-up" kit according to the manufacturer´s instructions.

7.1.5 Ligation

For ligation of digested inserts and corresponding vectors either the T4 DNA ligase or the "Rapid DNA Ligation Kit" were used according to the manufacturer´s instructions. The prepared reaction batches at a threefold molar ratio of insert to vector were incubated for at least 30 min at room temperature (RT). After ligation, a proportion of each of the ligation reaction mixtures was transformed into chemically competent *E. coli* cells.

7.1.6 Transformation of *E. coli*

For the amplification of recombinant plasmids, *E. coli* Top10 or *E. coli* Stbl3 cells were transformed, whereas the transformation of plasmids into BL21-RIPL chemically competent *E. coli* cells was required for protein production. *E. coli* cells were mixed with the ligation samples (transformation) or with 50-100 ng plasmid DNA (retransformation) and incubated on ice for 30 min. Cells were then heated for 45 s at 42°C (heat shock) and immediately chilled on ice. 250 µl LB medium was added and the samples were incubated shaking for 1 h at 37°C. Afterwards, the cells were plated on LB agar plates containing antibiotic. These plates were incubated at 37°C overnight and finally stored in the refrigerator.

7.1.7 Minipreparation of plasmid DNA

Pre-cultures were prepared by inoculating 5 ml LB medium containing antibiotic with a single *E. coli* colony containing the required plasmid from the selection plate. The cultures were incubated overnight, shaking at 37°C. The next day, plasmid DNA was isolated from 4 ml of the overnight cultures by using the "NucleoSpin Plasmid Kit", following the manufacturer´s protocol.

7.1.8 Maxipreparation of plasmid DNA

150 ml LB medium containing antibiotic was inoculated with 350 µl of a fresh pre-culture. The culture was incubated overnight, shaking at 37°C. The following large-scale plasmid isolation was performed using the "QIAGEN Plasmid Maxi Kit" according to the manufacturer´s instructions.

7.1.9 DNA sequencing

All newly generated plasmids were sequenced by Eurofins Genomics (Ebersberg) and assessed for the right order of nucleotides before they were further processed.

7.2 Cell culture methods

7.2.1 Storage of cell lines

For storage of cells, $1x10^7$ cells were pelleted by centrifugation (350 x g, 4 min), resuspended in 1 ml freezing medium (DMEM/RPMI, 20% (v/v) FCS (fetal calf serum), 10% (v/v) DMSO (dimethyl sulfoxide)) and transferred into cryo vials. Vials were frozen at -80°C in isopropanol-containing cryo-freezing containers which reduce the temperature by 1°C per min. For long-term storage, cell vials were transferred into liquid nitrogen.

7.2.2 Cultivation of cell lines

All mammalian cell lines were maintained at 37°C in a humidified atmosphere at 5% CO_2. Jurkat T cells were cultured in RPMI 1640 Medium supplemented with 10% FCS, 100 U/ml penicillin and 100 µg/ml streptomycin and kept at a density of 0.5 to $1.5x10^6$ cells per ml.

All adherent cell lines were cultured in DMEM supplemented with 10% FCS, 100 U/ml penicillin and 100 µg/ml streptomycin and maintained at 30-80% confluency. To split or seed cells, the cell layer was washed carefully with PBS and incubated with 0.5-2 ml

0.05% trypsin/EDTA solution until cells detached. Trypsinization was stopped by adding fresh medium and cells were diluted or seeded as required.

7.2.3 Transfection of Jurkat T cells by electroporation

Upon electroporation of cells, electric pulses lead to the temporary formation of pores in the cell membrane, which facilitate the uptake of DNA. For the transfection of Jurkat T cells, $8x10^6$ cells were resuspended in 400 µl medium and mixed with 5 µg DNA in a 4 mm electroporation cuvette. Cells were electroporated with a Gene Pulser X System at 220 V and 1000 µF (exponential program) and subsequently transferred into pre-warmed RPMI to allow them to recover. Cells were analyzed 24 - 72 hrs after electroporation.

7.2.4 Calcium phosphate transfection of HEK293 cells

Using this method, calcium cations and phosphate anions are brought together forming calcium phosphate [$Ca_3(PO_4)_2$] crystals. DNA to be transfected is bound by these crystals and can that way be absorbed by cells via endocytosis. The day before transfection, HEK293 cells were washed, trypsinized and counted. $2.5x10^6$ cells were seeded per 10 cm dish in 9 ml of supplemented DMEM. Prior to transfection, cells were 10 - 30% confluent. Transfection samples were prepared by mixing up to 10 µg DNA with 50 µl $CaCl_2$ (2.5 M) and 450 µl sterile H_2O. This mixture was then added dropwise into a 2 ml reaction tube containing 500 µl sterile 2x HBS, while constantly vortexing. For precipitate formation samples were incubated for 15 min at RT. Subsequently, solutions were distributed dropwise on cells. For DNA absorption and transient overexpression of the desired proteins, cells were incubated over night at 37°C.

7.2.5 Generation of OTULIN-, HOIP- and SNX27-deficient cells

KO cell lines were generated using the CRISPR/Cas9 system (Ran et al., 2013). Single guide RNAs (sgRNAs) targeting exon 2 of the *OTULIN* gene (5´-ATACATGAAAGAGGGGCATC-3´) or exon 1 of the *SNX27* gene (5´-GGCTACGGCTTCAACGTGCG-3´) were designed by means of two online tools (http://crispr.mit.edu/ and https://portals.broadinstitute.org/gpp/public/analysis-tools/sgrna-design). The sgRNA targeting exon 1 of the *RNF31/HOIP* gene (5´-GAGAGCTGGCTAGTAGCGGC-3´) was adopted from the literature (Yang et al., 2016). Two partially complementary oligos carrying overhangs of four nucleotides compatible for cloning into the PX458 backbone were synthesized for each KO (sequences listed in section 6.6.1). Oligo pairs were annealed (5 min at 95°C) and ligated into BbsI-digested

pSpCas9(BB)-2A-GFP (PX458) vector. This vector enables simultaneous expression of *S. pyogenes* Cas9, eGFP and sgRNAs targeting the respective gene.
Jurkat T cells were transfected with the manipulated PX458 vector as described in section 7.2.3. HEK293 cells were transfected using X-tremeGENE HP DNA Transfection Reagent according to the manufacturer's instructions. After 1-3 days, GFP-positive cells were sorted by A. Gewies using a MoFlow Cytometer (Cytomation). Sorted cells were seeded in 96-well plates at very low density (0.5 - 5 cells / well) to obtain clonal cell populations. After expansion, cell clones were lysed in RIPA buffer and screened for loss of the respective protein by WB. In addition, genomic DNA was isolated from cells using the "QIAamp DNA Mini Kit", following the manufacturer´s protocol. The DNA was amplified by PCR around the targeted site using the "Taq DNA Polymerase Kit" (primers listed in section 6.6.2) and sequenced by Eurofins Genomics in order to verify the KOs on genomic level. Jurkat KO clones were additionally checked for the expression of CD3 and CD28 by FACS.

7.2.6 Lentiviral transduction of KO cells

To generate cell lines stably expressing OTULIN WT and mutants, OTULIN-deficient cells were lentivirally transduced with different pHAGE-hΔCD2-T2A-OTULIN constructs. Using this construct, both the truncated human surface marker protein CD2 (ΔCD2) and OTULIN are translated from the same mRNA at equimolar levels. The ribosome skips the peptide bond formation at the C-terminus of the T2A peptide resulting in the generation of two distinct proteins instead of a long fusion protein (Szymczak et al., 2004).
For virus production, $1.5x10^6$ HEK293T cells were seeded in a 10 cm dish in 8 ml DMEM. The day after, cells were transfected with 1.5 µg of the packaging vector psPAX2, 1 µg of the lentiviral envelope plasmid pMD2.G and 2 µg of the respective pHAGE-hΔCD2-T2A construct using X-tremeGENE HP DNA Transfection Reagent according to the manufacturer's instructions. 72 hrs after transfection, the virus-containing supernatants were collected, sterile filtered (0.45 µm) and added to KO cells in the presence of 8 µg/ml polybrene. For lentiviral transduction of OTULIN-deficient Jurkat T cells, $5x10^5$ cells were incubated with 500 - 1500 µl supernatant. 24 hrs later, infected cells were washed three times with PBS and transferred into fresh RPMI medium. After a recovery phase of about one week, transduction efficiency was validated by flow cytometry after anti-CD2 staining of the cells. Moreover, cells were lysed in RIPA buffer and OTULIN expression was analyzed by WB after SDS-PAGE.

7.2.7 Stimulation of cells

Stimulation of Jurkat T cells was performed in 2 ml reaction tubes on a rotator at 37°C. For activation of the Wnt signaling pathway, $3x10^6$ Jurkat T cells were stimulated with 20 ng/ml recombinant human Wnt3a protein. Cells were treated with 20 ng/ml recombinant human TNFα to induce TNFR signaling. TCR stimulation was mimicked by CD3/CD28 co-ligation. $3x10^6$ Jurkat T cells were resuspended in 300 µl 'old' medium and incubated with 0.3 µg anti-CD3 and 1 µg anti-CD28 antibodies in the presence of cross-linking secondary antibodies (0.5 µg rat anti-mouse IgG1 and IgG2a). After stimulation, cells were lysed in 100 µl High Salt buffer and analyzed by WB following SDS-PAGE.

7.3 Flow cytometry

Cells were tested for surface protein expression using an Attune Acoustic Focusing Cytometer. This cytometer is equipped with a blue laser (488 nm), a red laser (638 nm) and different emission filters enabling the detection of different fluorophores.

7.3.1 Staining of surface molecules

To analyze surface expression of hΔCD2, hCD3 or hCD28, approximately $0.2x10^6$ cells were resuspended in 100 µl FACS buffer and incubated with the respective fluorophore-coupled antibody (listed in section 6.11.4) for 20 min at 4°C in the dark. Subsequently, cells were washed three times with PBS and resuspended in PBS or FACS buffer for the analysis by flow cytometry.

7.3.2 Determination of cell surface GLUT1 levels

U2OS cells were transfected with the respective pHAGE-hΔCD2-T2A construct (mock, OTULIN WT, OTULIN ΔETSL) using X-tremeGENE HP DNA Transfection Reagent according to the manufacturer's instructions. 48 hrs after transfection, cells were trypsinized and counted. 100,000 cells were resuspended in 95 µl Buffer A (Complete culture medium, 0.1% NaN_3 and 1 mM EDTA) and incubated with 10 µl GLUT1.RBD.GFP and 0.25 µl anti-CD2 antibody for 20 min at 37°C. After staining, cells were washed three times with Buffer B (PBS, 0.1% NaN_3, 1 mM EDTA and 2% FCS) and analyzed for OTULIN overexpression (ΔCD2 positive cells) and GLUT1 surface expression by flow cytometry. In order to quantify GLUT1 surface expression, median fluorescence intensities of the GLUT1.RBD.GFP signal were determined with the FlowJo software and normalized to mock. Data from three independent experiments (n=3) were analyzed and depicted as mean ±

standard deviation (SD). Statistical analysis was performed using the unpaired Student´s *t*-test (GraphPad Prism).

7.4 Synthesis of activity-based probes

7.4.1 Synthesis of bio-Ub^{G76Dha}-Ub (OTULIN ABP)

Biotin-Ahx-Ub^{G76Dha}-Ub (OTULIN ABP) was chemically synthesized by our collaboration partner Farid El Oualid (UbiQ). The detailed protocol is published in (Weber et al., 2017).

7.4.2 Synthesis of His$_{10}$-Ub^{G76Dha}-Ub ΔG76 (OTULIN ABP ΔG76)

In contrast to the OTULIN ABP synthesis (section 7.4.1), the synthesis of the His$_{10}$-Ub^{G76Dha}-Ub ΔG76 (OTULIN ABP ΔG76) was not based on solid-phase peptide synthesis, but on a recombinant precursor protein. The precursor protein His$_{10}$-Ub^{G76C}-Ub ΔG76, which carries a G76C substitution in the distal Ub and lacks the C-terminal glycine of the proximal Ub, was produced in *E. coli* BL21-CodonPlus (DE3)-RIPL cells and purified via affinity chromatography (see section 7.5.1). Subsequently, the Cys76 in the distal Ub moiety was coverted into Dha through oxidative elimination by our collaboration partner Farid El Oualid (UbiQ) (Weber et al., 2017).

7.5 Biochemical and immunological methods

7.5.1 Production and purification of recombinant proteins

C-terminally Strep-tag II (Strep)-tagged OTULIN constructs and N-terminally His$_{10}$ (His)-tagged diUb variants were expressed in *E. coli* BL21-CodonPlus (DE3)-RIPL cells and purified via affinity chromatography using the ÄKTA Purifier system. Bacteria carrying the respective plasmid were grown at 37°C in autoclaved LB medium containing 100 µg/ml ampicillin and 25 µg/ml chloramphenicol. At an OD$_{600}$ of 0.6 - 0.8, protein expression was induced by adding 0.5 mM IPTG and 200 ng/ml AHT. Proteins were produced overnight at 21°C. Cultures (1 l) were harvested by centrifugation (2,100 x g / 20 min / 4°C) and lysed by sonification in Strep Lysis buffer or His Binding buffer (10 ml). Lysates were cleared by centrifugation (51,000 x g / 20 min / 4°C). Extracts containing Strep-tagged proteins were applied on StrepTrap columns and unspecifically bound proteins were removed by rinsing the columns with Strep Washing buffer. Proteins were eluted using 1x Strep Elution buffer and desalted via HiTrap Desalting columns in Desalting buffer.

Cleared lysates containing His-tagged diUb variants were applied on HisTrap columns and unspecific proteins were washed away with His Washing buffer. DiUb constructs were eluted by a gradient of His Elution buffer and desalted via HiTrap Desalting columns in 50 mM sodium phosphate buffer (pH 8).
The expression and purification of recombinant proteins for crystallography and ITC studies was performed by Paul Elliott (MRC, Cambridge; University of Oxford).

7.5.2 SDS polyacrylamide gel electrophoresis (SDS-PAGE)

The analytical SDS-PAGE technique is used to separate proteins depending on their size by an electrical field. Depending on the size of the considered proteins, the acrylamide content of the separating gels and therefore their cross-linking level was adjusted (7.5 – 15%). Polymerization of the gels was induced by adding APS (ammonium persulfate) and TEMED. During polymerization, the separating gel was covered with isopropanol to obtain an even surface. 3% stacking gels containing pockets were added on top of fully polymerized separating gels.
All protein samples were treated with SDS-containing sample buffer (Roti-Load 1) and boiled at 95°C for 8 min. Thereby the proteins are denatured and covered by negatively charged SDS molecules. To estimate the molecular weight of the separated proteins, a prestained protein ladder was loaded in a well next to the samples. After loading, electrophoresis was performed in SDS Electrophoresis buffer at 90 – 120 V for approximately 2.5 hrs. Subsequently, the proteins in the gels were either visualized using Coomassie staining solution or the “Pierce Silver Stain Kit” or transferred onto PVDF membranes by Western Blotting (see section 7.5.3).

7.5.3 Western Blot (WB)

To enable immunodetection of proteins following separation by SDS-PAGE, proteins were electrophoretically transferred onto PVDF membranes using a semi-dry Western Blot transfer system. Before transfer, PVDF membranes were activated in methanol and subsequently equilibrated in Blotting buffer together with Whatman filter papers. The membrane and the SDS gel were placed between soaked filter papers in the blotting device, and the transfer was carried out for 110 min with a current of 90 mA per gel.
After WB transfer, membranes were agitated for 1 h in blocking solution to avoid unspecific binding of antibodies. Blocked membranes were incubated overnight with a specific primary antibody (in PBS-T with 2.5% milk, see section 6.11.1), shaking at 4°C. The next day, membranes were washed three times in PBS-T for 10 min to remove unbound antibody.

Horseradish peroxidase (HRP)-coupled secondary antibody (in PBS-T with 1.25% milk, see section 6.11.2) was added for 1 h at RT and finally, membranes were washed again with PBS-T.
To visualize proteins, membranes were covered with an enhanced chemoluminescence (ECL) substrate which is converted by the HRP. This enzymatic reaction is accompanied by light emission and can thus be detected using ECL film.

7.5.4 Labeling recombinant DUBs with OTULIN ABP or Ub-PA

Recombinant DUBs were diluted in DUB Reaction buffer and incubated for the indicated times at 30°C or 37°C with different amounts of OTULIN ABP or Ub-PA (amounts specified in the Figure Legends). Reactions were stopped by boiling in reducing SDS sample buffer, and proteins were separated by SDS-PAGE (see section 7.5.2). Gels were stained using Coomassie-based PageBlue Protein Staining Solution or the “Pierce Silver Stain Kit” in order to analyze DUB-diUb (DUB-ABP) or DUB-Ub complex formation.

7.5.5 Ub chain cleavage assay

$OTULIN_{cat}$ WT (aa 80-352, 500 pM) was diluted in DUB Reaction buffer with 0.03% BSA and incubated at 37°C for 25 min with 250 ng of Met1-tetraUb. For inhibition, OTULIN was treated with OTULIN ABP or PR-619 at the indicated concentrations (1 h, RT), prior to addition of the tetraUb chains.
In diUb cleavage assays, DUBs (500 nM) were incubated with 500 ng diUb in DUB Reaction buffer without BSA (1 h, 30°C). Cleavage reactions were stopped by boiling in 1x SDS sample buffer and analyzed by WB or Silver staining after SDS-PAGE.

7.5.6 Strep-PD

For Strep-tag II (Strep)-PDs, 20 µg recombinant $OTULIN_{cat}$-Strep (WT, C129A) were mixed with equimolar amounts of His_{10}-Ub-Ub WT or His_{10}-Ub^{G76A}-Ub in buffer A (total volume 500 µl) and incubated on the rotator for 2 hrs at 4°C. 20 µl was removed from each sample as an Input control (Input). Strep-Tactin Sepharose was pre-equilibrated in buffer A, added to the samples (60 µl of 50% slurry per sample) and incubated for 1 h with the protein mixtures to enable binding of $OTULIN_{cat}$-Strep to the resin. The resin was pelleted by centrifugation (2,500 x g / 4°C / 1 min) and another control sample was removed from each supernatant to check whether proteins had been depleted from the solution by the pull-down procedure. OTULIN-coupled resin was washed eight times with 1 ml of buffer B to get rid of weaker protein interactions and subsequently boiled in 25 µl of 2x reducing SDS sample buffer.

Control samples were denatured by boiling in 1x SDS sample buffer and analyzed together with the pull-down eluates by WB after SDS-PAGE.

7.5.7 Treatment of cell extracts with diUb probes

For the treatment of cell extracts with diUb probes, 2 – 3x10^6 HEK293 or Jurkat T cells were lysed in 250 µl co-IP buffer without protease inhibitors. Cleared extracts were divided into aliquots (20 – 50 µl reaction volume / sample). To analyze labeling of cellular DUBs or the formation of polyUb chains, different amounts of OTULIN ABP, OTULIN ABPΔG76 or Ub^{G76A}-Ub were added to the samples and incubated at 30 or 37°C for 2 – 60 min (indicated in the Figure Legends). Reactions were stopped by boiling in reducing sample buffer and analyzed by WB. For ATP depletion, aliquots were treated with 0.5 U Apyrase for 30 min before the addition of the OTULIN ABP. For linkage analyses of enriched polyUb chains, 44 µl aliquots were treated first with 1 µg OTULIN ABP for 30 min at 37°C before adding 5 µl of different linkage-specific 10x DUBs (from the "UbiCREST Deubiquitinase Enzyme Set") and incubating for further 30 min at 37°C.

7.5.8 Strep-PD from cell extracts

In order to identify the OTULIN interactome by LC-MS/MS, Strep-PDs were performed in extracts of OTULIN KO Jurkat T cells reconstituted with either SSF-tagged OTULIN WT or mock (SSF-tag only). Every sample was prepared in triplicate. For each sample, 2x10^8 cells were lysed in 1 ml co-IP buffer with phosphatase and protease inhibitors for 1 h at 4°C. Cell debris was removed from the lysates by centrifugation (20,000 x g, 20 min, 4°C), supernatants were transferred into new reaction tubes and diluted with 500 µl co-IP buffer. 15 µl was removed from each sample and mixed with SDS sample buffer to later assess by WB whether equal cell numbers were used. Strep-Tactin sepharose was pre-equilibrated in co-IP buffer and added to each sample (300 µl of 50% slurry / sample). The mixtures were incubated on a rotator for 16 hrs at 4°C to ensure efficient binding of SSF-OTULIN to the beads. The resin was sedimented by centrifugation (250 x g, 2 min, 4°C) and another 15 µl control sample was removed from each supernatant to check whether OTULIN had been depleted from the extracts by the PD procedure. Beads were washed three times with 1 ml co-IP buffer without inhibitors (250 x g, 2 min, 4°C) and subsequently boiled in 150 µl 2x reducing SDS sample buffer. 7.5 µl (5%) was removed for WB analysis, the rest was analyzed by LC-MS/MS.

7.5.9 His-PD / OTULIN ABPΔG76-PD

For His-PDs, $2x10^7$ Jurkat T cells were lysed in His Lysis buffer without protease inhibitors for 20 min at 4°C. Cell debris was removed from the lysate by centrifugation (20,000 x g, 10 min, 4°C). To check if equal cell numbers were used, 30 µl was removed from each sample (Input/lysate). Cell extracts were then incubated with 4 µg His_{10}-Ub^{G76Dha}-Ub ΔG76 (OTULIN ABP ΔG76) for 60 min at RT, enabling the coupling of active OTULIN and the probe. Ni-NTA Agarose was pre-equilibrated in lysis buffer, added to the samples (35 µl of 50% slurry per sample) and incubated on the turning wheel for 2 hrs at 4°C. By centrifugation (500 x g / 2 min / 4°C) beads were sedimented and subsequently washed 3 times with 1 ml of washing buffer (300 mM NaCl, 50 mM NaH_2PO_4, 0.2% NP-40, 10% glycerol, 20 mM imidazole, pH 8) to remove unspecifically binding proteins. OTULIN ABP ΔG76-bound protein complexes were eluted by boiling the beads in 2x reducing SDS sample buffer (25 µl) and analyzed by WB after SDS-PAGE.

7.5.10 Biotin-PD / OTULIN ABP-PD

For Biotin-PDs, $1x10^7$ HEK293 or $2x10^7$ Jurkat T cells were lysed in 500 µl co-IP buffer without protease inhibitors for 20 min at 4°C. Cell debris was removed from the lysate by centrifugation (20,000 x g, 10 min, 4°C). To determine if equal cell numbers were used, 30 µl was removed from each sample (input/lysate). For a pre-clearing step, cell extracts were mixed with 15 µl of High Capacitiy Streptavidin Agarose and incubated on the turning wheel for 1 h at 4°C. The beads were sedimented by centrifugation (2,500 x g / 2 min / 4°C) and 450 µl of the resulting supernatant were transferred into a new reaction tube. The pre-cleared cell extracts were then incubated at RT with 2 – 4 µg OTULIN ABP (15 – 60 min), enabling the covalent coupling of active OTULIN and the probe. To bind and precipitate the formed OTULIN-ABP complexes, 25 – 35 µl of streptavidin agarose was added and incubated with the samples on the turning wheel for 1 – 2 hrs at 4°C. After a first centrifugation step (2,500 x g / 4°C / 2 min), control samples (30 µl) were removed from each supernatant to monitor depletion of proteins by the pull-down procedure. Then, beads were washed three times with 1 ml co-IP buffer to remove unspecific interactions. Protein complexes were eluted by boiling beads in 25 µl 2x SDS sample buffer and analyzed by WB after SDS-PAGE.

To determine protein levels in input (prior to PD) and supernatant (after PD), control samples were denatured by boiling in SDS sample buffer and loaded in equal amounts on SDS gels for WB analysis. All protein band intensities were quantified using ImageJ software and

normalized to β-actin. The ratio of quantified proteins between the supernatant and input was calculated to obtain relative amounts of 'free', OTULIN-ABP unbound proteins.
To identify the OTULIN ABP interactome by LC-MS/MS, we used a larger quantity of cells ($5x10^7$ cells, lysed in 1 ml co-IP buffer) for the biotin-PDs. Pre-cleared lysates (950 µl) were incubated for 30 min at 30°C with (or without) Apyrase (4 U), to deplete cellular ATP. To inhibit DUBs, samples were incubated for a further 30 min at 30°C with (or without) PR-619 (250 µM). Extracts were then treated with (or without) OTULIN ABP (5 µg) for 15 min at RT prior to adding 35 µl streptavidin agarose to pull-down protein-ABP complexes (2 hrs, 4°C). In order to remove most non-covalent ABP interactors, beads were washed twice with co-IP buffer and subsequently twice with high-stringent 1% SDS-containing co-IP buffer. For the identification of OTULIN interactors, beads were washed four times with co-IP buffer (no SDS). PDs were eluted by boiling the beads in 50 µl 2x SDS sample buffer. 2.5 µl (5%) was removed for WB analysis, whereas the rest was analyzed by LC-MS/MS.

7.5.11 GFP-Trap

For transient overexpression of proteins, $2.5x10^6$ HEK293 cells were seeded in a 10 cm dish and transfected the next day using calcium phosphate transfection. One day after transfection, cells were washed with PBS and lysed in 500 µl co-IP buffer (20 min, 4°C). Lysates were cleared by centrifugation at 20,000 x g (10 min, 4°C). 30 µl was removed from each lysate and mixed with reducing SDS sample buffer (lysate control). Subsequently, extracts were incubated with 20 µl GFP-Trap beads (50% suspension), equilibrated in co-IP buffer, for 1 - 2 hrs on a rotator at 4°C. To pull down GFP-tagged proteins, samples were centrifuged at 2,500 x g (2 min, 4°C). Beads were washed three times in co-IP buffer without inhibitors and finally resuspended in 25 µl 2x SDS sample buffer. PD eluates as well as lysate control samples were analyzed by antibody detection on WB membranes after SDS-PAGE.
For the analysis of interactions between SNX27 and cargos, cells were lysed in Cargo buffer without salt, according to (Gallon et al., 2014).

7.5.12 Immunoprecipitation (IP)

For IPs of endogenous proteins, $2.5\text{-}5x10^7$ cells were lysed in 500 µl co-IP buffer (20 min, 4°C). For IPs of overexpressed proteins from HEK293 extracts, fewer cells ($\sim1x10^7$) were lysed one day after transfection. Lysates were centrifuged at 20,000 x g (10 min, 4°C) and incubated with the respective antibodies on a rotator overnight at 4°C. The next day, 15 - 25 µl Protein G Sepharose (50% suspension) was added and incubated for another

1 - 2 hrs at 4°C. IPs were washed three times with 1 ml co-IP buffer without inhibitors (700 x g, 2 min, 4°C) and subsequently denatured by boiling in 25 µl 2x SDS sample buffer. IPs and lysate controls were analyzed by WB after SDS-PAGE.

7.5.13 Size exclusion chromatography analysis of cell extracts

Gel filtration analyses of cell extracts were performed on an ÄKTApurifier System. $1x10^8$ Jurkat T cells were washed with PBS and lysed in 400 µl SEC lysis buffer for 30 min at 4°C. Lysates were initially centrifuged at 20,000 x g (20 min at 4°C) and subsequently subjected to an ultracentrifugation step (125,000 x g, 30 min, 4°C). The resulting supernatants were filtered using Proteus Mini Clarification Spin Columns (Generon; 14,000 x g, 2 min, 4°C) to get rid of particles that are larger than 0.2 µm. Extracts were loaded onto a Superdex 200 10/300 GL column equilibrated in SEC buffer. 0.5 ml fractions were collected and mixed with SDS sample buffer to analyze the elution profile of the respective proteins by WB after SDS-PAGE.

7.5.14 Confocal microscopy

U2OS cells were transfected with GFP-SNX27 and RFP-OTULIN constructs using X-tremeGENE HP DNA Transfection Reagent according to the manufacturer's instructions. 10 hrs after transfection, 30,000 cells per well were seeded in 12-well plates on round cover glasses coated with Poly-L-lysine solution. The following day, cells were fixed with 4% Roti-Histofix (10 min, RT), washed twice with PBS-T and permeabilized in Permeabilization buffer for 15 min. Then, cells were washed again with PBS-T, blocked in Blocking solution for 1 h and incubated with primary antibody in blocking solution overnight at 4°C. The next day, cells were washed three times with PBS-T, incubated with fluorophore-labeled secondary antibody in blocking solution (1 h, RT) and washed again twice with PBS-T. After nuclear counterstain with DAPI in PBS, cover glasses were washed in PBS and mounted on SuperFrost slides using mounting medium (provided by Annalisa Schaub). Images were acquired using a Leica SP5 confocal laser scanning microscope (63x magnification) by Annalisa Schaub.

7.6 X-ray crystallography of the OTULIN-ABP and OTULIN-SNX27 complexes

The expression and purification of $OTULIN_{cat}$ (aa 80-352) and SNX_{PDZ} (aa 40-135) for crystallography, as well as the crystallization, structure determination and structure refinement, was performed by our collaboration partner Paul Elliott (MRC, Cambridge; University of Oxford). The detailed protocol for X-ray crystallograpghy of the OTULIN-ABP

complex is published in (Weber et al., 2017). The structure of the OTULIN-ABP complex has been deposited with the Protein Data Bank under the accession code PDB ID: 5OE7.

7.7 LC-MS/MS

The mass spectrometric analysis including protein digest, LC-MS/MS and data analysis was performed by Adan Pinto-Fernandez and Sarah Bonham (Benedikt M. Kessler group, University of Oxford). The detailed protocol is published in (Weber et al., 2017). Volcano plots were generated using FDR(false discovery rate)=0.01 and s0=2 or s0=0.2 as cutoff parameters.

The mass spectrometry proteomics data have been deposited to the ProteomeXchange Consortium via the PRIDE (Vizcaino et al., 2016) partner repository with the dataset identifier PXD006868.

8. Abbreviations

°C	degree Celsius
aa	amino acid
ABP	activity-based probe
AHT	anhydrotetracycline
Ahx	aminohexanoic
Ala	alanine
AMC	7-amino-4-methylcoumarin
AMPA	α-amino-3-hydroxy-5-methyl-4-isoxazolepropionic acid
AP-1	activator protein 1
APS	ammonium persulfate
Arp2/3	actin-related protein 2/3
Asn	asparagine
Asp	aspartic acid
ATP	adenosine triphosphate
BAR	Bin/Amphiphysin/Rvs
bio	biotin
BSA	bovine serum albumin
cIAP1/2	cellular inhibitor of apoptosis 1 and 2
CO_2	carbon dioxide
CYLD	Cylindromatosis
Cys	cysteine
Da	dalton
DGKζ	diacylglycerol kinase ζ
Dha	dehydroalanine
DMEM	Dulbecco´s Modified Eagle Medium
DMSO	dimethyl sulfoxide
DNA	deoxyribonucleic acid
DSB	double-strand break
DSCR3	Down´s syndrome critical region 3
DTT	dithiothreitol
DUB	deubiquitinating enzyme
DVL2	Dishevelled 2
E. coli	*Escherichia coli*
E1, E2, E3 enzymes	ubiquitin-activating, ubiquitin-conjugating, ubiquitin-ligating enzyme
EDTA	ethylenediaminetetraacetic acid
ERK	extracellular-signal-regulated kinase
FCS	fetal calf serum
FDR	false discovery rate
FERM	4.1, ezrin, radixin, moesin
g	gram
GFP	green fluorescent protein

Gln	glutamine
Glu	glutamic acid
GLUT1	glucose transporter 1
Gly	glycine
h, hrs	hour, hours
HCl	hydrochloric acid
HECT	Homologous to the E6AP Carboxyl Terminus
His	histidine
HOIL-1	Heme-oxidized IRP2 Ub ligase-1, also termed RBCK1 or RNF54
HOIP	HOIL-1-interacting protein, also termed RNF31 or ZIBRA
IKK	inhibitor of κB kinase
IL-1R	interleukin-1 receptor
Ile	isoleucine
IP	immunoprecipitation
IRAK	interleukin-1 receptor-associated kinase
ITC	isothermal calorimetry
IκBα	inhibitor of NF-κB alpha
KCl	potassium chloride
K_D	equilibrium dissociation constant
KO	knockout
l	liter
LB (medium / agar)	Lysogeny-Broth (medium / agar)
LC-MS/MS	liquid chromatography–tandem mass spectrometry
Leu	leucine
LUBAC	linear ubiquitin chain assembly complex
Lys	lysine
m	meter
M	molar concentration
MAPK	mitogen-activated protein kinase
MeOH	methanol
Met	methionine
MilliQ-H_2O	ultrapure water
min	minute
MINDY	motif interacting with ubiquitin (MIU)- containing novel DUB family
MW	molecular weight
MYD88	myeloid differentiation primary response 88
NaCl	sodium chloride
NEMO	NF-κB essential modulator
NF-κB	nuclear factor kappa B
NHEJ	non-homologous end joining
NMDA	N-methyl-D-aspartate
NOD2	nucleotide-binding oligomerization domain-containing protein 2
NZF	nuclear protein localization 4 zinc finger
O_2	oxygen

OD	optical density
ORAS	OTULIN-related autoinflammatory syndrome
OTULIN	ovarian tumor domain-containing DUB with linear linkage specificity
PA	propargylamide
PBS	phosphate buffered saline
PCR	polymerase chain reaction
PD	pull-down
PDZ	post-synaptic density 95/discs large/zonula occludens
PDZbm	PDZ-binding motif
Phe	phenylalanine
PHLPP1	PH Domain and Leucine Rich Repeat Protein Phosphatase 1
PI(3)P	phosphatidylinositol 3-phosphate
PIM	PUB-interacting motif
PNGase	peptide:N-glycosidase
PRR	pattern recognition receptor
PUB	peptide:N-glycanase/UBA- or UBX-containing proteins
PX	phox-homology
RBR	RING-between-RING
RFP	Red fluorescent protein
RING	Really Interesting New Gene
RIPK1	receptor-interacting serine/threonine protein kinase 1
RT	room temperature
s	second
SDS-PAGE	sodium dodecyl sulfate-polyacrylamide gel electrophoresis
sgRNA	single guide ribonucleic acid
SHARPIN	Shank-associated RH domain-interacting protein, also termed hSIPL1
SNX	Sorting Nexin
SPATA2	Spermatogenesis-associated protein 2
SSF	2xStrep-tag II-Flag
TAB2/3	TAK1-binding proteins 2 and 3
TAK1	transforming growth factor β-activated kinase 1
TEMED	tetramethylethylenediamine
TGN	trans-Golgi network
Thr	threonine
TLR	Toll-like receptor
TNFR1	tumor necrosis factor receptor 1
TNFα	tumor necrosis factor α
TRADD	TNFR1-associated death domain protein
TRAF	TNF receptor associated factor
Tris	tris(hydroxymethyl)aminomethane
Tyr	tyrosine
U	enzyme unit
Ub	ubiquitin
UBA domain	ubiquitin-associated domain
UBAN	ubiquitin binding in ABIN and NEMO

UBD	ubiquitin-binding domain
UbiCREST	Ubiquitin Chain Restriction Analysis
UBP	ubiquitin-binding protein
UCH	ubiquitin C-terminal hydrolase
USP	ubiquitin-specific protease
UV	ultraviolet
v/v	volume per volume
Val	valine
VME	vinyl methyl ester
VPS	vacuolar protein sorting-associated protein
w/v	weight per volume
WASH	Wiskott-Aldrich syndrome protein and SCAR homologue
WT	wild type
ZnF-UBP	zinc-finger ubiquitin-binding protein
β2-AR	beta-2 adrenergic receptor

9. References

Abdul Rehman, S.A., Kristariyanto, Y.A., Choi, S.Y., Nkosi, P.J., Weidlich, S., Labib, K., Hofmann, K., and Kulathu, Y. (2016). MINDY-1 Is a Member of an Evolutionarily Conserved and Structurally Distinct New Family of Deubiquitinating Enzymes. Molecular cell *63*, 146-155.

Altun, M., Kramer, H.B., Willems, L.I., McDermott, J.L., Leach, C.A., Goldenberg, S.J., Kumar, K.G., Konietzny, R., Fischer, R., Kogan, E.*, et al.* (2011). Activity-based chemical proteomics accelerates inhibitor development for deubiquitylating enzymes. Chemistry & biology *18*, 1401-1412.

Amerik, A., Swaminathan, S., Krantz, B.A., Wilkinson, K.D., and Hochstrasser, M. (1997). In vivo disassembly of free polyubiquitin chains by yeast Ubp14 modulates rates of protein degradation by the proteasome. The EMBO journal *16*, 4826-4838.

Balana, B., Maslennikov, I., Kwiatkowski, W., Stern, K.M., Bahima, L., Choe, S., and Slesinger, P.A. (2011). Mechanism underlying selective regulation of G protein-gated inwardly rectifying potassium channels by the psychostimulant-sensitive sorting nexin 27. Proceedings of the National Academy of Sciences of the United States of America *108*, 5831-5836.

Beal, R.E., Toscano-Cantaffa, D., Young, P., Rechsteiner, M., and Pickart, C.M. (1998). The hydrophobic effect contributes to polyubiquitin chain recognition. Biochemistry *37*, 2925-2934.

Bernardes, G.J., Chalker, J.M., Errey, J.C., and Davis, B.G. (2008). Facile conversion of cysteine and alkyl cysteines to dehydroalanine on protein surfaces: versatile and switchable access to functionalized proteins. Journal of the American Chemical Society *130*, 5052-5053.

Boisson, B., Laplantine, E., Dobbs, K., Cobat, A., Tarantino, N., Hazen, M., Lidov, H.G., Hopkins, G., Du, L., Belkadi, A.*, et al.* (2015). Human HOIP and LUBAC deficiency underlies autoinflammation, immunodeficiency, amylopectinosis, and lymphangiectasia. The Journal of experimental medicine *212*, 939-951.

Boisson, B., Laplantine, E., Prando, C., Giliani, S., Israelsson, E., Xu, Z., Abhyankar, A., Israel, L., Trevejo-Nunez, G., Bogunovic, D.*, et al.* (2012). Immunodeficiency, autoinflammation and amylopectinosis in humans with inherited HOIL-1 and LUBAC deficiency. Nature immunology *13*, 1178-1186.

Borodovsky, A., Kessler, B.M., Casagrande, R., Overkleeft, H.S., Wilkinson, K.D., and Ploegh, H.L. (2001). A novel active site-directed probe specific for deubiquitylating enzymes reveals proteasome association of USP14. The EMBO journal *20*, 5187-5196.

Borodovsky, A., Ovaa, H., Kolli, N., Gan-Erdene, T., Wilkinson, K.D., Ploegh, H.L., and Kessler, B.M. (2002). Chemistry-Based Functional Proteomics Reveals Novel Members of the Deubiquitinating Enzyme Family. Chemistry & biology *9*, 1149-1159.

Bremm, A., Freund, S.M., and Komander, D. (2010). Lys11-linked ubiquitin chains adopt compact conformations and are preferentially hydrolyzed by the deubiquitinase Cezanne. Nature structural & molecular biology *17*, 939-947.

Burd, C., and Cullen, P.J. (2014). Retromer: a master conductor of endosome sorting. Cold Spring Harbor perspectives in biology *6*.

Cai, L., Loo, L.S., Atlashkin, V., Hanson, B.J., and Hong, W. (2011). Deficiency of sorting nexin 27 (SNX27) leads to growth retardation and elevated levels of N-methyl-D-aspartate receptor 2C (NR2C). Molecular and cellular biology *31*, 1734-1747.

Chau, V., Tobias, J.W., Bachmair, A., Marriott, D., Ecker, D.J., Gonda, D.K., and Varshavsky, A. (1989). A multiubiquitin chain is confined to specific lysine in a targeted short-lived protein. Science (New York, NY) *243*, 1576-1583.

Chen, Z., and Pickart, C.M. (1990). A 25-kilodalton ubiquitin carrier protein (E2) catalyzes multi-ubiquitin chain synthesis via lysine 48 of ubiquitin. The Journal of biological chemistry *265*, 21835-21842.

Chen, Z.J., and Sun, L.J. (2009). Nonproteolytic functions of ubiquitin in cell signaling. Molecular cell *33*, 275-286.

Ciechanover, A., Elias, S., Heller, H., and Hershko, A. (1982). "Covalent affinity" purification of ubiquitin-activating enzyme. The Journal of biological chemistry *257*, 2537-2542.

Clague, M.J., Heride, C., and Urbe, S. (2015). The demographics of the ubiquitin system. Trends in cell biology *25*, 417-426.

Clairfeuille, T., Mas, C., Chan, A.S., Yang, Z., Tello-Lafoz, M., Chandra, M., Widagdo, J., Kerr, M.C., Paul, B., Merida, I.*, et al.* (2016). A molecular code for endosomal recycling of phosphorylated cargos by the SNX27-retromer complex. Nature structural & molecular biology *23*, 921-932.

Collins, B.M., Norwood, S.J., Kerr, M.C., Mahony, D., Seaman, M.N., Teasdale, R.D., and Owen, D.J. (2008). Structure of Vps26B and mapping of its interaction with the retromer protein complex. Traffic (Copenhagen, Denmark) *9*, 366-379.

Cravatt, B.F., Wright, A.T., and Kozarich, J.W. (2008). Activity-based protein profiling: from enzyme chemistry to proteomic chemistry. Annu Rev Biochem *77*, 383-414.

Cullen, P.J. (2008). Endosomal sorting and signalling: an emerging role for sorting nexins. Nature reviews Molecular cell biology *9*, 574-582.

Cullen, P.J., and Korswagen, H.C. (2011). Sorting nexins provide diversity for retromer-dependent trafficking events. Nature cell biology *14*, 29-37.

Damgaard, R.B., Nachbur, U., Yabal, M., Wong, W.W., Fiil, B.K., Kastirr, M., Rieser, E., Rickard, J.A., Bankovacki, A., Peschel, C.*, et al.* (2012). The ubiquitin ligase XIAP recruits LUBAC for NOD2 signaling in inflammation and innate immunity. Molecular cell *46*, 746-758.

Damgaard, R.B., Walker, J.A., Marco-Casanova, P., Morgan, N.V., Titheradge, H.L., Elliott, P.R., McHale, D., Maher, E.R., McKenzie, A.N.J., and Komander, D. (2016). The Deubiquitinase OTULIN Is an Essential Negative Regulator of Inflammation and Autoimmunity. Cell *166*, 1215-1230.e1220.

de Jong, A., Merkx, R., Berlin, I., Rodenko, B., Wijdeven, R.H.M., El Atmioui, D., Yalçin, Z., Robson, C.N., Neefjes, J.J., and Ovaa, H. (2012). Ubiquitin-Based Probes Prepared by Total Synthesis To Profile the Activity of Deubiquitinating Enzymes. Chembiochem *13*, 2251-2258.

Derivery, E., Sousa, C., Gautier, J.J., Lombard, B., Loew, D., and Gautreau, A. (2009). The Arp2/3 activator WASH controls the fission of endosomes through a large multiprotein complex. Developmental cell *17*, 712-723.

Dikic, I., Wakatsuki, S., and Walters, K.J. (2009). Ubiquitin-binding domains - from structures to functions. Nature reviews Molecular cell biology *10*, 659-671.

Doyle, D.A., Lee, A., Lewis, J., Kim, E., Sheng, M., and MacKinnon, R. (1996). Crystal structures of a complexed and peptide-free membrane protein-binding domain: molecular basis of peptide recognition by PDZ. Cell *85*, 1067-1076.

Draber, P., Kupka, S., Reichert, M., Draberova, H., Lafont, E., de Miguel, D., Spilgies, L., Surinova, S., Taraborrelli, L., Hartwig, T.*, et al.* (2015). LUBAC-Recruited CYLD and A20 Regulate Gene Activation and Cell Death by Exerting Opposing Effects on Linear Ubiquitin in Signaling Complexes. Cell reports *13*, 2258-2272.

Duwel, M., Welteke, V., Oeckinghaus, A., Baens, M., Kloo, B., Ferch, U., Darnay, B.G., Ruland, J., Marynen, P., and Krappmann, D. (2009). A20 negatively regulates T cell receptor signaling to NF-kappaB by cleaving Malt1 ubiquitin chains. Journal of immunology (Baltimore, Md : 1950) *182*, 7718-7728.

Eddins, M.J., Varadan, R., Fushman, D., Pickart, C.M., and Wolberger, C. (2007). Crystal structure and solution NMR studies of Lys48-linked tetraubiquitin at neutral pH. Journal of molecular biology *367*, 204-211.

Edelmann, M.J., Iphofer, A., Akutsu, M., Altun, M., di Gleria, K., Kramer, H.B., Fiebiger, E., Dhe-Paganon, S., and Kessler, B.M. (2009). Structural basis and specificity of human otubain 1-mediated deubiquitination. The Biochemical journal *418*, 379-390.

Ekkebus, R., van Kasteren, S.I., Kulathu, Y., Scholten, A., Berlin, I., Geurink, P.P., de Jong, A., Goerdayal, S., Neefjes, J., Heck, A.J.R.*, et al.* (2013). On Terminal Alkynes That Can React with Active-Site Cysteine Nucleophiles in Proteases. Journal of the American Chemical Society *135*, 2867-2870.

Elliott, P.R., Leske, D., Hrdinka, M., Bagola, K., Fiil, B.K., McLaughlin, S.H., Wagstaff, J., Volkmar, N., Christianson, J.C., Kessler, B.M.*, et al.* (2016). SPATA2 Links CYLD to LUBAC, Activates CYLD, and Controls LUBAC Signaling. Molecular cell *63*, 990-1005.

Elliott, P.R., Nielsen, S.V., Marco-Casanova, P., Fiil, B.K., Keusekotten, K., Mailand, N., Freund, S.M., Gyrd-Hansen, M., and Komander, D. (2014). Molecular basis and regulation of OTULIN-LUBAC interaction. Molecular cell *54*, 335-348.

Emmerich, C.H., Bakshi, S., Kelsall, I.R., Ortiz-Guerrero, J., Shpiro, N., and Cohen, P. (2016). Lys63/Met1-hybrid ubiquitin chains are commonly formed during the activation of innate immune signalling. Biochemical and biophysical research communications *474*, 452-461.

Emmerich, C.H., Ordureau, A., Strickson, S., Arthur, J.S., Pedrioli, P.G., Komander, D., and Cohen, P. (2013). Activation of the canonical IKK complex by K63/M1-linked hybrid ubiquitin chains. Proceedings of the National Academy of Sciences of the United States of America *110*, 15247-15252.

Faesen, A.C., Luna-Vargas, M.P., Geurink, P.P., Clerici, M., Merkx, R., van Dijk, W.J., Hameed, D.S., El Oualid, F., Ovaa, H., and Sixma, T.K. (2011). The differential modulation of USP activity by internal regulatory domains, interactors and eight ubiquitin chain types. Chemistry & biology *18*, 1550-1561.

Fiil, B.K., Damgaard, R.B., Wagner, S.A., Keusekotten, K., Fritsch, M., Bekker-Jensen, S., Mailand, N., Choudhary, C., Komander, D., and Gyrd-Hansen, M. (2013). OTULIN restricts Met1-linked ubiquitination to control innate immune signaling. Molecular cell *50*, 818-830.

Fiil, B.K., and Gyrd-Hansen, M. (2014). Met1-linked ubiquitination in immune signalling. The FEBS journal *281*, 4337-4350.

Frost, A., Perera, R., Roux, A., Spasov, K., Destaing, O., Egelman, E.H., De Camilli, P., and Unger, V.M. (2008). Structural basis of membrane invagination by F-BAR domains. Cell *132*, 807-817.

Fujita, H., Rahighi, S., Akita, M., Kato, R., Sasaki, Y., Wakatsuki, S., and Iwai, K. (2014). Mechanism underlying IkappaB kinase activation mediated by the linear ubiquitin chain assembly complex. Molecular and cellular biology *34*, 1322-1335.

Gallon, M., Clairfeuille, T., Steinberg, F., Mas, C., Ghai, R., Sessions, R.B., Teasdale, R.D., Collins, B.M., and Cullen, P.J. (2014). A unique PDZ domain and arrestin-like fold interaction reveals mechanistic details of endocytic recycling by SNX27-retromer. Proceedings of the National Academy of Sciences of the United States of America *111*, E3604-3613.

Gallon, M., and Cullen, P.J. (2015). Retromer and sorting nexins in endosomal sorting. Biochemical Society transactions *43*, 33-47.

Gerlach, B., Cordier, S.M., Schmukle, A.C., Emmerich, C.H., Rieser, E., Haas, T.L., Webb, A.I., Rickard, J.A., Anderton, H., Wong, W.W*., et al.* (2011). Linear ubiquitination prevents inflammation and regulates immune signalling. Nature *471*, 591-596.

Ghai, R., Tello-Lafoz, M., Norwood, S.J., Yang, Z., Clairfeuille, T., Teasdale, R.D., Merida, I., and Collins, B.M. (2015). Phosphoinositide binding by the SNX27 FERM domain regulates its localization at the immune synapse of activated T-cells. Journal of cell science *128*, 553-565.

Haas, T.L., Emmerich, C.H., Gerlach, B., Schmukle, A.C., Cordier, S.M., Rieser, E., Feltham, R., Vince, J., Warnken, U., Wenger, T*., et al.* (2009). Recruitment of the linear ubiquitin chain assembly complex stabilizes the TNF-R1 signaling complex and is required for TNF-mediated gene induction. Molecular cell *36*, 831-844.

Haj-Yahya, N., Hemantha, H.P., Meledin, R., Bondalapati, S., Seenaiah, M., and Brik, A. (2014). Dehydroalanine-based diubiquitin activity probes. Organic letters *16*, 540-543.

Harhaj, E.W., and Dixit, V.M. (2012). Regulation of NF-kappaB by deubiquitinases. Immunological reviews *246*, 107-124.

Hayden, M.S., and Ghosh, S. (2012). NF-kappaB, the first quarter-century: remarkable progress and outstanding questions. Genes & development *26*, 203-234.

Heger, K., Wickliffe, K.E., Ndoja, A., Zhang, J., Murthy, A., Dugger, D.L., Maltzman, A., de Sousa, E.M.F., Hung, J., Zeng, Y*., et al.* (2018). OTULIN limits cell death and inflammation by deubiquitinating LUBAC. Nature *559*, 120-124.

Hershko, A., and Ciechanover, A. (1998). The Ubiquitin System. Annual Review of Biochemistry *67*, 425-479.

Hospenthal, M.K., Freund, S.M., and Komander, D. (2013). Assembly, analysis and architecture of atypical ubiquitin chains. Nature structural & molecular biology *20*, 555-565.

Hospenthal, M.K., Mevissen, T.E.T., and Komander, D. (2015). Deubiquitinase-based analysis of ubiquitin chain architecture using Ubiquitin Chain Restriction (UbiCRest). Nature protocols *10*, 349-361.

Hrdinka, M., Fiil, B.K., Zucca, M., Leske, D., Bagola, K., Yabal, M., Elliott, P.R., Damgaard, R.B., Komander, D., Jost, P.J*., et al.* (2016). CYLD Limits Lys63- and Met1-Linked Ubiquitin at Receptor Complexes to Regulate Innate Immune Signaling. Cell reports *14*, 2846-2858.

Hrdinka, M., and Gyrd-Hansen, M. (2017). The Met1-Linked Ubiquitin Machinery: Emerging Themes of (De)regulation. Molecular cell *68*, 265-280.

Hsu, V.W., Bai, M., and Li, J. (2012). Getting active: protein sorting in endocytic recycling. Nature reviews Molecular cell biology *13*, 323-328.

Hu, M., Li, P., Li, M., Li, W., Yao, T., Wu, J.W., Gu, W., Cohen, R.E., and Shi, Y. (2002). Crystal structure of a UBP-family deubiquitinating enzyme in isolation and in complex with ubiquitin aldehyde. Cell *111*, 1041-1054.

Hu, M., Li, P., Song, L., Jeffrey, P.D., Chenova, T.A., Wilkinson, K.D., Cohen, R.E., and Shi, Y. (2005). Structure and mechanisms of the proteasome-associated deubiquitinating enzyme USP14. The EMBO journal *24*, 3747-3756.

Hubeau, M., Ngadjeua, F., Puel, A., Israel, L., Feinberg, J., Chrabieh, M., Belani, K., Bodemer, C., Fabre, I., Plebani, A.*, et al.* (2011). New mechanism of X-linked anhidrotic ectodermal dysplasia with immunodeficiency: impairment of ubiquitin binding despite normal folding of NEMO protein. Blood *118*, 926-935.

Hung, A.Y., and Sheng, M. (2002). PDZ domains: structural modules for protein complex assembly. The Journal of biological chemistry *277*, 5699-5702.

Husnjak, K., and Dikic, I. (2012). Ubiquitin-binding proteins: decoders of ubiquitin-mediated cellular functions. Annu Rev Biochem *81*, 291-322.

Ikeda, F. (2015). Linear ubiquitination signals in adaptive immune responses. Immunological reviews *266*, 222-236.

Ikeda, F., Deribe, Y.L., Skanland, S.S., Stieglitz, B., Grabbe, C., Franz-Wachtel, M., van Wijk, S.J., Goswami, P., Nagy, V., Terzic, J.*, et al.* (2011). SHARPIN forms a linear ubiquitin ligase complex regulating NF-kappaB activity and apoptosis. Nature *471*, 637-641.

Ivarsson, Y. (2012). Plasticity of PDZ domains in ligand recognition and signaling. FEBS letters *586*, 2638-2647.

Ivins, F.J., Montgomery, M.G., Smith, S.J., Morris-Davies, A.C., Taylor, I.A., and Rittinger, K. (2009). NEMO oligomerization and its ubiquitin-binding properties. The Biochemical journal *421*, 243-251.

Iwai, K., and Tokunaga, F. (2009). Linear polyubiquitination: a new regulator of NF-kappaB activation. EMBO Reports *10*, 706-713.

Jia, D., Gomez, T.S., Billadeau, D.D., and Rosen, M.K. (2012). Multiple repeat elements within the FAM21 tail link the WASH actin regulatory complex to the retromer. Molecular biology of the cell *23*, 2352-2361.

Johannes, L., and Wunder, C. (2011). The SNXy flavours of endosomal sorting. Nature cell biology *13*, 884-886.

Kamadurai, H.B., Souphron, J., Scott, D.C., Duda, D.M., Miller, D.J., Stringer, D., Piper, R.C., and Schulman, B.A. (2009). Insights into ubiquitin transfer cascades from a structure of a UbcH5B approximately ubiquitin-HECT(NEDD4L) complex. Molecular cell *36*, 1095-1102.

Kerr, M.C., Bennetts, J.S., Simpson, F., Thomas, E.C., Flegg, C., Gleeson, P.A., Wicking, C., and Teasdale, R.D. (2005). A novel mammalian retromer component, Vps26B. Traffic (Copenhagen, Denmark) *6*, 991-1001.

Keusekotten, K., Elliott, P.R., Glockner, L., Fiil, B.K., Damgaard, R.B., Kulathu, Y., Wauer, T., Hospenthal, M.K., Gyrd-Hansen, M., Krappmann, D.*, et al.* (2013). OTULIN antagonizes LUBAC signaling by specifically hydrolyzing Met1-linked polyubiquitin. Cell *153*, 1312-1326.

Kirisako, T., Kamei, K., Murata, S., Kato, M., Fukumoto, H., Kanie, M., Sano, S., Tokunaga, F., Tanaka, K., and Iwai, K. (2006). A ubiquitin ligase complex assembles linear polyubiquitin chains. The EMBO journal *25*, 4877-4887.

Komander, D., Clague, M.J., and Urbé, S. (2009a). Breaking the chains: structure and function of the deubiquitinases. Nature Reviews Molecular Cell Biology *10*, 550.

Komander, D., Lord, C.J., Scheel, H., Swift, S., Hofmann, K., Ashworth, A., and Barford, D. (2008). The structure of the CYLD USP domain explains its specificity for Lys63-linked polyubiquitin and reveals a B box module. Molecular cell *29*, 451-464.

Komander, D., and Rape, M. (2012). The Ubiquitin Code. Annual Review of Biochemistry *81*, 203-229.

Komander, D., Reyes-Turcu, F., Licchesi, J.D.F., Odenwaelder, P., Wilkinson, K.D., and Barford, D. (2009b). Molecular discrimination of structurally equivalent Lys 63-linked and linear polyubiquitin chains. EMBO reports *10*, 466-473.

Koumandou, V.L., Klute, M.J., Herman, E.K., Nunez-Miguel, R., Dacks, J.B., and Field, M.C. (2011). Evolutionary reconstruction of the retromer complex and its function in Trypanosoma brucei. Journal of cell science *124*, 1496-1509.

Kovtun, O., Leneva, N., Bykov, Y.S., Ariotti, N., Teasdale, R.D., Schaffer, M., Engel, B.D., Owen, D.J., Briggs, J.A.G., and Collins, B.M. (2018). Structure of the membrane-assembled retromer coat determined by cryo-electron tomography. Nature *561*, 561-564.

Kulathu, Y., Akutsu, M., Bremm, A., Hofmann, K., and Komander, D. (2009). Two-sided ubiquitin binding explains specificity of the TAB2 NZF domain. Nature structural & molecular biology *16*, 1328-1330.

Kupka, S., De Miguel, D., Draber, P., Martino, L., Surinova, S., Rittinger, K., and Walczak, H. (2016a). SPATA2-Mediated Binding of CYLD to HOIP Enables CYLD Recruitment to Signaling Complexes. Cell reports *16*, 2271-2280.

Kupka, S., Reichert, M., Draber, P., and Walczak, H. (2016b). Formation and removal of poly-ubiquitin chains in the regulation of tumor necrosis factor-induced gene activation and cell death. The FEBS journal *283*, 2626-2639.

Laskowski, R.A., Jablonska, J., Pravda, L., Varekova, R.S., and Thornton, J.M. (2018). PDBsum: Structural summaries of PDB entries. Protein science : a publication of the Protein Society *27*, 129-134.

Lauffer, B.E., Melero, C., Temkin, P., Lei, C., Hong, W., Kortemme, T., and von Zastrow, M. (2010). SNX27 mediates PDZ-directed sorting from endosomes to the plasma membrane. The Journal of cell biology *190*, 565-574.

Lee, S., Chang, J., and Blackstone, C. (2016). FAM21 directs SNX27-retromer cargoes to the plasma membrane by preventing transport to the Golgi apparatus. Nature communications *7*, 10939.

Li, C., Shah, S.Z., Zhao, D., and Yang, L. (2016). Role of the Retromer Complex in Neurodegenerative Diseases. Frontiers in aging neuroscience *8*, 42.

Li, G., Liang, Q., Gong, P., Tencer, A.H., and Zhuang, Z. (2014). Activity-based diubiquitin probes for elucidating the linkage specificity of deubiquitinating enzymes. Chemical communications (Cambridge, England) *50*, 216-218.

Liu, S., and Chen, Z.J. (2011). Expanding role of ubiquitination in NF-kappaB signaling. Cell research *21*, 6-21.

Loo, L.S., Tang, N., Al-Haddawi, M., Dawe, G.S., and Hong, W. (2014). A role for sorting nexin 27 in AMPA receptor trafficking. Nature communications *5*, 3176.

Lorenz, S. (2018). Structural mechanisms of HECT-type ubiquitin ligases. Biological chemistry *399*, 127-145.

Lork, M., Verhelst, K., and Beyaert, R. (2017). CYLD, A20 and OTULIN deubiquitinases in NF-kappaB signaling and cell death: so similar, yet so different. Cell death and differentiation *24*, 1172-1183.

Lucas, M., Gershlick, D.C., Vidaurrazaga, A., Rojas, A.L., Bonifacino, J.S., and Hierro, A. (2016). Structural Mechanism for Cargo Recognition by the Retromer Complex. Cell *167*, 1623-1635.e1614.

Lucas, M., and Hierro, A. (2017). Retromer. Current biology : CB *27*, R687-r689.

Lunn, M.L., Nassirpour, R., Arrabit, C., Tan, J., McLeod, I., Arias, C.M., Sawchenko, P.E., Yates, J.R., 3rd, and Slesinger, P.A. (2007). A unique sorting nexin regulates trafficking of potassium channels via a PDZ domain interaction. Nature neuroscience *10*, 1249-1259.

MacNeil, A.J., and Pohajdak, B. (2007). Polarization of endosomal SNX27 in migrating and tumor-engaged natural killer cells. Biochemical and biophysical research communications *361*, 146-150.

Martinez-Fonts, K., and Matouschek, A. (2016). A Rapid and Versatile Method for Generating Proteins with Defined Ubiquitin Chains. Biochemistry *55*, 1898-1908.

Matsumoto, M.L., Dong, K.C., Yu, C., Phu, L., Gao, X., Hannoush, R.N., Hymowitz, S.G., Kirkpatrick, D.S., Dixit, V.M., and Kelley, R.F. (2012). Engineering and structural characterization of a linear polyubiquitin-specific antibody. Journal of molecular biology *418*, 134-144.

McGouran, J.F., Gaertner, S.R., Altun, M., Kramer, H.B., and Kessler, B.M. (2013). Deubiquitinating enzyme specificity for ubiquitin chain topology profiled by di-ubiquitin activity probes. Chemistry & biology *20*, 1447-1455.

Mevissen, T.E., Hospenthal, M.K., Geurink, P.P., Elliott, P.R., Akutsu, M., Arnaudo, N., Ekkebus, R., Kulathu, Y., Wauer, T., El Oualid, F.*, et al.* (2013). OTU deubiquitinases reveal mechanisms of linkage specificity and enable ubiquitin chain restriction analysis. Cell *154*, 169-184.

Mevissen, T.E.T., and Komander, D. (2017). Mechanisms of Deubiquitinase Specificity and Regulation. Annu Rev Biochem *86*, 159-192.

Mevissen, T.E.T., Kulathu, Y., Mulder, M.P.C., Geurink, P.P., Maslen, S.L., Gersch, M., Elliott, P.R., Burke, J.E., van Tol, B.D.M., Akutsu, M.*, et al.* (2016). Molecular basis of Lys11-polyubiquitin specificity in the deubiquitinase Cezanne. Nature *538*, 402-405.

Mulder, M.P., El Oualid, F., ter Beek, J., and Ovaa, H. (2014). A native chemical ligation handle that enables the synthesis of advanced activity-based probes: diubiquitin as a case study. Chembiochem *15*, 946-949.

Muller-Rischart, A.K., Pilsl, A., Beaudette, P., Patra, M., Hadian, K., Funke, M., Peis, R., Deinlein, A., Schweimer, C., Kuhn, P.H.*, et al.* (2013). The E3 ligase parkin maintains mitochondrial integrity by increasing linear ubiquitination of NEMO. Molecular cell *49*, 908-921.

Norwood, S.J., Shaw, D.J., Cowieson, N.P., Owen, D.J., Teasdale, R.D., and Collins, B.M. (2011). Assembly and solution structure of the core retromer protein complex. Traffic (Copenhagen, Denmark) *12*, 56-71.

Ohashi, E., Tanabe, K., Henmi, Y., Mesaki, K., Kobayashi, Y., and Takei, K. (2011). Receptor sorting within endosomal trafficking pathway is facilitated by dynamic actin filaments. PLoS One *6*, e19942.

Ovaa, H. (2007). Active-site directed probes to report enzymatic action in the ubiquitin proteasome system. Nature reviews Cancer *7*, 613-620.

Ozkaynak, E., Finley, D., and Varshavsky, A. (1984). The yeast ubiquitin gene: head-to-tail repeats encoding a polyubiquitin precursor protein. Nature *312*, 663-666.

Pascoe, H.G., Gutowski, S., Chen, H., Brautigam, C.A., Chen, Z., Sternweis, P.C., and Zhang, X. (2015). Secondary PDZ domain-binding site on class B plexins enhances the affinity for PDZ-RhoGEF. Proceedings of the National Academy of Sciences of the United States of America *112*, 14852-14857.

Rahighi, S., Ikeda, F., Kawasaki, M., Akutsu, M., Suzuki, N., Kato, R., Kensche, T., Uejima, T., Bloor, S., Komander, D.*, et al.* (2009). Specific recognition of linear ubiquitin chains by NEMO is important for NF-kappaB activation. Cell *136*, 1098-1109.

Ran, F.A., Hsu, P.D., Wright, J., Agarwala, V., Scott, D.A., and Zhang, F. (2013). Genome engineering using the CRISPR-Cas9 system. Nature protocols *8*, 2281-2308.

Renatus, M., Parrado, S.G., D'Arcy, A., Eidhoff, U., Gerhartz, B., Hassiepen, U., Pierrat, B., Riedl, R., Vinzenz, D., Worpenberg, S.*, et al.* (2006). Structural basis of ubiquitin recognition by the deubiquitinating protease USP2. Structure (London, England : 1993) *14*, 1293-1302.

Reyes-Turcu, F.E., Horton, J.R., Mullally, J.E., Heroux, A., Cheng, X., and Wilkinson, K.D. (2006). The ubiquitin binding domain ZnF UBP recognizes the C-terminal diglycine motif of unanchored ubiquitin. Cell *124*, 1197-1208.

Reyes-Turcu, F.E., Shanks, J.R., Komander, D., and Wilkinson, K.D. (2008). Recognition of polyubiquitin isoforms by the multiple ubiquitin binding modules of isopeptidase T. The Journal of biological chemistry *283*, 19581-19592.

Rincon, E., Saez de Guinoa, J., Gharbi, S.I., Sorzano, C.O., Carrasco, Y.R., and Merida, I. (2011). Translocation dynamics of sorting nexin 27 in activated T cells. Journal of cell science *124*, 776-788.

Rincon, E., Santos, T., Avila-Flores, A., Albar, J.P., Lalioti, V., Lei, C., Hong, W., and Merida, I. (2007). Proteomics identification of sorting nexin 27 as a diacylglycerol kinase zeta-associated protein: new diacylglycerol kinase roles in endocytic recycling. Molecular & cellular proteomics : MCP *6*, 1073-1087.

Ritorto, M.S., Ewan, R., Perez-Oliva, A.B., Knebel, A., Buhrlage, S.J., Wightman, M., Kelly, S.M., Wood, N.T., Virdee, S., Gray, N.S.*, et al.* (2014). Screening of DUB activity and specificity by MALDI-TOF mass spectrometry. Nature communications *5*, 4763.

Rittinger, K., and Ikeda, F. (2017). Linear ubiquitin chains: enzymes, mechanisms and biology. Open biology *7*.

Rivkin, E. (2013). The linear ubiquitin-specific deubiquitinase Gumby/Fam105b regulates angiogenesis. *498*, 318-324.

Rotin, D., and Kumar, S. (2009). Physiological functions of the HECT family of ubiquitin ligases. Nature reviews Molecular cell biology *10*, 398-409.

Sasaki, K., and Iwai, K. (2015). Roles of linear ubiquitinylation, a crucial regulator of NF-kappaB and cell death, in the immune system. Immunological reviews *266*, 175-189.

Sato, Y., Fujita, H., Yoshikawa, A., Yamashita, M., Yamagata, A., Kaiser, S.E., Iwai, K., and Fukai, S. (2011). Specific recognition of linear ubiquitin chains by the Npl4 zinc finger (NZF) domain of the HOIL-1L subunit of the linear ubiquitin chain assembly complex. Proceedings of the National Academy of Sciences of the United States of America *108*, 20520-20525.

Sato, Y., Goto, E., Shibata, Y., Kubota, Y., Yamagata, A., Goto-Ito, S., Kubota, K., Inoue, J., Takekawa, M., Tokunaga, F.*, et al.* (2015). Structures of CYLD USP with Met1- or Lys63-linked diubiquitin reveal mechanisms for dual specificity. Nature structural & molecular biology *22*, 222-229.

Sato, Y., Yoshikawa, A., Yamashita, M., Yamagata, A., and Fukai, S. (2009). Structural basis for specific recognition of Lys 63-linked polyubiquitin chains by NZF domains of TAB2 and TAB3. The EMBO journal *28*, 3903-3909.

Schaeffer, V., Akutsu, M., Olma, M.H., Gomes, L.C., Kawasaki, M., and Dikic, I. (2014). Binding of OTULIN to the PUB domain of HOIP controls NF-kappaB signaling. Molecular cell *54*, 349-361.

Scharschmidt, E., Wegener, E., Heissmeyer, V., Rao, A., and Krappmann, D. (2004). Degradation of Bcl10 induced by T-cell activation negatively regulates NF-kappa B signaling. Molecular and cellular biology *24*, 3860-3873.

Schimmack, G., Schorpp, K., Kutzner, K., Gehring, T., Brenke, J.K., Hadian, K., and Krappmann, D. (2017). YOD1/TRAF6 association balances p62-dependent IL-1 signaling to NF-kappaB. eLife *6*.

Schlicher, L., Wissler, M., Preiss, F., Brauns-Schubert, P., Jakob, C., Dumit, V., Borner, C., Dengjel, J., and Maurer, U. (2016). SPATA2 promotes CYLD activity and regulates TNF-induced NF-kappaB signaling and cell death. EMBO Reports *17*, 1485-1497.

Seaman, M.N., Gautreau, A., and Billadeau, D.D. (2013). Retromer-mediated endosomal protein sorting: all WASHed up! Trends in cell biology *23*, 522-528.

Setsuie, R., Sakurai, M., Sakaguchi, Y., and Wada, K. (2009). Ubiquitin dimers control the hydrolase activity of UCH-L3. Neurochemistry international *54*, 314-321.

Shimizu, S., Fujita, H., Sasaki, Y., Tsuruyama, T., Fukuda, K., and Iwai, K. (2016). Differential Involvement of the Npl4 Zinc Finger Domains of SHARPIN and HOIL-1L in Linear Ubiquitin Chain Assembly Complex-Mediated Cell Death Protection. Molecular and cellular biology *36*, 1569-1583.

Shimizu, Y., Taraborrelli, L., and Walczak, H. (2015). Linear ubiquitination in immunity. Immunological reviews *266*, 190-207.

Shinde, S.R., and Maddika, S. (2017). PTEN Regulates Glucose Transporter Recycling by Impairing SNX27 Retromer Assembly. Cell reports *21*, 1655-1666.

Simonetti, B., and Cullen, P.J. (2018). Actin-dependent endosomal receptor recycling. Current opinion in cell biology *56*, 22-33.

Smit, J.J., Monteferrario, D., Noordermeer, S.M., van Dijk, W.J., van der Reijden, B.A., and Sixma, T.K. (2012). The E3 ligase HOIP specifies linear ubiquitin chain assembly through its RING-IBR-RING domain and the unique LDD extension. The EMBO journal *31*, 3833-3844.

Sowa, M.E., Bennett, E.J., Gygi, S.P., and Harper, J.W. (2009). Defining the human deubiquitinating enzyme interaction landscape. Cell *138*, 389-403.

Steinberg, F., Gallon, M., Winfield, M., Thomas, E.C., Bell, A.J., Heesom, K.J., Tavare, J.M., and Cullen, P.J. (2013). A global analysis of SNX27-retromer assembly and cargo specificity reveals a function in glucose and metal ion transport. Nature cell biology *15*, 461-471.

Stieglitz, B., Morris-Davies, A.C., Koliopoulos, M.G., Christodoulou, E., and Rittinger, K. (2012). LUBAC synthesizes linear ubiquitin chains via a thioester intermediate. EMBO Reports *13*, 840-846.

Stieglitz, B., Rana, R.R., Koliopoulos, M.G., Morris-Davies, A.C., Schaeffer, V., Christodoulou, E., Howell, S., Brown, N.R., Dikic, I., and Rittinger, K. (2013). Structural basis for ligase-specific conjugation of linear ubiquitin chains by HOIP. Nature *503*, 422-426.

Strachan, J., Roach, L., Sokratous, K., Tooth, D., Long, J., Garner, T.P., Searle, M.S., Oldham, N.J., and Layfield, R. (2012). Insights into the molecular composition of endogenous unanchored polyubiquitin chains. Journal of proteome research *11*, 1969-1980.

Sun, L., Hu, X., Chen, W., He, W., Zhang, Z., and Wang, T. (2016). Sorting nexin 27 interacts with Fzd7 and mediates Wnt signalling. Bioscience reports *36*, e00296.

Sundell, G.N., Arnold, R., Ali, M., Naksukpaiboon, P., Orts, J., Guntert, P., Chi, C.N., and Ivarsson, Y. (2018). Proteome-wide analysis of phospho-regulated PDZ domain interactions. Molecular systems biology *14*, e8129.

Szymczak, A.L., Workman, C.J., Wang, Y., Vignali, K.M., Dilioglou, S., Vanin, E.F., and Vignali, D.A. (2004). Correction of multi-gene deficiency in vivo using a single 'self-cleaving' 2A peptide-based retroviral vector. Nature biotechnology *22*, 589-594.

Takiuchi, T., Nakagawa, T., Tamiya, H., Fujita, H., Sasaki, Y., Saeki, Y., Takeda, H., Sawasaki, T., Buchberger, A., Kimura, T*., et al.* (2014). Suppression of LUBAC-mediated linear ubiquitination by a specific interaction between LUBAC and the deubiquitinases CYLD and OTULIN. Genes to cells : devoted to molecular & cellular mechanisms *19*, 254-272.

Teasdale, R.D., and Collins, B.M. (2012). Insights into the PX (phox-homology) domain and SNX (sorting nexin) protein families: structures, functions and roles in disease. The Biochemical journal *441*, 39-59.

Tello-Lafoz, M., Martinez-Martinez, G., Rodriguez-Rodriguez, C., Albar, J.P., Huse, M., Gharbi, S., and Merida, I. (2017). Sorting nexin 27 interactome in T-lymphocytes identifies zona occludens-2 dynamic redistribution at the immune synapse. Traffic (Copenhagen, Denmark) *18*, 491-504.

Temkin, P., Lauffer, B., Jager, S., Cimermancic, P., Krogan, N.J., and von Zastrow, M. (2011). SNX27 mediates retromer tubule entry and endosome-to-plasma membrane trafficking of signalling receptors. Nature cell biology *13*, 715-721.

Tokunaga, F., Nakagawa, T., Nakahara, M., Saeki, Y., Taniguchi, M., Sakata, S., Tanaka, K., Nakano, H., and Iwai, K. (2011). SHARPIN is a component of the NF-kappaB-activating linear ubiquitin chain assembly complex. Nature *471*, 633-636.

Tokunaga, F., Sakata, S., Saeki, Y., Satomi, Y., Kirisako, T., Kamei, K., Nakagawa, T., Kato, M., Murata, S., Yamaoka, S.*, et al.* (2009). Involvement of linear polyubiquitylation of NEMO in NF-kappaB activation. Nature cell biology *11*, 123-132.

Valdes, J.L., Tang, J., McDermott, M.I., Kuo, J.C., Zimmerman, S.P., Wincovitch, S.M., Waterman, C.M., Milgram, S.L., and Playford, M.P. (2011). Sorting nexin 27 protein regulates trafficking of a p21-activated kinase (PAK) interacting exchange factor (beta-Pix)-G protein-coupled receptor kinase interacting protein (GIT) complex via a PDZ domain interaction. The Journal of biological chemistry *286*, 39403-39416.

van Weering, J.R., Sessions, R.B., Traer, C.J., Kloer, D.P., Bhatia, V.K., Stamou, D., Carlsson, S.R., Hurley, J.H., and Cullen, P.J. (2012). Molecular basis for SNX-BAR-mediated assembly of distinct endosomal sorting tubules. The EMBO journal *31*, 4466-4480.

van Weering, J.R., Verkade, P., and Cullen, P.J. (2010). SNX-BAR proteins in phosphoinositide-mediated, tubular-based endosomal sorting. Seminars in cell & developmental biology *21*, 371-380.

Varadan, R., Assfalg, M., Haririnia, A., Raasi, S., Pickart, C., and Fushman, D. (2004). Solution conformation of Lys63-linked di-ubiquitin chain provides clues to functional diversity of polyubiquitin signaling. The Journal of biological chemistry *279*, 7055-7063.

Vijay-Kumar, S., Bugg, C.E., and Cook, W.J. (1987). Structure of ubiquitin refined at 1.8 A resolution. Journal of molecular biology *194*, 531-544.

Virdee, S., Ye, Y., Nguyen, D.P., Komander, D., and Chin, J.W. (2010). Engineered diubiquitin synthesis reveals Lys29-isopeptide specificity of an OTU deubiquitinase. Nature chemical biology *6*, 750-757.

Vizcaino, J.A., Csordas, A., Del-Toro, N., Dianes, J.A., Griss, J., Lavidas, I., Mayer, G., Perez-Riverol, Y., Reisinger, F., Ternent, T.*, et al.* (2016). 2016 update of the PRIDE database and its related tools. Nucleic acids research *44*, 11033.

Wagner, S.A., Satpathy, S., Beli, P., and Choudhary, C. (2016). SPATA2 links CYLD to the TNF-alpha receptor signaling complex and modulates the receptor signaling outcomes. The EMBO journal *35*, 1868-1884.

Wang, X., Zhao, Y., Zhang, X., Badie, H., Zhou, Y., Mu, Y., Loo, L.S., Cai, L., Thompson, R.C., Yang, B.*, et al.* (2013). Loss of sorting nexin 27 contributes to excitatory synaptic dysfunction by modulating glutamate receptor recycling in Down's syndrome. Nature medicine *19*, 473-480.

Weber, A., Elliott, P.R., Pinto-Fernandez, A., Bonham, S., Kessler, B.M., Komander, D., El Oualid, F., and Krappmann, D. (2017). A Linear Diubiquitin-Based Probe for Efficient and Selective Detection of the Deubiquitinating Enzyme OTULIN. Cell chemical biology *24*, 1299-1313.e1297.

Yang, Y.K., Yang, C., Chan, W., Wang, Z., Deibel, K.E., and Pomerantz, J.L. (2016). Molecular Determinants of Scaffold-induced Linear Ubiquitinylation of B Cell Lymphoma/Leukemia 10 (Bcl10) during T Cell Receptor and Oncogenic Caspase Recruitment Domain-containing Protein 11 (CARD11) Signaling. The Journal of biological chemistry *291*, 25921-25936.

Ye, Y., Akutsu, M., Reyes-Turcu, F., Enchev, R.I., Wilkinson, K.D., and Komander, D. (2011). Polyubiquitin binding and cross-reactivity in the USP domain deubiquitinase USP21. EMBO Reports *12*, 350-357.

Ye, Y., Blaser, G., Horrocks, M.H., Ruedas-Rama, M.J., Ibrahim, S., Zhukov, A.A., Orte, A., Klenerman, D., Jackson, S.E., and Komander, D. (2012). Ubiquitin chain conformation regulates recognition and activity of interacting proteins. Nature *492*, 266-270.

Ye, Y., and Rape, M. (2009). Building ubiquitin chains: E2 enzymes at work. Nature reviews Molecular cell biology *10*, 755-764.

Zerbino, D.R., Achuthan, P., Akanni, W., Amode, M.R., Barrell, D., Bhai, J., Billis, K., Cummins, C., Gall, A., Giron, C.G.*, et al.* (2018). Ensembl 2018. Nucleic acids research *46*, D754-d761.

Zhang, J., Clark, K., Lawrence, T., Peggie, M.W., and Cohen, P. (2014). An unexpected twist to the activation of IKKbeta: TAK1 primes IKKbeta for activation by autophosphorylation. The Biochemical journal *461*, 531-537.

Zheng, N., and Shabek, N. (2017). Ubiquitin Ligases: Structure, Function, and Regulation. Annu Rev Biochem *86*, 129-157.

Zhou, Q., Yu, X., Demirkaya, E., Deuitch, N., Stone, D., Tsai, W.L., Kuehn, H.S., Wang, H., Yang, D., Park, Y.H.*, et al.* (2016). Biallelic hypomorphic mutations in a linear deubiquitinase define otulipenia, an early-onset autoinflammatory disease. Proceedings of the National Academy of Sciences of the United States of America *113*, 10127-10132.

Zinngrebe, J., Montinaro, A., Peltzer, N., and Walczak, H. (2014). Ubiquitin in the immune system. EMBO Reports *15*, 28-45.

10. Appendix

10.1 Publications

Results of this thesis are part of:

Weber, A., Elliott, P.R., Pinto-Fernandez, A., Bonham, S., Kessler, B.M., Komander, D., El Oualid, F., and Krappmann, D. (2017). A Linear Diubiquitin-Based Probe for Efficient and Selective Detection of the Deubiquitinating Enzyme OTULIN. Cell chemical biology *24*, 1299-1313.e1297.

Weber, A., Elliott, P.R., Pinto-Fernandez, A., Bonham, S., Harrison, L., Schaub, A., Kutzner, K., Keusekotten, K., Pfluger, P.T., El Oualid, F., Kessler, B.M., Komander, D., Krappmann, D. Regulation of the endosomal SNX27-retromer by OTULIN.
Submitted.

10.2 Acknowledgements

First, I would like to express my gratitude to my supervisor Daniel Krappmann. Thank you for the great project, your support and your contagious enthusiasm.

I also want to thank the members of my thesis committee for reviewing my thesis: Prof. Dr. Barbara Conradt, Prof. Dr. Christof Osman, Prof. Dr. Heinrich Jung, Prof. Dr. Kai Papenfort and Prof. Dr. Bettina Kempkes.

Special thanks go to the members of my HELENA thesis committee for helpful discussions and advices: Dierk Niessing, Oliver Plettenburg and Robert Janowski.

I am very thankful to our collaboration partners, who contributed to this study: Paul Elliott, Adan Pinto-Fernandez, Sarah Bonham, Benedikt Kessler, David Komander and Farid El Oualid.

I had great pleasure of working with all the fantasic colleagues of the Krappmann lab. Thank you for the cheerful and amicable working atmosphere!

Finally, I am deeply grateful to my family in Stuttgart and Munich, and especially to Simon! Without your love, support and patience, this thesis would not have been possible. Thank you!

10.3 Eidesstattliche Erklärung

Ich versichere hiermit an Eides statt, dass meine Dissertation selbständig und ohne unerlaubte Hilfsmittel angefertigt worden ist.
Die vorliegende Dissertation wurde weder ganz, noch teilweise bei einer anderen Prüfungskommission vorgelegt.
Ich habe noch zu keinem früheren Zeitpunkt versucht, eine Dissertation einzureichen oder an einer Doktorprüfung teilzunehmen.

München, den 9. Januar 2019 *Aurelia Weber*

.....

Aurelia Weber